Jinsong Zhou · Zhongyang Luo
Yanqun Zhu · Mengxiang Fang

Mercury Emission and its Control in Chinese Coal-Fired Power Plants

ZHEJIANG UNIVERSITY PRESS
浙江大学出版社

Springer

Jinsong Zhou
Zhongyang Luo
Yanqun Zhu
Mengxiang Fang

Mercury Emission and its Control in Chinese Coal-Fired Power Plants

Jinsong Zhou
Zhongyang Luo
Yanqun Zhu
Mengxiang Fang

Mercury Emission and its Control in Chinese Coal-Fired Power Plants

With 137 figures, 72 of them in color

ZHEJIANG UNIVERSITY PRESS
浙江大学出版社

Springer

Authors
Prof. Jinsong Zhou
College of Mechanical and Energy Engineering, Zhejiang University 310027, P.R. China
E-mail: zhoujs@zju.edu.cn

Prof. Zhongyang Luo
College of Mechanical and Energy Engineering, Zhejiang University 310027, P.R. China
E-mail: zyluo@zju.edu.cn

Dr. Yanqun Zhu
College of Mechanical and Energy Engineering, Zhejiang University 310027, P.R. China
E-mail: yqzhu@zju.edu.cn

Prof. Mengxiang Fang
College of Mechanical and Energy Engineering, Zhejiang University 310027, P.R. China
E-mail: mxfang@zju.edu.cn

ISSN 1995-6819 e-ISSN 1995-6827
Advanced Topics in Science and Technology in China

Zhejiang University Press, Hangzhou

ISBN 978-3-642-37873-7 ISBN 978-3-642-37874-4 (eBook)
Springer Heidelberg New York Dordrecht London

Library of Congress Control Number: 2013935586

Printed on acid-free paper

Springer is part of Springer Science+Business Media (www.springer.com)

Preface

Coal-fired mercury emission is one of the main factors causing global mercury pollution problems. The United Nations Environment Program (UNEP) pointed out that coal-fired power plants are the biggest human mercury emission source. In China, coal consumption is huge. And mercury emission pollution was gradually revealed in recent years. Actively developing coal-fired mercury pollution emission control research and exploring reasonable, effective and economic mercury control methods and approaches, are important topics for Chinese sustainable development in light of the current use of coal as main energy source.

This book mainly introduces Zhejiang University's experiences and achievements in the research field of coal-fired mercury emissions and control during the last decade. All these studies were funded by the Chinese National Natural Science Foundations: Transformation Mechanics and Emission Reduction of Mercury in Coal Combustion (No. 59906010, 2000-2002), and Stabilization Mechanisms of Mercury During Its Control in Coal-Fired Flue Gas (No. 50476056, 2005-2007); the Chinese National Basic Research Priorities (973) Program: Mercury Transformation and Its Control for Coal-Fired Utilization (No. G1999022212-08, 1999-2003); the Chinese High Tech Research and Development (863) Program: Advanced Mercury Control Technology on the Basis of Semi-Dry Method (No. 2001AA529040, 2002-2004), and Estimation of Mercury Emission from Coal Use in China (No. 2005AA520080, 2005-2007), and the Chinese Doctor Station Foundation: Mercury Speciation Transformation and Removal in the Conventional Combustion Pollutants Control Process (No. 20050335057, 2006-2008).

This book is the technical report to introduce mercury emission and its control from coal-fired power plants in China. The book focuses on coal consumption and air pollutant control in coal-fired power plants, and the ongoing research status of mercury emission and its control in China. The book mainly describes the mercury sampling methods and measurements of coal-fired flue gas, the estimation of mercury emission from coal-fired power plants in China, the research into mercury speciation transformation during coal combustion, the research of mercury control and mercury stability in byproducts.

The preparation of this book has been made possible thanks to the

contributions of Dr. Changxing Hu, Dr. Sheng He, Dr. Hongliang Gao, Dr. Jianli Ren, Dr. Jianming Zheng, Dr. Xiaoyu Hua, Xujie Wu, Xiangjian Shi, Guangkai Wang, Le Zhang, and Qiankun Li, etc.

The authors
Hangzhou, China
Mar. 18, 2013

Contents

1

Controlling Pollutants in Coal-Fired Power Plants in China

1.1 Introduction

Coal is an important source of energy in China. According to the data from the National Bureau of Statistics of China, 3,570 million tons coal was consumed in 2011, which was about 72.8% of the primary energy used in China. Although new sources of energy are now being used, it is estimated that the use of coal will still be above 60% of the total primary energy production by the year 2020. The typical way of utilizing coal is through burning. Emissions such as sulfur oxides (SO_x), nitrogen oxides (NO_x), and trace mercury (Hg), etc., from burning coal have caused serious pollution problems. In fact, coal-fired power plants are the main sources of mercury emissions[1]. In 2005, about 495 tons of mercury came from coal-fired power plants and other sources. Considering the rapid economic growth and industrial expansion of China, the annual growth of mercury emissions is expected to reach 20 – 30 tons[2]. Hu estimated that there were about 193.6 tons of mercury emissions from coal-fired power plants in China in 2005. This figure amounts to 12% of global mercury emissions[3].

More than 140 countries, including China, reached an agreement under the Environment Program Management Committee of the United Nations in February 2009. Through this agreement, the participating countries pledged to a treaty on reducing global mercury pollution. At present, a few developed countries plan to fix limit standards on mercury emissions in future. The United States Environmental Protection Agency (US EPA)[4] proposed new mercury emissions control rules in March 2011.

In China, government and related agencies have focused on measures to control mercury emissions from coal-fired power plants in the country. The government has started funding research on finding ways to control mercury emissions. In 2010, the State Environmental Protection Department explicitly requested carrying out atmospheric mercury pollution control pilot projects in coal-fired power plants from 2011 to 2015. China has announced emission standards of air pollutants for thermal

power plants (GB 13223-2011), including mercury emission control standards, in July 2011. This chapter discusses the coal consumption and air pollution control devices of coal-fired power plants in China, and the current status and control of mercury emissions in the country.

1.2 Coal Consumption and Air Pollutant Control in Coal-Fired Power Plants in China

For a long time, the use of coal as the main source of energy has played a key role in the structure of energy consumption in China. The percentage of coal consumption in total energy in China from 1990 to 2007[5,6,7] is shown in Fig. 1.1.

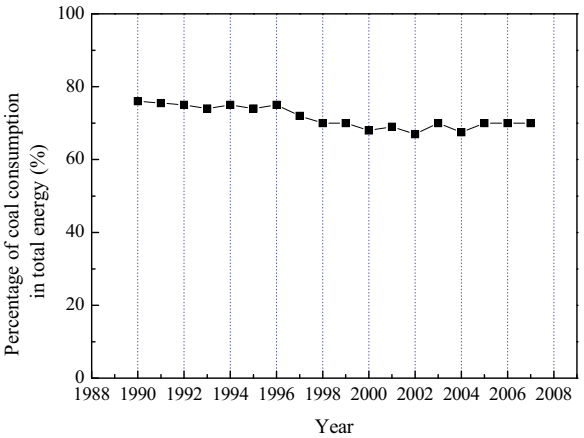

Fig. 1.1 Percentage of coal consumption in total energy from 1990 to 2007 in China

As can be seen, coal consumption occupied a high proportion of total energy in China. The percentage of coal consumption was lowest at 65.6% in 2002, increasing to 68.7% in 2009. It is estimated that coal consumption can reach 62.6% in 2015 and continue to reach levels above 50% in 2050. So, not only now, but also for quite a long period, though the proportion of coal in the energy consumption structure will drop year by year, the role of coal as the main source of energy in China shall remain.

The capacity and coal consumption of electric power generation in China are shown in Fig. 1.2. Coal-fired power plants are the most popular type of electric power generation in China. The average installed capacity of coal-fired power plants was about 75.2% of the total installed capacity from 1990 to 2008. In 2008, the capacity of electric power generation was 792.5 GW, including 601.3 GW from coal-fired power plants, which was about 75.9% of the total. In all, these plants have consumed a total of 1.34 billion tons of coal.

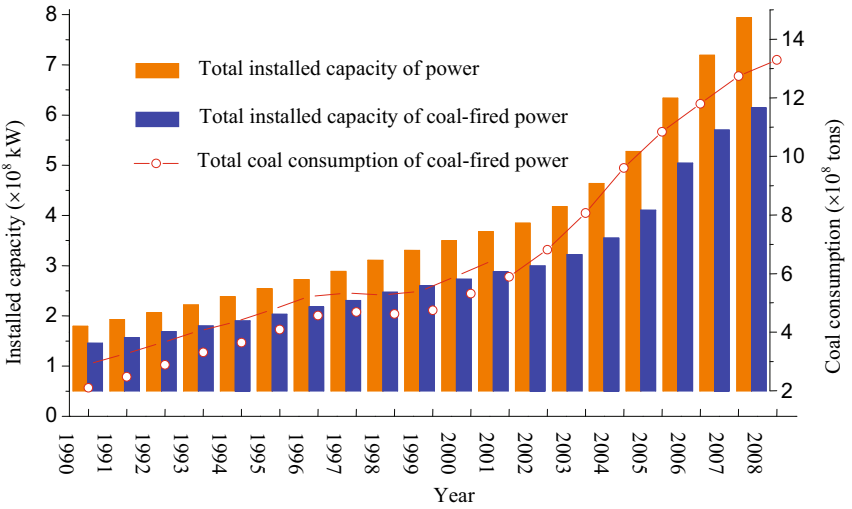

Fig. 1.2 Capacity and coal consumption of electric power generation in China from 1990 to 2008

Conventional pollutant emission control technologies for particles SO_2 and NO_x has progressed in recent years in China. Currently, most coal-fired power plants are equipped with dust-cleaning equipment，such as electrostatic precipitators (ESP) or fabric filters (FF). Desulfurization technology has also rapidly developed[8]. In 2005, the capacity of coal-fired power plants equipped with a desulfurization unit was 12.3%. However, in 2009, this capacity was about 78% (about 470.0 GW). In addition, SO_2 emissions from coal-fired power plants appeared to have decreased for the first time. Wet limestone-gypsum desulfurization is mainly used as flue gas desulfurization technology in China. By 2007, 26 sets of flue gas NO_x-controlled devices had been installed in coal-fired power plants in China, with a total capacity reaching 11,250 MW. Most power plants used selective catalytic reduction (SCR) technology, except four units of 600 MW that adopted selective non-catalytic reduction (SNCR). At present, nearly 200 sets of NO_x-controlled devices for 105.0 GW capacity have passed environmental assessments[9]. Given the rapidly increasing demands for environmental protection requirements, more coal-fired units must be equipped with flue gas desulfurization and NO_x-controlled devices. However, although these conventional pollutant control technologies can affect gaseous mercury ($Hg_{(g)}$) emissions, the ability to control $Hg_{(g)}$ depends on mercury speciation.

1.3 Research of Mercury Emissions and Their Control in China

1.3.1 Mercury Emissions in China

According to the UNEP report released in 2008, China, the United States and India are the three countries with the largest mercury emissions, with an aggregate rate of about 57% of total global emissions. It is said that by 2008, mercury emissions in China were twice those of the United States and India combined, with nearly 50% of mercury emissions coming from the burning of fossil fuels in China.

Some reports show that in China average mercury concentration in coal is 0.22 mg/kg, which is more than 0.13 mg/kg of the world average. Many scholars used different methods to estimate mercury emissions from coal-fired plants in China. Feng *et al*.[10] estimated mercury emissions in the atmosphere to be 296 tons; if the present pollution control facilities are maintained, the annual amount of mercury emissions can increase by 5.3%. Wang *et al*.[11] studied the mercury concentration in Chinese coal and the emissions of mercury from coal-fired industries and estimated the mercury emissions in the atmosphere in China in 1995 to be about 213.8 tons. Mercury emissions from coal-fired industries reached 2493.8 tons in the years 1978–1995, with emissions growing at an average annual rate of 4.8%. David and Streets *et al*.[12] analyzed the national statistical yearbook data for 1999 and estimated the mercury emissions to be 536(±236) tons, 38% of which came from coal-fired industries. Meanwhile, Jiang *et al*.[13] divided mercury emission sources into 65 various types according to the following criteria: economic sector, flue type, method of burning and pollutant emission control technology. They established a mercury emission inventory of coal-fired industries in the provinces according to coal consumption, mercury concentration in coal and the mercury emission factor in China. The two sets of data released by the US Geological Survey (USGS) showed that the average mercury concentration in Chinese coal was 0.15 and 0.20 mg/kg, respectively. Both were higher than the global average mercury concentration of 0.13 mg/kg. In addition, the two data sets also indicated $Hg_{(g)}$ emissions from coal-fired industries in 2000 at 161.6 and 219.5 tons, respectively. At present, about 35% of total mercury comes from electric power industries. China has an unequal distribution of mercury emissions from coal-fired industries, and provinces with major emissions include Henan, Shandong, Guizhou, Guangdong and Jiangsu.

Ren *et al*.[14] reported that the average annual growth rate of $Hg_{(g)}$ emissions coming from the coal-fired power plants in China from 1999 to 2003 was 9.59% and that for non-$Hg_{(g)}$ emissions was 8.49%. There were 86.8 and 28.94 tons of $Hg_{(g)}$ and non-$Hg_{(g)}$ emissions, respectively, from coal-fired power plants in 2003. Wang *et al*.[15] estimated that the mercury emission was about 256 tons from the coal-fired industry in 2003. According to actual test data of coal-fired power plants, Hu *et al*.[3] estimated the total mercury emissions from coal-fired power plants in 2005 to be 193.6 tons, including 147.0 tons of $Hg_{(g)}$.

The assumptions made by Wang, however, have yet to be proven by field test or research. To date, the accuracy of such estimations still awaits validation. Thus, it is important to study the mercury emission characteristics of the typical coal-fired sources in order to establish a thorough, comprehensive, and accurate mercury emission inventory of coal-fired power plants in China.

1.3.2 Mercury Emission Control Technologies in China

Coal-fired mercury control technologies have developed gradually in recent years. Various mercury pollution control technologies used in coal-fired power plants are presented in Fig. 1.3. Mercury pollution control technologies of coal-fired plants can be roughly divided into three types: those done before, during, and after the burning of coal.

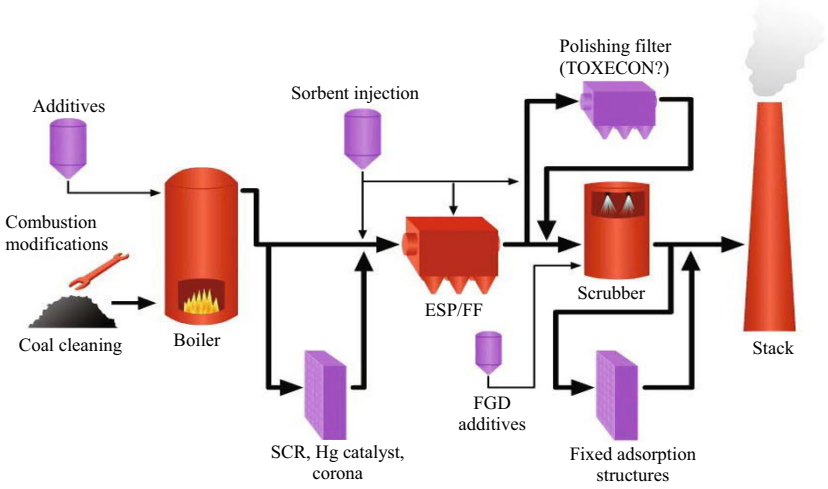

Fig. 1.3 Mercury pollution control technical methods for coal-fired power plants

Examples of mercury control technology applied before burning include coal washing, coal drying technologies, etc. Coal washing is an effective mode of reducing $Hg_{(g)}$ emissions. In general, the mercury removal rate of flotation technology is between the ranges of 21%–37%. This technology is applied depending on the coal type, method of washing, separation technology, and mercury concentration in coal[16]. The coal washing technology is a relatively old technology, whereas the application of coal heating dry technology is fairly recent. Coal drying technology, on the other hand, can remove about 70% of mercury in the coal before burning. However, the rate of washed coal in China is still low and most coal-fired power plants have not yet adopted the use of "washed" coal.

At present, studies of mercury control during burning have focused on the improvement of the combustion mode and additive combustion method. Research

shows that the circulating fluidized-bed coal combustion method is helpful in reducing mercury emissions. In fact, only 4.5% of mercury in coal is emitted to the atmosphere when burning high chlorine bituminous coal[17]. Incorporating the additive during the burning process changes the distribution of mercury speciation in the flue gas. Currently, brominated additive is used to control mercury emissions. On-site application research shows that total mercury removal efficiency can reach 80% when 4 ppm bromine is added to the coal[18].

Mercury control technology after burning refers to the removal of mercury from the coal-fired flue gas. This technology can be divided into several methods explained below. First, it uses sorbent to adsorb mercury in flue gas. However, the mechanism involved in adsorbing mercury is unclear, and there are many arguments surrounding its effectiveness. The popular absorbents are activated carbon, coal fly ash, calcium material, zeolite, and so on.

Second, it uses existing flue gas pollution control devices of coal-fired power plants to reduce mercury emissions. At present, existing flue gas pollution control devices include particle-control equipment (ESP or FF), NO_x-control equipment (SCR), and flue gas desulfurization equipment (WFGD). It can simultaneously control mercury, particulates, SO_2, and NO_x pollutants using the existing pollutant control devices.

Third, it develops new mercury pollution control technologies, such as corona discharge plasma technology and electrocatalytic oxidization combined treatment technology, for comprehensive control.

Currently, except for the mercury emissions control technology used in the laboratories, there is no particular technology being used for coal-fired power plants in China. However, ESP, WFGD, and SCR pollutant control equipment that has certain mercury control functions is widely used. The mercury removal efficiency of such equipment depends on the speciation distribution of mercury in flue gas, which is mainly affected by coal type. Table 1.1 shows the average mercury removal efficiency rates of existing pollutant control technologies with different coal types[19,20].

Table 1.1 Mercury removal efficiency of existing pollution control technology with different coal types

Existing pollution control technology	Mercury removal efficiency (%)		
	Bituminite	Sub-bituminite	Lignite
Particle control			
Cold-ESP	46/36	16/3	0/04
Hot-ESP	12/9	13/6	-/-
FF	83/90	72/72	-/-
Wet dust removal	14/-	0/9	33/-
SO_2 control			
Dry spray+FF	98/98	3/24	17/0
Hot-ESP+WFGD	55/49	33/29	-/-
Cold-ESP+WFGD	81/75	35/29	44/44
FF+WFGD	96/98	-/-	-/-

1.4 Outline of the Book

The aim of this book is to introduce mercury emissions and their control in coal-fired power plants in China. The whole book is divided into 5 chapters. Chapter 1 discusses the controlling pollutants in coal-fired power plants in China, including coal consumption and air pollutant control in coal-fired power plants, and the ongoing research status of mercury emissions and their control in China. Chapter 2 describes mercury sampling methods and measurements in coal-fired power plants, including the introduction of sampling objects in coal-fired power plants, the process of mercury sampling, results of mercury sampling and measurement, mercury balance analysis, mercury removal with current pollutant control devices, and so on. Chapter 3 presents an estimation of mercury emissions from coal-fired power plants in China, including mercury emission factor, mercury emission estimation from coal-fired power plants, the future development trend forecasts, and so on. Chapter 4 touches on mercury speciation transformation during coal combustion, including experimental research on the release of mercury from coal combustion, mercury speciation transformation after coal combustion, modeling research on mercury speciation transformation during coal combustion, and so on. Chapter 5 discusses mercury control and mercury stability in byproducts, including experimental research on the absorption of $Hg_{(g)}$, mercury absorption with normal sorbents and mercury absorption with treated sorbents, as well as the absorption mechanism on the active carbon surface, mercury stability in desulfurization gypsum, mercury stability on the active carbon surface, and so on.

1.5 Summary

The hazards of mercury pollution have attracted growing public interest in recent years. Thus, the effective control of mercury emissions from coal-fired power plants has also gained worldwide interest. Mercury emission and control are significantly related to the energy consumption structure of a country. In line with this, the current chapter presents the structure of the coal consumption and mercury control technology in China, and other related issues.

In China, coal is one of the main sources of energy, occupying a high ratio of the total energy consumption in the country. This coal-based energy consumption structure is expected to continue well into the future. Control methods of coal-fired mercury emission pollution can be divided into three categories: mercury control technologies before burning, such as coal washing technology and heat treatment technology, that are not commonly used in China; mercury control technologies during burning, which are focused on improving combustion methods and additive combustion means; and mercury control technologies after burning, such as using sorbents to achieve the adsorption removal of mercury and existing pollution control devices of coal-fired power plants in order to control $Hg_{(g)}$ emissions.

References

[1] U.S. Environmental Protection Agency. *Mercury Study Report to Congress Volume 1: Executive Summary.* Office of Air Quality Planning and Standards and Office of Research and Development, EPA-452/R-97-003. Washington, DC: U.S. Government Printing Office, 1997.

[2] Pombo R.W., Gibbons J. Mercury in perspective: Fact and fiction about the debate over mercury. http://www.heartland.org/custom/semod_policybot/pdf/17467.pdf, 2005.

[3] Hu C.X. Mercury Emission from Coal-Fired Power Plant in China and Stability Adsorption Mechanism of Mercury on Activated Carbon. Ph.D thesis, Zhejiang University, 2007.

[4] U.S. Environmental Protection Agency. Clean Air Mercury Rules. http://www.epa.gov/mercuryrule/indux.htm, Mar 2005.

[5] Guan W.H., Gu C.L., Lin Z.S. Study on the change of energy consumption structure in China. *Journal of Natural Resources*, 21(3): 401-407, 2005.

[6] The Primary Energy Consumption Structure of Major Country in 2006. Shanxi Energy and Conservation, 2008.

[7] 2008 China Statistical Yearbook.

[8] Li Z. Sustainable Utilization of Coal in China. Beijing, 2009.

[9] Wang J.N. Pollution Control of Coal-Fired Electric Industry in China. Beijing, 2009.

[10] Feng X.B., Hong Y.T., Ni J.Y., Zhou B., Wang Y. Distribution and occurrence mode of mercury in some coals of Guizhou province and its environmental impact. *Coal Geology & Exploration*, 2: 14-17, 1998.

[11] Wang Q.C., Shen W.G., Ma Z.W. The estimation of mercury emission from coal combustion in China. *China Enivronmental Science*, 19(4): 318-321, 1999.

[12] Streets D.G., Hao J.M., Wu Y. Anthropogenic mercury emissions in China. *Atmospheric Environment*, 39: 7789-7806, 2005.

[13] Jiang J.K., Hao J.M., Wu Y., Streets D.G., Duan L., Tian H.Z. Development of mercury emission inventory from coal combustion in China. *Environmental Science*, 26(2): 35-39, 2005.

[14] Ren J.L., Zhou J.S., Luo Z.Y., Zhong Y.J., Cen K.F. Forecasting model for mercury emission by coal-fired power plants. *Power Engineering*, 25(4): 587-592, 2005.

[15] Wang S.X., Liu M., Jiang J.K., Hao J.M., Wu Y., Streets D.G. Estimate the mercury emissions from non-coal sources in China. *Environmental Science*, 27(12): 2401-2406, 2006.

[16] Brian W., Ren A.L. Development of mercury emission control measures coal-fired power plant. *Hebei Journal of Industrial Science & Technology*, 25: 401-404, 2008.

[17] Liu K.L., Gao Y., Riley J.T. An investigation of mercury emission from FBC systems fired with high-chlorine coals. *Energy & Flues*, 15(5): 1173-1180, 2001.

[18] Lix X., Jiang Y. Development and situation of mercury control technology of coal-fired power plants in America. *High-Technology & Industrialization*, 3: 92-95, 2009.

[19] Economic and Social Council of UN. Control of Mercury Emissions from

Coal-Fired Electric Utility Boilers, EB.AIR/WG.5/2002/6. 4 July, 2002.

[20] Licata A., Balles E., Schüttenhelm W. Mercury Control Alternatives for Coal-Fired Power Plants. Presented at Power Gen 2002 Orlando, FL, 2002.

2

Mercury Sampling and Measurement in Coal-Fired Power Plants

2.1 Introduction

Fossil-fuel combustion is the major anthropogenic emission source of mercury. In China, a coal-fired power plant is the most common method of producing electric energy. Numerous studies have been conducted to research the characteristics of mercury emissions from the coal-fired power plants in China. Many factors, such as the amount and type of coal, the manner of combustion, the conventional pollutant-control devices, will affect the mercury emission for its special physical-chemical characteristics. In order to study the mercury sampling and measurement in coal-fired electric power plants in China, 6 sets of typical coal-fired boiler systems were chosen. The basic conditions of these boiler systems are shown in Table 2.1.

Table 2.1 Basic conditions of 6 typical coal-fired boiler systems

No.	Location	Unit capacity (MW)	Combustion method	Coal type	Mercury in coal (mg/kg)	Pollutant control device
1	Zhejiang	300	Four-corner	Shenhua mixed coal	0.145	ESP
2	Zhejiang	600	Front and back walls	Shenhua mixed coal	0.161	ESP
3*	Beijing	2*100	Four-corner	Zhun'ge'er mixed coal	0.088	ESP+WFGD+LNB**
4	Jiangsu	300	Four-corner	Shanxi coal	0.208	ESP
5	Anhui	300	Four-corner	Huibei mixed coal	0.188	ESP+WFGD
6	Fujian	300	Four-corner	Jingbei mixed coal	0.140	SCR+ESP+WFGD***

Note: *Both 100 MW boilers with two ESPs and one WFGD; **Lower NO_x burner; ***WFGD with sea water

In the following part, we will introduce the process and results of the sampling tests of the above-mentioned typical coal-fired power plants using the Ontario Hydro method (OH Method, U.S. Standard Mercury Sampling Method), Continuous Emission Monitor (CEM) method, and 324 method. We also discuss the distribution of mercury speciation in flue gas from coal-fired power plants as well as the impact of various air pollutant control devices on mercury speciation.

2.2 Mercury Measurement Method in Coal-Fired Power Plants

Many mercury measurement methods are being used in the study of mercury emissions, but many among these are still being studied. These methods can be divided into two kinds: the manual analysis method and the on-line analysis method, which is also called CEM. Depending on the test procedure and the measuring method, the manual analysis methods can be further divided into the wet chemical and the dry adsorption methods. The manual analysis requires a longer time, whereas the on-line analytical technique can analyze mercury concentration and speciation in real-time.

2.2.1 Manual Analysis Method

There are two kinds of wet chemical mercury testing methods: the measurement method of total mercury (for example, the EPA 101A method and EPA 29 method, etc.) and the measurement method of mercury speciation (for example, the OH method, the Tris Buffer method, and the EPA 101B method, etc.). Dry sorbent methods usually refer to the flue gas mercury sorbent speciation (FMSS) and the quicksilver emissions monitor (QSEM).

The OH method is the choice of over 80 American coal-fired power plants for measuring mercury concentration and speciation. However, it is very complex for mercury sampling and analyzing in the coal-fired flue gas testing field. Many factors, such as coal type, fly ash, gas velocity, temperature, and so on, can directly affect the accuracy and reliability of the test data. The mass balance of test results can also reflect the reliability of the sampling analysis of mercury from coal-fired power plants. According to Takahisa's research, it is acceptable for the mass balance to be within the range of 70% – 130%[1].

2.2.2 Continuous Emission Monitoring

CEM is a developing technology that can conduct real-time monitoring and analysis. It is based on advanced analysis technology, such as cold atomic absorption

spectrometry (CVAAS), cold vapor atomic fluorescence (CVAFS), atomic excitation spectrometry (AES), new chemical sensors, and so on[2].

The process of CEM is the same as that of other flue gas pollution emission monitoring systems. First, the analyzed object is obtained from the flue gas using the sampler. The potential interferential components in the sampling gas, such as HCl, SO_2, SO_3 and other acidic gases, are eliminated before they go through the detector. The concentration and speciation of mercury is then detected by the detector. However, the continuous monitoring of mercury is complex because of the existence of different mercury speciation, which are generally divided into elemental mercury (Hg^0), oxidized mercury (Hg^{2+}) and particle mercury (Hg^p). The CEM detector only detects Hg^0. All the non-Hg^0 and Hg^{2+} should be transformed to gaseous Hg^0 through a transformation system for measuring total mercury by CEM. Except for mercury chloride ($HgCl_2$) as the main form of Hg^{2+}, research indicated that there are still other Hg^{2+} forms[3].

In theory, Hg^p can be converted into gaseous Hg^0. However, most mercury CEMs only measure total $Hg_{(g)}$ (TGM). A negative deviation should be introduced into the measurement of TGM because the Hg^p cannot be measured in actual conditions. Furthermore, the fly ash on a filter can capture $Hg_{(g)}$ during sampling, which will enlarge the negative deviation. Therefore, it is very important to monitor Hg^p during the analysis by CEM. A similar problem also exists during the quantitative transformation of $HgCl_2$. The $HgCl_2$ is water-soluble and more active; thus, its quantity might decrease due to the adsorption that occurs while sampling.

2.3 Process of Mercury Sampling

For the present study, the sampling and analyzing of flue gas mercury were mostly conducted using the OH method. At the same time, the CEM was also used to monitor $Hg_{(g)}$ in some testing. Coal, fly ash, slag, and slurry liquid of WFGD were also analyzed during the testing. Solid and liquid mercury samples were collected at the same time of sampling $Hg_{(g)}$. Mercury in the collected samples was mostly analyzed by the direct detection method with MA2000 instrument, or the AFS detection method with pretreatment by microwave digestion.

Flue gas mercury concentrations at the inlet and outlet of existing pollution control devices were tested by sampling or on-line analysis, which can study the mercury control capabilities of different conventional pollution control devices. Six different coal-fired boilers with different pollution control equipment were chosen in this mercury emission research. The detailed sampling conditions of the typical coal-fired boiler systems are shown in Table 2.2. The concentration and speciation analyses of flue gas mercury from No. 1 and No. 2 coal-fired boilers were conducted according to the OH method; those from No. 3 and No. 5 were conducted using the CEM method; and those from No. 4 and No. 6 were conducted according to both the OH and CEM methods. In addition, the 324 method was also adopted during the test of the Nos. 4, 5, and 6 coal-fired boilers.

Table 2.2 Sampling conditions of 6 typical coal-fired boiler systems

No.	Method	Measure point	Boiler load (MW）
1	OH	OH blank	-
		Before ESP	300
		Before ESP	212
		After ESP	300
		After ESP	210
2	OH	Before ESP	600
		Before ESP	453
		After ESP	600
		After ESP	450
3	CEM	After ESP	100
		After ESP	80
		After ESP	100
		After WFGD	100
4	OH	OH blank	-
		Before ESP	300
		After ESP	300
	CEM	After ESP	300
	324	After ESP	300
5	CEM	After ESP	210
		After WFGD	200
		After WFGD	200
	324	After WFGD	200
6	OH	OH blank	-
		Before SCR	270
		Before SCR	270
		Before ESP	274
		After ESP	284
		After WFGD	230
	CEM	After ESP	230–270
		After WFGD	280–300
	324	After ESP	230–270

2.4 Results of Mercury Sampling and Measurement

Tables 2.3–2.5 show the test results of concentration and speciation of flue gas mercury emissions into the atmosphere from the coal-fired boilers using OH, CEM

and 324 method, respectively. $Hg_{(g)}$ was the main speciation, which was about 86.5%–97.8% of the total mercury emission. Hg^p was only 2.1%–13.5% of the total. It is difficult to control gaseous Hg^0 by existing conventional pollution control devices because Hg^0, as a primary $Hg_{(g)}$, has special characteristics, including higher volatility, a lower water-solubility and a stable speciation, which can induce global pollution with the help of atmospheric motion. Hg^{2+} is another type of $Hg_{(g)}$. Common Hg^{2+} is water-soluble and can be captured by most wet flue gas cleaning technologies. Once it is emitted to the atmosphere, water soluble Hg^{2+} is deposited, thus polluting the vicinity of the mercury emission source.

Table 2.6 shows the concentration of total $Hg_{(g)}$ and ratio of mercury speciation in the flue gas emitted into the atmosphere. The ratio of Hg^0 and that of Hg^{2+} was nearly equal when only the ESP was in place; the ratio of Hg^{2+} decreased when both ESP and WFGD were in place; and the ratio of Hg^0 and the concentration of total $Hg_{(g)}$ decreased further when SCR, ESP, and WFGD were in place (Tables 2.3 to 2.6). This occurred because the SCR catalyzed Hg^0 to Hg^{2+} under a certain condition and then the WFGD captured most Hg^{2+}.

Table 2.3 Concentration and speciation of flue gas mercury emissions into the atmosphere (OH method)

Location	Unit capacity (MW)	Combustion method	Pollutant control device	Hg^0 (μg/(N·m^3))	Hg^{2+} (μg/(N·m^3))	Hg_p (μg/(N·m^3))	Total Hg (μg/(N·m^3))	Percentage of total Hg (%)		
								Hg^0	Hg^{2+}	Hg_p
Zhejiang	300	Four-corner	ESP	4.8468	3.3678	1.2831	9.4976	51.0	35.5	13.5
Zhejiang	600	Front and back walls	ESP	7.4813	6.0838	1.9357	15.5007	48.3	39.2	12.5
Jiangsu	300	Four-corner	ESP	5.6532	6.5371	0.8708	13.0612	43.4	49.3	7.3
Fujian	300	Four-corner	SCR+ESP +FGD	0.4460	2.3660	0.0310	2.843	15.7	83.2	1.1

Table 2.4 Concentration and speciation of flue gas mercury (excluding Hg^p) emissions into the atmosphere (CEM method)

Location	Unit capacity (MW)	Combustion method	Pollutant control device	Hg^0 (μg/(N·m^3))	Hg^{2+} (μg/(N·m^3))	Total gaseous (μg/(N·m^3))	Percentage of total gaseous Hg (%)	
							Hg^0	Hg^{2+}
Jiangsu	300	Four-corner	ESP	8.79	6.86	13.0612	56.2	43.8
Beijing	2*100	Four-corner	ESP+FGD	1.97	1.11	3.08	64.0	36.0
Anhui	300	Four-corner	ESP+FGD	6	0.28	6.28	95.5	4.5
Fujian	300	Four-corner	SCR+ESP +FGD	≈0	—	—	—	—

Table 2.5 Concentrations and speciation of flue gas mercury (excluding Hg^p) emissions into the atmosphere (324 method)

Location	Measure point	Sampling	Hg^0 (μg/(N·m^3))	Hg^{2+} (μg/(N·m^3))	Total gaseous Hg (μg/(N·m^3))	Percentage of total gaseous Hg (%)	
						Hg^0	Hg^{2+}
Jiangsu	After ESP	324_A	5.63	8.51	14.14	39.8	60.2
		324_B	3.45	7.67	11.12	31.0	69.0
Anhui	After WFGD	324_A	4.87	0.42	5.29	92.1	7.9
		324_B	5.41	0.81	6.22	87.0	13.0
Anhui	After ESP	324_A	1.31	13.75	15.06	8.7	91.3

Table 2.6 Concentrations of total $Hg_{(g)}$ and ratio of mercury speciation emissions into the atmosphere (OH method)

Location	Unit capacity (MW)	Combustion way	Pollutant control device	Total $Hg_{(g)}$ (μg/(N·m^3))	Percentage of total gaseous Hg (%)	
					Hg^0	Hg^{2+}
Zhejiang	300	Four-corner	ESP	8.2145	59.0	41.0
Zhejiang	600	Front and back walls	ESP	13.565	55.2	44.8
Jiangsu	300	Four-corner	ESP	12.1903	46.4	53.6
Fujian	300	Four-corner	SCR+ESP+FGD	2.812	15.9	84.1

2.5 Mercury Balance Analysis

Mercury balance analysis is an effective way by which to ensure the accuracy of test results. The mercury mass balance ratio of each boiler is defined as the ratio of output mercury quality to input mercury quality. In this reported testing, the mercury mass balance ratio of each boiler ranged within (100±22)% (Table 2.7), indicating that the test results were accurate.

Table 2.7 Mercury mass balance analysis of each typical coal-fired boiler

No.	Input		Output				Mass balance (%)
	Hg from coal	Other	Gaseous	Fly ash	Bottom ash	WFGD production	
1	1	—	0.8148	0.1167	0.0040	—	93.55
2	1	—	0.7213	0.1848	0.0050	—	91.11
3	1	0.0011	0.2479	0.1787	—	0.6208	104.85
4	1	—	0.7525	0.1757	0.0040	—	93.22
5	1	0.0007	0.2453	0.0964	—	0.8810	122.34
6	1	0.0024	0.0717	0.0827	0.0002	0.9061	106.31

2.6 Mercury Removal by Existing Pollutant Control Devices

High-efficiency pollution control devices, such as the flue gas dedusting system, desulfurization system, and deNO_x system can partly decrease $Hg_{(g)}$ emissions into the atmosphere. Different pollution control devices have different influences on mercury emissions.

2.6.1 Mercury Removal by deNO_x System

At present, two kinds of methods are mainly used to reduce NO_x emissions in coal-fired power plants, namely the flue SCR and the selective non-catalytic reduction (SNCR). The mercury speciation in flue gas is related to the temperature and the ammonia concentration of flue gas in SCR, but also to the main component of coal, such as chloride, sulfur, calcium, etc.

The SCR reactor of boiler No. 6 was arranged between the economizer and air preheater, which belonged to a high dust arrangement. At a high temperature of flue gas (340 °C), the catalyst had high activity. Test data showed that most of the Hg^0 converted to Hg^{2+} with the catalyst of SCR, indicating a high conversion efficiency of 85.1%. The rising proportion of Hg^{2+} helped in the removal of mercury through the WFGD device.

2.6.2 Mercury Removal by Dedusting System

All coal-fired power plants were equipped with dust removal devices, and of these 90% employed ESP. In this work, each EPS was located after the air preheater and had a dedusting efficiency of over 99%. Accordingly, most of the Hg^p could be captured in this way, and the Hg control efficiency was about 24%. The FF device and the wet dust removal device are two other kinds of dedusting systems. FF can reduce mercury emissions by capturing fly ash; at the same time, the fly ash layer accumulated on the FF also adsorbs mercury. Thus, FF could reduce 28% of total mercury emissions into the atmosphere. Although the wet dust removal has a high efficiency, it consumes a great amount of power, which is not good at controlling micro-particles. Research showed most mercury was enriched in micro fly ash.

Table 2.8 shows the published mercury removal efficiency of three main particulate control devices[4,5,6]. According to these results, the mercury removal efficiency of ESP was about 30%, that of wet dust removal was below 10%, and that of cyclone dust removal was almost zero. There has been very little research on the impact of flue gas cleaning devices on the mercury emission factor in coal-fired power plants in China. Most comparative data used in this study referred to the test results of developed countries.

Table 2.8 Hg removal efficiency of three main particulate control devices

Type	Streets (2005)	US EPA (2002)	US EPA (1997)	Wang *et al.* (2000)	Zhu *et al.* (2002)
ESP	30.6	36.0	30.4	25.7	30.3
Wet dust removal	6.5	8.7	4.3	—	—
Cyclone dust removal	0.1	0.1	0.0	—	—

The 6 particulate control devices chosen in this study were all ESPs. Based on the test results, Table 2.9 shows the calculated Hg emission factor (EMF) of ESP in 6 typical coal-fired power plants in China.

As shown in Table 2.9, the average EMF based on test results of 6 ESPs was 0.875, which was higher than that evaluated by other scholars. For example, Streets *et al.*[5] estimated that the EMF of ESP was 0.694 in coal-fired power plants in China. Wang *et al.*[4] believed it was 0.743, whereas Zhu *et al.*[6] believed it was 0.697.

Table 2.9 Hg EMF of 4 ESPs in China

Location	Total Hg before ESP (g/h)	Total Hg after ESP (g/h)	Hg removal efficiency (%)	EMF
Zhejiang	15.52	15.39	0.8	0.992
Zhejiang	34.10	33.16	2.7	0.973
Jiangsu	37.53	22.11	41.1	0.589
Fujian	18.02	17.03	5.5	0.945

2.6.3 Mercury Removal by WFGD

The limestone-gypsum wet desulphurization process, is a kind of WFGD technology, which is widely used in China. WFGD can reduce SO_2 emissions as well as remove most of the gaseous Hg^{2+} in flue gas. However, WFGD does not work with Hg^0; it can even increase Hg^0 emissions because it can cause the Hg^{2+} adsorbed into sulphite to be released again.

Chlorine concentration in coal can affect seriously the speciation of $Hg_{(g)}$, which is one of the important factors for mercury removal with WFGD. When chlorine concentration in coal ranges from 50 to 100 ppm, the flue gas Hg removal efficiency of ESP+WFGD could range within 30% – 60%, with an average mercury removal efficiency of about 49%. At the same level of chlorine concentration, mercury removal efficiency of FF+WFGD could reach 88%[7].

Table 2.10 shows the mercury removal efficiency of the WFGD bench-scale experiments[8]. The range of mercury removal efficiency in the present work ranged from 0 to 61.7%, and the average mercury removal efficiency was about 31%.

Table 2.10 Hg removal efficiency of WFGD in bench-scale experiment

Type of WFGD/ Hg concentration in flue gas (g/(N·m^3))	Hg removal efficiency (%)	References
Limestone / 9.9	10.87	Radian, 1993a (EPRI)
Limestone	0.00	Radian, 1993b (EPRI)
Limestone / 8.1	22.63	Interpoll, 1990a (NSP)
Limestone / 11.6	59.3	Interpoll, 1991 (NSP)
Lime / 6.0	45.91	EPRI, 1993a
Limestone / 10.0	12.05	Battelle, 1993a (DOE)
Limestone / 12.5	20.15	Radian, 1994b (EPRI)
Lime / 5.6	61.67	Radian, 1994c (EPRI)
Limestone / 9.5	45.10	Southern Research Ins., 1995a
Average	30.85	—

When the boiler was burning the lignite, the mercury removal efficiency of the WFGD reached less than 5%. This occurred because Hg^0 showed the most speciation in the lignite flue gas, which prevented WFGD from removing the mercury. When the boiler was burning high-Cl coal, the proportion of gaseous Hg^{2+} rose in the flue gas, which allowed WFGD to easily capture mercury. This indicated that the mercury removal capacity of WFGD was decided mainly by the characteristics of the coal being burned.

Based on the test results, the calculated mercury removal efficiency and mercury emission factor of WFGD are presented in Table 2.11.

Table 2.11 Hg removal efficiency and EMF of 3 WFGDs in China

Location	WFGD Type	Total gaseous Hg before WFGD (g/h)	Total gaseous Hg after WFGD (g/h)	Hg removal efficiency (%)	EMF
Beijing	Limestone-gypsum	4.36	1.25	71.4	0.286
Anhui	Limestone-gypsum	13.59	2.95	78.3	0.217
Fujian*	Sea-water	15.05	0.86	94.3	0.057

Note: *SCR was equipped before the WFGD

2.7 Summary

Accurate measurement of flue gas mercury is the key factor in the study of mercury control technology. In this section, the tests of 6 typical coal-fired power plants in China were described in detail. Through data analysis, mercury speciation in power plants, as well as the impact and the performance of air pollution control devices on demercuration, have been mainly discussed.

Mercury emissions from 6 coal-fired power plants came mainly in the form of $Hg_{(g)}$, accounting for about 87% to 98% of the total mercury concentration, whereas the Hg^p occupied a small proportion, accounting for only 2% to 13%. When there was only ESP as a cleaning device, the ratio of gaseous Hg^0 was almost the same as that of gaseous Hg^{2+} in the flue gas after the ESP. On the basis of ESP, when WFGD

was added, the proportion of Hg^0 was higher than that of Hg^{2+}.

According to the test data, the emission factor of ESP mercury in coal-fired power plants was approximately 0.875 on average. The mercury removal efficiency of ESP in power plants was associated with coal varieties, ESP structure, and other factors. In addition, ESP mainly removed Hg^p.

The role of mercury removal was played by WFGD through washing, especially for water-soluble Hg^{2+}. The dissolution effect of WFGD limestone and slurry became more prominent. It could be estimated in this study that the emission factor of WFGD demercuration was 0.252.

Test data showed that SCR transformed most of the gaseous Hg^0 into the gaseous Hg^{2+}, presenting a conversion efficiency of about 85%. At high temperature, $Hg_{(g)}$ effectively reacted with the oxidation catalyst. The degree of oxidation was related to coal types, gas composition, catalyst nature, temperature, and so on.

References

[1] Takahisa Y., Kazuo A. Mercury emissions from a coal-fired power plant in Japan. *The Science of the Total Environment*, 259: 97-103, 2000.

[2] Wockel. A Present Situation of CEM Systems for Mercury. *The Air & Waste Management Association's 89th Annual Meeting & Exhibition, June*, 1996.

[3] Hedges S., Ryan J., Stevens R. Workshop on Source Emission and Ambient Air Monitoring of Mercury. Bloomington, MN, September 13-14, 1999. EPA/625/R-00/002 (NTIS B2001-100963). National Risk Management and National Exposure Research Laboratory, Cincinnati, OH. June 2000.

[4] Wang Q.C., Shen W.G., Ma Z.W. The estimation of mercury emission from coal combustion in China. *China Enivronmental Science*, 19(4): 318-321, 1999.

[5] Streets D.G., Hao J.M., Wu Y. Anthropogenic mercury emissions in China. *Atmospheric Environment*, 39: 7789-7806, 2005.

[6] Zhu Z.J., Xu L., Tan Y., *et al.* Research on characteristics of mercury distribution incombustion products for a 300MW pulverized coal-fired boiler. *Power Engineering*, 22: 3-5, 2002.

[7] Pavlish J.H., Sondreal E.A., Mann M.D. Status review of mercury control options for coal-fired power plants. *Flue Processing Technology*, 82: 89-165, 2003.

[8] EPRI. http://mydocs.epri.com/docs/public/EPRI_MC.html.

3

Estimation of Mercury Emissions from Coal-Fired Power Plants in China

3.1 Introduction

As the main energy source in China, the key role of coal in the industry is well secured although its proportion in total primary energy consumption is predicted to shrink in the future. It is predicted that coal shall remain as the cornerstone of energy security in the protection of the stability and the rapid development of the national economy over the next several decades. The mercury in coal is released during combustion, and some is captured by air pollution control devices. However, most of the $Hg_{(g)}$ is emitted into the flue gas, which leads to air pollution. Therefore, determining the mercury emission factor and estimating the mercury emission in China are important tasks. This section mainly introduces the processes of determining the estimated formula of mercury emissions, estimating mercury emissions in coal-fired flue gas, and predicting the future trend of mercury control in China.

3.2 Estimated Formula of Mercury Emissions

The following Eq. (3-1) was used to estimate the annual amount of Hg emitted into the atmosphere from each coal-fired power plant. Eq. (3-1) considered some basic conditions, such as coal type (coal production), coal cleaning, coal consumption each year, boiler type, dust removal equipment, desulfuration, and so on.

$$E = \frac{C_{\mathrm{Hg}}}{10^6} \times M_{\mathrm{coal}} \times ccf \times \prod EMF_i \tag{3-1}$$

where C_{Hg} is the Hg concentration in coal (mg/kg); M_{coal} is the coal consumption each year (tons/yr); ccf is the coal cleaning factor; EMF_i is the mercury emission factor of different burner and different pollution control devices.

To estimate total annual Hg emissions into the atmosphere from coal-fired power plants in China, the following formula was used:

$$E_{\text{total}} = \sum_{j=0}^{n} eef_j \times E_j \tag{3-2}$$

where f is the proportion of one type of coal-fired power plant in total number of coal-fired power plants; and j is one type of coal-fired power plant ($1 \le j \le n$); E_j is the total mercury emission of the j^{th} type of coal-fired power plan.

The Hg EMF_i of burners and flue gas pollution control devices in coal-fired power plants are shown in Table 3.1.

Table 3.1 Hg EMF_i of each device in coal-fired power plants

Devices	EMF
Four-corner burner	0.998
Wet-type dust collector	0.935
ESP	0.867
FGD	0.252
SCR+ESP+FGD	0.124

3.3 Estimation of Mercury Emissions from Coal-Fired Power Plants in China

Coal production in China amounts to thousands of millions of tons each year, accounting for 40% of the world coal production. Around 50% of this amount of coal production is used in coal-fired power plants. Fig. 3.1 shows the trend of coal consumption in coal-fired power plants from 1990 to 2005 in China.

According to a survey of coal consumption among coal-fired power plants in China, out of the total coal used, washed coal accounted for only 8% of the total. More than 90% of the total coal-fired boilers widely used in China are pulverized coal burners. Of these, the four-corner burner is one of the most used burners in pulverized coal boilers. Since the mid-80s, ESP has been used instead of mechanical filters and cyclone separators, with a 4% – 5% increase in speed each year. Before 1996, ESP was about 63.3% of the total dust cleaning equipment, and the rest consisted of wet dust cleaning equipment. From 1996 to 2000, this increased to 86.3% and increased even further after 2000 to 95%. Almost all of the more than 300 MW coal-fired power plants are equipped with ESPs.

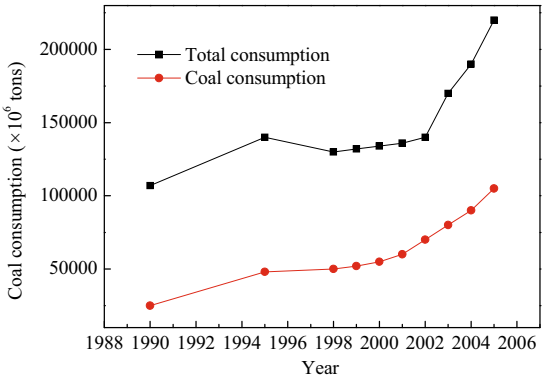

Fig. 3.1 Coal consumption of coal-fired power plants in China from 1990 to 2005

Before 2000, dust cleaning equipment was the only flue gas pollution-control device in coal-fired power plants in China. According to statistics, in 2000 flue gas desulfurization devices were installed to cover about 4,000 MW of power output, accounting for just 1% of the total installed capacity of coal-fired power plants in China. In 2005, the amount of new gas desulfurization devices increased to cover 104,000 MW of power output, which was more than the total of 46,000 MW recorded 10 years before. At the end of 2010, the amount of desulfurization reached 460,000 MW in China. At present, SCR has already started to be used for controlling the NO_x emissions in China.

Based on the flue gas cleaning devices recorded in 2002, coal-fired power plants could be divided into two types in China: one type was only equipped with ESP (about 88% of the total coal-fired power plants), and the other was equipped with ESP and WFGD (about 12% of the total).

According to the above analysis, the calculated mercury emissions into the atmosphere from 1990 to 2005 from coal-fired power plants in China are presented in Fig. 3.2. The comparison in the growth rate of coal consumption and mercury emissions from 1990 to 2005 of coal-fired power plants in China is shown in Fig. 3.3. Based on Figs. 3.2 and 3.3, the increment of mercury emissions from coal-fired power plants was not maintained at the same speed, which was similar to the trend in coal consumption from 1990 to 2005.

WFGD can remove great amounts of Hg^{2+} by washing. With the increasing use of WFGD, coal-fired power plants emitted lesser mercury per ton of coal consumption from 2003 to 2005 (Figs. 3.2 and 3.3). Mercury emissions from coal-fired plants reached 119.7, 134.3, and 150.6 tons in 2003, 2004 and 2005, respectively. With the assumption that the use of pollution devices was the same as in 2002, the mercury emissions would be 131.6, 147.6 and 165.1 tons in 2003, 2004 and 2005, respectively, which were 11.8, 13.3, and 14.5 tons more than those actual mercury emissions in 2003, 2004 and 2005. When SCR was used, WFGD removed more mercury because there was more Hg^{2+} existing in the tail of the flue gas.

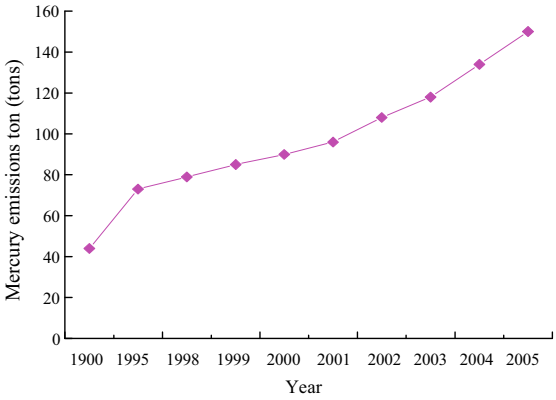

Fig. 3.2 Mercury emissions into the atmosphere from coal-fired power plants in China from 1990 to 2005

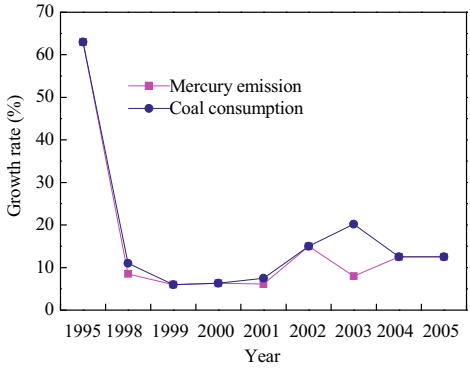

Fig. 3.3 Growth rate of coal consumption and mercury emissions of coal-fired power plants in China from 1990 to 2005

Table 3.2 compares the mercury emissions from coal-fired power plants in China, which was estimated by this study and other researchers. Mercury emissions in 1995, as estimated by this study, are closer to that estimated by Wang *et al.*[1]. However, estimation of mercury emissions in 1999, as reported by Streets *et al.*[2], was less than that recorded in the present work. Furthermore, Streets *et al.*[2] determined the EMF of ESP as 0.694, which was less than the value of 0.867 calculated in the current work. The estimated mercury concentration in coal of only 0.15 mg/kg in 2000, as reported by Jiang *et al.*[3], was also less than that recorded in the present study.

In 1999, the U.S. EPA estimated that 43 tons of mercury was emitted from 1149 units at 464 coal-fired power plants in the US. In that report, it was estimated that the amount of mercury emissions would reach 60 tons by 2010. Mercury emissions of coal-fired power plants in China nearly doubled those of the U.S in 1999, even exceeding those recorded in the U.S. in 2010.

Table 3.2 Mercury emissions estimated from coal-fired power plants in China (tons)

Year	Wang *et al*. (2006)	Jiang *et al*. (2005)	Streets *et al*. (2005)	This study
1995	72.86	-	-	73.4
1999	-	-	68	85.1
2000	-	76.83	-	90.5

3.4 The Future Development Trend Forecasts

Over the next decades, it is predicted that coal shall remain as the most important energy source in China. In addition, the proportion of coal consumed by the electric power industry to total coal consumption is predicted to increase from 48% in 2005 to 64% in 2020.

The proportion of washed coal to total coal used by coal-fired power plants in China from 1999 to 2004 decreased because of the increased cost of burning washed coal. However, the use of washed coal is predicted to increase in the future. Although the SCR device configuration of coal-fired power plants in China is small at present, it is estimated that the proportion of coal-fired power plants with SCR can reach 5% in 2010 and 10% in 2020. Coal-fired power plants in China in the future shall still be 100% equipped with ESP.

There are about 30% of coal-fired power plants that have been equipped with desulfurization equipment in China since 2006. It is predicted that the proportion of those equipped plants can reach 50% in 2010 and 70% in 2020. In general, coal-fired power plants with SCR configuration in China are also equipped with the desulfurization equipment. The total EMF of coal-fired power plants with simultaneous configurations of SCR, ESP and WFGD is only 0.124.

The mercury emissions from coal-fired power plants reached 161.3 and 172.2 tons in 2007 and 2008, respectively. Coal-fired power plants with WFGD comprised 50% of the total coal-fired power plants and those with SCR comprised 5% of the total in 2010. Mercury emissions from coal-fired power plants in 2010 reached 179.4 tons, although coal used in 2010 increased to 66.8 million tons compared with the amount used in 2008. In 2020, coal-fired power plants with WFGD reached 70% of total coal-fired power plants and those with SCR are expected to account for 10% of the total. Accordingly, mercury emissions from coal-fired power plants in 2020 are predicted to reach 207.0 tons.

Growth rates of coal consumption and mercury emissions of coal-fired power plants in China from 2005 to 2020 are shown in Fig. 3.4. The growth rate of mercury emissions was lower than that of coal consumption; the growth rate of mercury emissions was even negative in 2010 (Fig. 3.4). This indicated that active mercury pollution control measures can lessen the increase in mercury emissions, thus reducing environmental pollution.

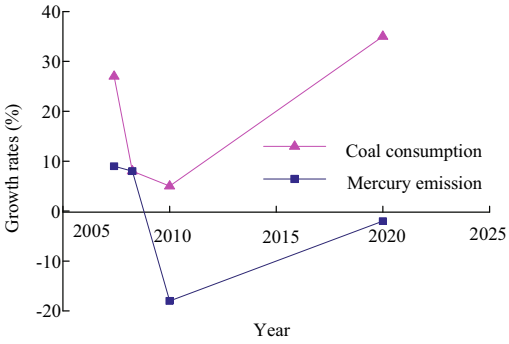

Fig. 3.4 Growth rates of coal consumption and mercury emissions of coal-fired power plants in China from 2005 to 2020

3.5 Summary

Estimating mercury emissions is the first step in understanding the current situation of mercury pollution in China, conducting research on mercury pollution control, and developing emission control methods. In this section, with a focus on the estimation of mercury emissions as well as data for coal consumption and various air pollution control facilities in China, we accurately estimated mercury emissions in recent years and made a prediction for the development of mercury control approaches in China.

From 2000 to 2002, the growth rate of mercury emissions from coal-fired power plants in China was estimated to have accelerated by 10%. From 2002 to 2005, the growth rate increased to 12%. Increased ESP could effectively reduce mercury emissions into the atmosphere. Moreover, desulfurization equipment WFGD could remove most of the mercury in an oxidized state by washing.

In 2007 and 2008, mercury emission of coal-fired power plants in China was predicted to reach 161.3 and 172.2 tons, respectively. By 2010, the proportion of FGD equipment would increase to 50%. Meanwhile, the SCR configuration increased from 1% in 2007 to 5% in 2008. Mercury emissions of all coal-fired power plants comprised only 179.4 tons. In 2020, the ratio of FGD equipment was expected to increase from 50% in 2010 to 70%, whereas the SCR equipment was expected to increase from 5% in 2010 to 10%. The mercury emissions of all coal-fired power plants could reach a total of 207.0 tons by that time.

Although coal consumption in thermal power plants was predicted to increase over the next decades, the controlled volume of mercury emissions of coal-fired power plants could offset the increased volume of coal consumption of thermal power plants, even leading to declining mercury emissions. This might be possible due to the increase in coal washing practice and the extensive use of flue gas cleaning devices. In the future, improvement in the proportion of coal after washing and the extensive use of flue gas control devices, including desulphurization and

denitrification equipment (e.g., FGD and SCR) in coal-fired power plants, could significantly reduce mercury emissions of coal-fired power plants in China.

References

[1] Wang Q.C., Shen W.G., Ma Z.W. The estimation of mercury emission from coal combustion in China. *China Enivronmental Science*, 19(4): 318-321, 1999.

[2] Streets D.G., Hao J.M., Wu Y. Anthropogenic mercury emissions in China. *Atmospheric Environment*, 39: 7789-7806, 2005.

[3] Jiang J.K., Hao J.M., Wu Y., Streets D.G., Duan L., Tian H.Z. Development of mercury emission inventory from coal combustion in China. *Environmental Science*, 26(2): 35-39, 2005.

4

Mercury Speciation Transformation During Coal Combustion

4.1 Introduction

During the coal combustion process and the cooling process of flue gas, mercury experiences a complex physical and chemical transformation. Various factors will affect the speciation distribution of mercury in flue gas. Such factors include the type of coal being used, temperature, reaction conditions, flue gas composition, fly ash composition, and so on.

Mercury is a volatile element, and mercury compounds in coal are thermally unstable. There is a special characteristic that when the temperature is higher than 700 °C, mercury compounds will be decomposed into Hg^0. In the coal combustion chamber where the temperature is usually more than 1,000 °C, almost all mercury compounds in coal, such as pyrite and cinnabar containing mercury, are converted to gaseous Hg^0.

When the temperature gradually decreases as the flue gas flows through the various heat transfer equipment, the Hg speciation continuously changes. Some gaseous Hg^0 are adsorbed by coal cinders or fly ash through several methods of physical adsorption, chemical absorption, and chemical reaction to form Hg^p, which may exist as a speciation of $HgCl_2$, HgO, $HgSO_4$, HgS, etc., on the surface of a particle. Some gaseous Hg^0 react with other flue gas components to form Hg^{2+} compounds when the flue gas temperature falls. Many researchers believe that chlorine containing substances play a key role in the process of Hg oxidation. The reaction between Hg^0 and Cl is usually considered as one of the main mechanisms for mercury transformation in the cooling flue gas. Gaseous Hg^{2+} in the flue gas is mostly considered to be $HgCl_2(g)$[1]. Some Hg^{2+} compounds are emitted as the gaseous form with the other flue gases. There is still some gaseous Hg^0 existing in the flue gas without changing speciation.

In this chapter we will describe in depth the mercury speciation transformation during coal combustion using different research methods. We mainly focus on the mercury emissions from coal of different combustion types, such as grate-firing,

suspension and fluidized-bed combustion; the research of the reaction kinetic model on mercury speciation transformation in flue gas; the equilibrium thermochemical analysis of mercury speciation transformation after coal combustion; and modeling research on mercury speciation transformation during coal combustion.

4.2 Mercury Emissions from Coal of Different Combustion Types

The mercury emission characteristics of pulverized coal using three general combustion methods (i.e., grate-firing, suspension, and fluidized-bed combustion methods) were studied using a quartz tube furnace, a small-scale pulverized coal furnace, and a medium-scale circulating fluidized-bed test. The speciation distribution of flue gas mercury was analyzed using the OH method.

4.2.1 Mercury Speciation during Coal Pyrolyzing and Burning in a Fixed Bed

Distribution of mercury speciation during coal pyrolysis and coal burning was researched. In the experiment, Changguang (CG) coal was chosen to analyse the mercury speciation distribution at different temperatures of 700, 900 and 1,200 °C during coal pyrolysis and burning, respectively.

As shown in Fig. 4.1, the Hg^0 concentration in the flue gas was reduced to 77% from 95% when the thermal pyrolysis temperature of coal increased from 700 to 1,200 °C. When coal burning, the Hg^0 concentration in the flue gas was reduced to 45% from 83% with the temperature increasing from 700 to 1,200 °C (Fig. 4.2). Hg^0 was the main speciation in both the above conditions. However, the Hg^0 concentration in pyrolyzing was higher than that in burning.

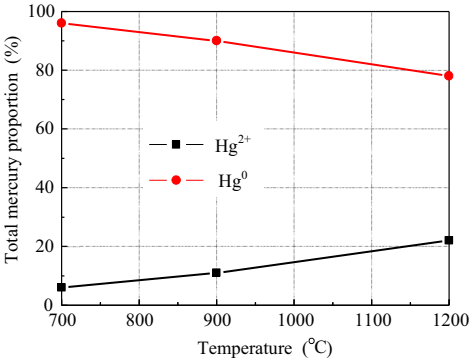

Fig. 4.1 Temperature influence on mercury speciation during coal pyrolyzing

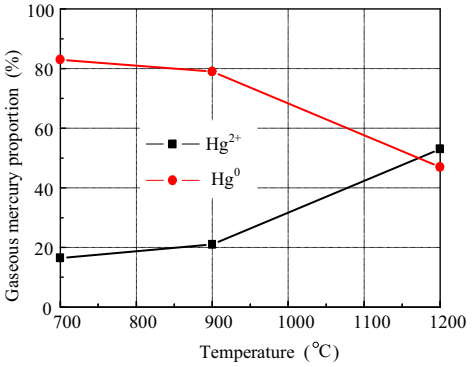

Fig. 4.2 Temperature influence on mercury speciation during coal burning

Fig. 4.3 shows the distribution of $Hg_{(g)}$ and Hg^p in flue gas when both Xinwen (XW) and CG pulverized coals were used as combustion as the layer condition in the quartz tube. The Hg^p speciation was about 20% of the total flue gas Hg. The remaining Hg was all $Hg_{(g)}$, and there was a little Hg in the ash. In the actual pulverized coal combustion flue gas, the Hg concentration in fly ash ranged between 23%–26% of the total Hg. The $Hg_{(g)}$ directly discharged into the atmosphere was in the range of 56%–69%. Future studies on mercury emissions during coal combustion should focus on the mercury speciation transformation law in the flue gas. At the same time, flue gas Hg control research should focus on the Hg direct discharge in the flue gas to the atmosphere.

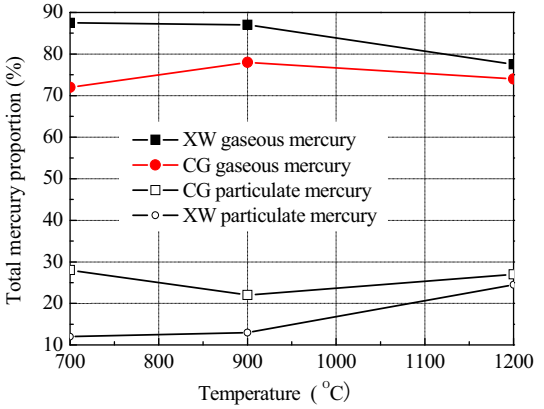

Fig. 4.3 Distribution of gaseous and Hg^p in burning coal sample

Typically, the Hg speciation distribution in flue gas of coal combustion is different from that of coal pyrolysis. As shown in Fig. 4.4 and Fig. 4.5, the Hg^0 concentration was less during coal combustion. As the combustion temperature increased, the Hg^0 concentration quickly decreased.

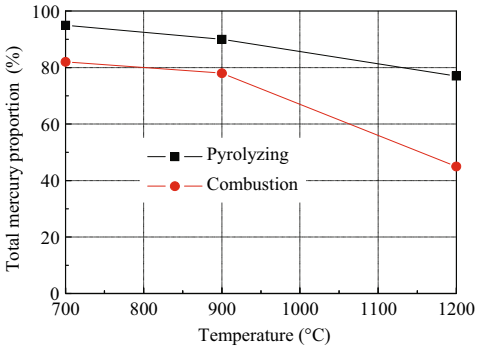

Fig. 4.4 Effect of temperature on Hg^0 during pyrolyzing and burning

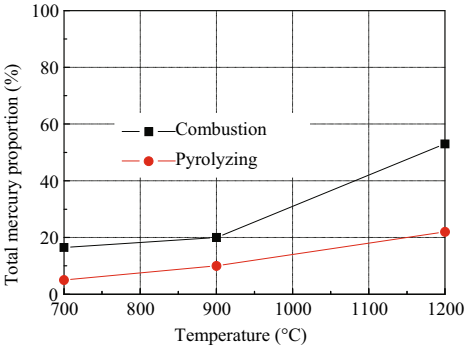

Fig. 4.5 Effect of temperature on Hg^{2+} during pyrolyzing and burning

During pyrolyzing, Hg^0 reaction functions with Cl from Cl_2 and HCl in flue gas were concluded as follows:

$$Hg^0_{(g)} + Cl_{2(g)} \rightarrow HgCl_{2(s,g)} \quad (4\text{-}1)$$

$$Hg^0_{(g)} + 2HCl_{(g)} \rightarrow HgCl_{2(s,g)} + H_{2(g)} \quad (4\text{-}2)$$

$$Hg^0 + Cl \rightarrow HgCl \quad (4\text{-}3)$$

$$HgCl + Cl \rightarrow HgCl_2 \quad (4\text{-}4)$$

$$HgCl + HCl \rightarrow HgCl_2 + H \quad (4\text{-}5)$$

$$HgCl + Cl_2 \rightarrow HgCl_2 + Cl \quad (4\text{-}6)$$

During burning, Hg^0 reaction functions in the flue gas were concluded as follows:

$$2Hg_{(g)} + O_2 \rightarrow 2HgO_{(s,g)} \quad (4\text{-}7)$$

$$2Hg^0_{(g)} + 4HCl_{(g)} + O_{2(g)} \rightarrow 2HgCl_{2(s,g)} + 2H_2O_{(g)} \quad (4\text{-}8)$$

$$4Hg^0_{(g)} + 4HCl_{(g)} + O_{2(g)} \rightarrow 4HgCl + 2H_2O_{(g)} \quad (4\text{-}9)$$

Both HgO and $HgCl_2$ generated in the reaction, Eqs. (4-7), (4-8) and (4-9), were compounds of Hg^{2+}. When the temperature reached more than 300 °C, the positive

reaction shown in Eq. (4-7) rapidly occurred. When the temperature reached over 400 °C, the reverse reaction shown in Eq. (4-7) rapidly occurred, and part of HgO decomposed into mercury and oxygen. The resultant HgCl in reaction Eq. (4-9) had an unstable form, which further occurred in reaction Eqs. (4-4), (4-5), and (4-6) to produce stabilized $HgCl_2$.

4.2.2 Mercury Speciation in Flue Gas When Coal Combustion Is in a State of Suspension

Yanzhou (YZ) and CG coals were used to study the mercury speciation in the suspension pulverized coal boiler at different temperatures of 1,300, 1,200, and 1,100 °C. The results showed that total $Hg_{(g)}$ (including Hg^{2+} and Hg^0) ranged from 10 to 15 μg/(N·m^3). The distributions of mercury speciation in the flue gas are shown in Figs. 4.6 and 4.7 when YZ and CG coals were burning, respectively. The speciation distributions of the $Hg_{(g)}$ of the YZ and CG coals were similar in that Hg^0 concentration was higher than Hg^{2+} concentration at different temperatures.

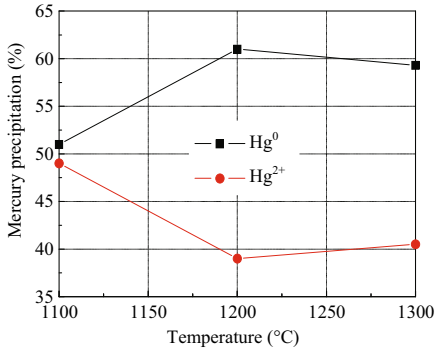

Fig. 4.6 $Hg_{(g)}$ speciation distribution of YZ coal combustion in a state of suspension

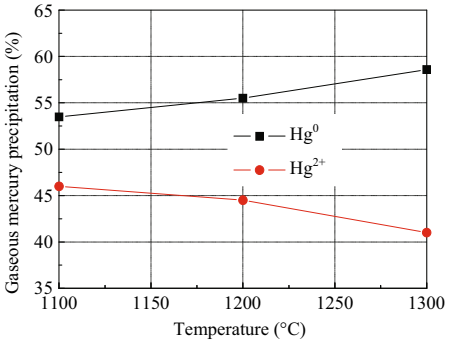

Fig. 4.7 $Hg_{(g)}$ speciation distribution of CG coal combustion in a state of suspension

Mercury in the flue gas included gaseous mercury and Hg^p. The latter was partly removed by dust collection devices. Carbon in fly ash had the ability to adsorb mercury, which mostly depended on the flue gas temperature, carbon concentration of fly ash, and surface properties, and so on. The finer fly-ash particles adsorbed more mercury on the surface. There was more than 90% of mercury that existed in the fly-ash particles whose size was less than 0.125 mm. The proportion of mercury entering the fly ash was about 27% for layer combustion and about 23% for pulverized coal suspension combustion. The ratio of mercury in the bottom ash was estimated to be about 20%. Fig. 4.8 shows the distribution of gaseous mercury and Hg^p in the flue gas of burning pulverized coal in suspension. The Hg^p and $Hg_{(g)}$ were about 20% and 80% of the total mercury, respectively, indicating that most mercury was emitted into the atmosphere in gaseous form.

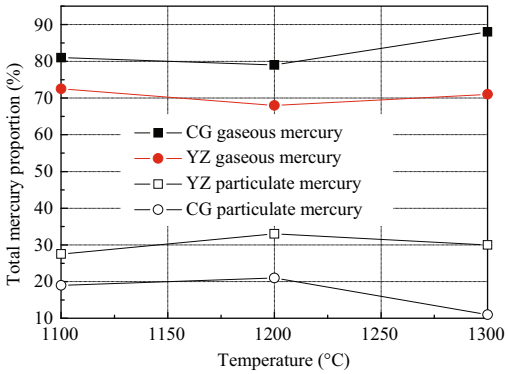

Fig. 4.8 Distribution of $Hg_{(g)}$ and Hg^p in flue gas when coal combustion is in a state of suspension

From the perspective of chemical reaction dynamics, the cooling rate of flue gas can affect the reaction between Hg^0 and other flue gas components. The combustion experiment was conducted at a temperature of 1,300 °C. Under the same conditions, the effect of the sampling cooling rate between a sampling point temperature of 415 °C and the solution adsorption point temperature of 125 °C in the Hg speciation distribution was also studied. The results are shown in Table 4.1.

Table 4.1 Effect of sampling cooling rate on the Hg speciation distribution

Experiments	Cooling rate (K/s)	Concentration (μg/(N·m^3))		Ratio (%)	
		Hg^{2+}	Hg^0	Hg^{2+}	Hg^0
No. 1	490	5.76	8.49	40	60
No. 2	360	6.77	6.68	50	60

During the two sampling processes, the sampling cooling rate changed by altering the distance between the sampling point and the solution adsorption point. Residence time was lengthy at the low sampling cooling rate, thus enhancing the opportunities for reactions between Hg^0 and other flue gas components and improving the oxidization from Hg^0 to Hg^{2+}.

Generally, the flue gas cooling rate and residence time in the cooling section have a significant effect on the measurement of mercury speciation in flue gas and the mercury emission control. During the measurement, for example, sampling in a high temperature area of flue gas, the sampling inlet temperature was high, and the sample gas was cooled during the transportation from the sampling pipe to the absorption bottle. Hg^0 in sampling gas could react with other flue gas components and could increase Hg^{2+}. Thus, the measurement results did not present the real Hg speciation situation at sampling points. To reduce the impact of flue gas cooling on the transformation of mercury speciation, the sample gas should be rapidly cooled to ice water temperature from the sampling points by some special means.

4.2.3 Mercury Speciation in Flue Gas When Coal Combustion Is in a Fluidized-Bed

Studies of the characteristics of mercury emissions from combustion of bituminous coal were conducted on a circulating fluidized-bed (CFB). The mercury concentrations in mixed coal and in flue gas from the CFB combustion were analyzed.

The coals used in the study included Huaibei bituminous (HB-B) coal, $2^{\#}$ bituminous ($2^{\#}$-B) coal, Chafei Stone (CF-S) coal and Qingping Stone (QP-S) coal, which were all crushed to a size of less than 10 mm. These samples were proportionately mixed according to the research requests. The impact of limestone on mercury emission was also studied. The sampling and analyzing of mercury concentration in the flue gas and ash was conducted in accordance with the OH method.

Table 4.2 lists the concentrations of Hg^{2+}, Hg^0, and total concentration of $Hg_{(g)}$ in the standard flue gas volume flow unit under different combustion conditions. The results show that the $Hg_{(g)}$ concentrations in the flue gas in each condition ranged from 6.8 to 9.3 $\mu g/(N \cdot m^3)$. All concentration values were less than 10 $\mu g/(N \cdot m^3)$.

Table 4.2 Hg speciation distribution in flue gas with combustion of four mixed coals in CFB respectively

Conditions	No. 1	No. 2	No. 3	No. 4
Mixing ratio of coal	QP-S 60% HB-B 40%	QP-S 60% HB-B 40% Limestone	CF-S 60% $2^{\#}$-B 40%	CF-S 60% $2^{\#}$-B 40% Limestone
Hg^{2+} ($\mu g/m^3$)	3.6	2.6	2.5	2.7
Hg^0 ($\mu g/m^3$)	5.2	4.2	5.3	6.6
total Hg ($\mu g/m^3$)	8.8	6.8	7.8	9.3

The proportions of Hg^{2+} and Hg^0 that accounted for the total $Hg_{(g)}$ in the flue gas under different combustion conditions are shown in Fig. 4.9 and Fig. 4.10, respectively. The proportion of Hg^{2+} to the $Hg_{(g)}$ in the flue gas ranged from 30% to 41%, whereas the proportion of Hg^0 ranged from 59% to 70%. The concentration of Hg^0 was about 20% higher than that of Hg^{2+} under conditions 1 and 2; however, the

concentration was about 30% higher under conditions 3 and 4. In the mixed combustion of QP-S coal and HB-B coal, the oxidation of Hg^0 in the flue gas was a little higher than that in the mixed combustion of CF-S coal and 2#-B coal, indicating a possible relationship to the types of coal.

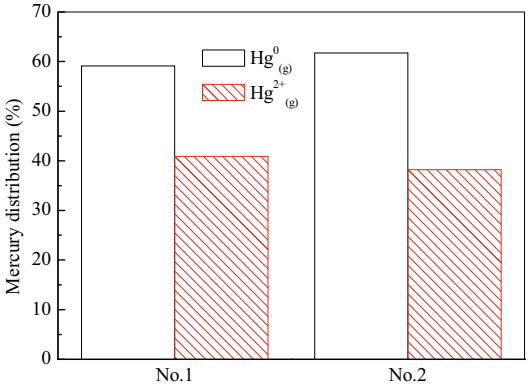

Fig. 4.9 Ratio of Hg^0 and Hg^{2+} in No. 1 and No. 2 conditions

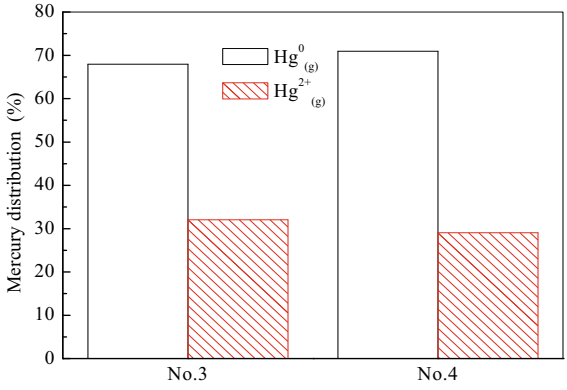

Fig. 4.10 Ratio of Hg^0 and Hg^{2+} in No. 3 and No. 4 conditions

The ratios of $Hg_{(g)}$ and Hg^p in different conditions are shown in Fig. 4.11 and Fig. 4.12, respectively. The mercury in the flue gas had two gaseous forms (Hg^{2+} and Hg^0) and Hg^p. The latter was the mercury in the fly-ash particles. The concentrations of $Hg_{(g)}$ and Hg^p were in the flue gas in a gas-solid two-phase. The ratio of $Hg_{(g)}$ in the total mercury ranged from 46% to 75%, whereas Hg^p in fly ash particles took up 59% – 70%. Overall, in No. 1 and No. 3 conditions, without limestone, the $Hg_{(g)}$ in the flue gas had a higher ratio at 68% and 75%, respectively; however, the proportion of Hg^p was lower. In No. 2 and No. 4 conditions, with limestone, the

$Hg_{(g)}$ in flue gas decreased greatly; however, the Hg^p concentrations in flue gas increased by 22% and 18%, respectively.

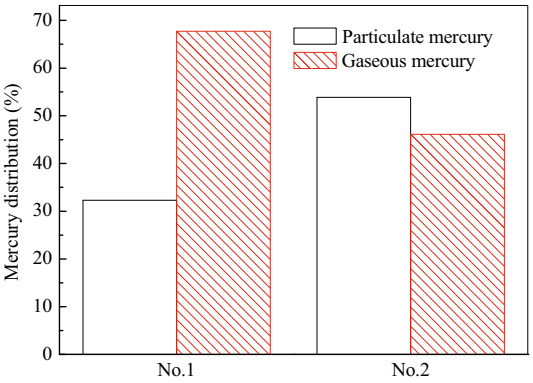

Fig. 4.11 Ratio of $Hg_{(g)}$ and Hg^p in No. 1 and No. 2 conditions

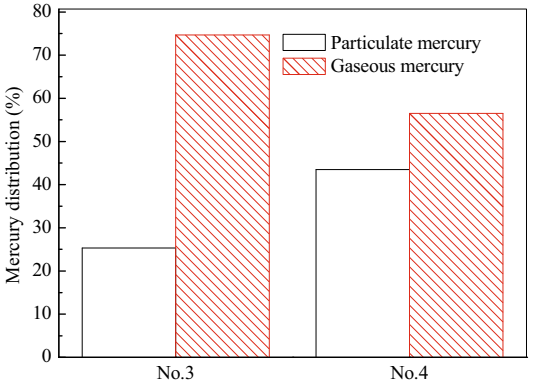

Fig. 4.12 Ratio of $Hg_{(g)}$ and Hg^p in No. 3 and No. 4 conditions

The mercury concentrations per unit mass (μg/g) in coal, fly ash, and bottom ash under different working conditions are presented in Table 4.3. Mercury concentrations in coal were 0.2977 and 0.3911 μg/g, respectively, and those in fly ash ranged within 0.2569 – 0.3315 μg/g. Meanwhile, the mercury concentration in the bottom ash ranged within 0.0192 – 0.0362 μg/g. The concentration of mercury in the bottom ash was much lower than that in coal because most of the mercury evaporated into gas at the high combustion temperature. Mercury concentration in the fly ash was much higher compared with the bottom ash, which was different from other major metal trace elements. This difference can be attributed to the relatively lower temperature environment of the tail flue gas. Mercury vapor condensed on, or was adsorbed by, the surface, thus increasing mercury concentration in the fly ash. The mercury concentration in the fly ash can potentially pollute water and soil.

Table 4.3 Ratios of mercury concentration in fly ash and bottom ash

Conditions	No. 1	No. 2	No. 3	No. 4
Mixing ratio of coal	QP-S 60% HB-B 40%	QP-S 60% HB-B 40% Limestone	CF-S 60% 2#-B 40%	CF-S 60% 2#-B 40% Limestone
Hg in coal (μg/g)	0.2977	0.2977	0.3911	0.3911
Hg in fly ash (μg/g)	0.2719	0.2569	0.3315	0.3124
Hg in bottom ash (μg/g)	0.0215	0.0320	0.0192	0.0362

CFB has received great attention since its introduction as a novel clean coal combustion technology in the 1970s. CFB can realize high efficiency from various flues during burning at low temperature, especially of low-quality and high-sulfur coal. It can attain desulfurization using cheap and easy methods with the limestone during burning and can reach 90% desulfurization efficiency, making it an efficient low-pollution power generation technology. This section is focused on the impact of limestone on mercury emission.

Fig. 4.13 and Fig. 4.14 show the ratios of the mercury concentrations in flue gas, fly ash and bottom ash before and after the addition of limestone, respectively. Adding limestone changed the proportion of mercury in the bottom ash, fly ash, and flue gas. The addition adjusted the proportion of $Hg_{(g)}$ in flue gas, thus reducing the $Hg_{(g)}$. For example, burning of QP-S coal mixed with HB-B coal reduced the $Hg_{(g)}$ from 66% to 43% after limestone addition. Burning of CF-S coal mixed with $2^{\#}$-B coal reduced $Hg_{(g)}$ in the flue gas from 71% to 52%. However, the Hg^p concentration in the fly ash increased slightly. For example, in conditions 1 and 2, the mercury concentrations in fly-ash increased nearly 20% after limestone addition, whereas in conditions 3 and 4, the mercury concentrations in fly ash increased to 16%. The mercury concentration in the bottom ash also slightly increased, but the proportion of mercury concentration in the bottom ash was low, which ranged within 3%–8%. Nearly 90% of mercury existed in the flue gas (including $Hg_{(g)}$ and Hg^p in fly ash). According to historical statistics, the ratio of the mercury concentration in fly ash was about 20% of that in coal, which value was higher than that in this report. The reason was that the proportion of stone coal was larger, and the ash in stone coal was very high (more than 70% in mass), which also caused a large concentration of fly ash in the flue gas. As a result, the chance of contact between the fly ash's surface and $Hg_{(g)}$ increased to form the Hg^p. The $Hg_{(g)}$ in the flue gas was partially transferred and adsorbed into the fly ash. The addition of limestone had changed the distribution ratio of mercury in gas and moved it in the direction of forming Hg^p, which was easy to be captured by a particle collection device.

After adding limestone, the mercury concentration in fly ash increased significantly, which indicated that limestone could help in controlling $Hg_{(g)}$ emission in an easy way to transform to Hg^p. Generally, limestone reduced the free $Hg_{(g)}$ in the atmosphere, which was useful in the purification of the environment. However, at the same time, mercury was transformed to solid ash, which might be potentially dangerous on the environment depending on the stability of mercury in the ash. One way of trying to deal with fly ash and bottom ash was to grind the ash into cement to form a block. By checking the experiment, the released mercury proved to be very small.

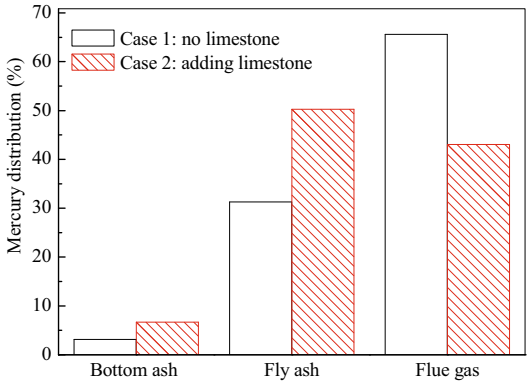

Fig. 4.13 Ratio of Hg in different ashes in No. 1 and No. 2 conditions

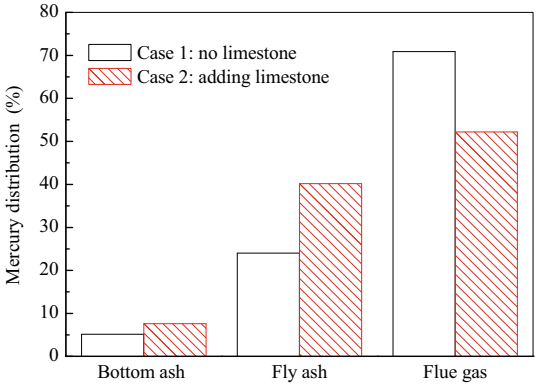

Fig. 4.14 Ratio of Hg in different ashes in No. 3 and No. 4 conditions

4.2.4 Mercury Emission in Different Combustion Types

By heating coal in a fixed quartz tube furnace, the behavior of mercury emission was checked. In the pulverized coal boiler and circulating fluidized-bed bench tests, the transformation of mercury speciation from coal in the two combustion types of suspension combustion and fluidized-bed combustion were also studied.

4.2.4.1 Ratio of Hg(g) and Hg^p in Flue Gas

The ratios of $Hg_{(g)}$ and Hg^p in flue gas with three combustion methods are shown in Figs. 4.15 and 4.16. The data in the figures were treated as the average values based on all experimental conditions. From the experimental results of coal burning in a fixed bed and a state of suspension, the ratios of $Hg_{(g)}$ and Hg^p were found to be similar. The proportion of $Hg_{(g)}$ was about 80% of total mercury in the fluidized-bed

combustion method, because stone-coal comprised 60% of the mixed coal. The mercury concentration in the stone-coal was more than that in other coal. As a result, the proportion of Hg^p in the total mercury increased. The proportion of $Hg_{(g)}$ comprising the total flue gas mercury content was in the range of 46%–75%, and the average was 62%. The proportion of Hg^p was 25%–54%, and the average was 39%. The ratio of $Hg_{(g)}$, Hg^p in the flue gas from the three different combustion methods indicated that $Hg_{(g)}$ was the main speciation emission when coal was fired.

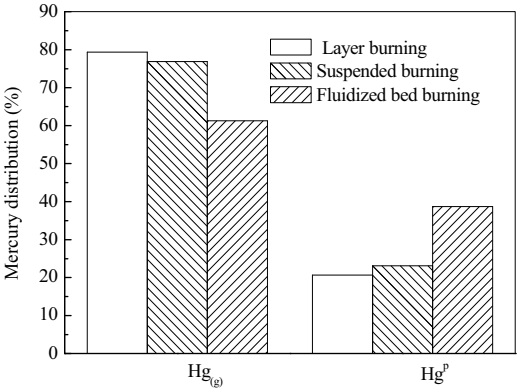

Fig. 4.15 Ratio of $Hg_{(g)}$ and Hg^p with different combustion methods

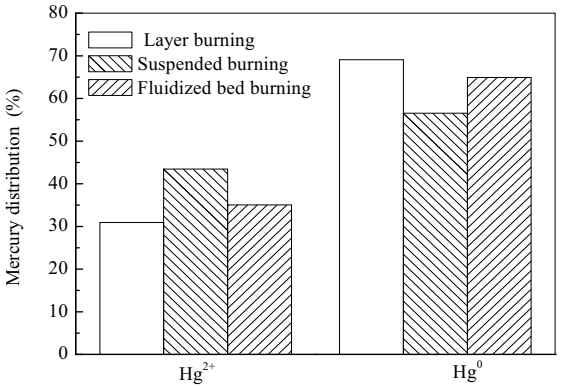

Fig. 4.16 Ratio of Hg^0 and Hg^{2+} with different combustion methods

4.2.4.2 Ratios of Hg^{2+} and Hg^0 in $Hg_{(g)}$

The ratios of Hg^{2+} and Hg^0 in $Hg_{(g)}$ using three combustion methods are shown in Fig. 4.16. The data in Fig. 4.16 were the average results of all experimental conditions. In the experiment of coal burning in a fixed bed, the Hg^0 concentration in flue gas decreased gradually, whereas Hg^{2+} concentration increased gradually when the temperature increased. When coal burned at different temperatures, the character-

istics of mercury emissions were very similar. However, there were some differences. The proportion of Hg^{2+} in the total $Hg_{(g)}$ was from 17% to 54%, and the average proportion was 69%. The proportion of Hg^0 was from 46% to 83%, and the average proportion was 31%.

When pulverized coal burned in a state of suspension, the proportion of Hg^{2+} in the total $Hg_{(g)}$ was from 40% to 50%, and the average was 44%. That of Hg^0 was from 50% to 60%, and the average was 56%. The total $Hg_{(g)}$ concentrations in flue gas were in the range of 10 – 15 μg/(N·m^3).

In the fluidized-bed combustion, the proportion of Hg^{2+} in the total $Hg_{(g)}$ was from 30% to 41%, and the average was 35%. The proportion of Hg^0 in the total $Hg_{(g)}$ was from 59% to 70%, and the average was 65%. The $Hg_{(g)}$ concentrations in all conditions of flue gas were in the range of 6.8 – 9.3 μg/(N·m^3), and less than 10 μg/(N·m^3).

Given the conditions of the three different combustion methods, the speciation distributions of Hg^{2+} and Hg^0 were similar. Coal burning in a fixed bed increased the Hg^0 concentration, which may be attributed to the shorter gas cooling process and the shorter reaction time in the experiment. The concentration of $Hg_{(g)}$, when using the fluidized-bed combustion method, was slightly lower than that when using the suspension combustion method. This may be attributed to the high proportion of burning stone coal, the addition of limestone in some conditions, and the high concentration of fly ash. These factors enhanced the mercury adsorption by particles, thus reducing the concentration of $Hg_{(g)}$.

4.3 Research on Reaction Kinetics of Mercury Speciation Transformation in Flue Gas

Mercury is an extremely volatile element. Most mercury compounds are thermally unstable and tend to decompose into Hg^0 when the temperature is higher than 700 °C. At temperatures of coal combustion, almost all the mercury is converted into Hg^0 in the boiler. Therefore, during the coal burning, mercury is converted into gaseous Hg^0 and flows into the flue gas regardless of its original classification (organically or inorganically combining state). During the cooling process, the temperature of flue gas gradually decreased when the gas passed through the heat transmission equipment. Gaseous mercury underwent a more complicated physical and chemical reaction with other flue gas components . Finally, Hg^0 usually existed in all three forms, namely, Hg^0, Hg^{2+} and Hg^p.

The Hg^{2+} in flue gas was mainly the result of the reaction between chlorine-containing substances (e.g., Cl_2, HCl, and Cl) and mercury. Therefore, the mercury speciation in flue gas mainly was $HgCl_2$. And mercury also reacted with O_2, SO_x, and NO_x to produce HgO, $HgSO_4$, and so on. The research on the oxidation process of mercury in flue gas must consider the effect of the gas components, such

as the O_2 concentration in flue gas ranged from 4%–10%, that of SO_2 ranged from 100–2,000 ppm, and that of NO ranged from 100–1,000 ppm.

In this section, the reaction kinetic model was established and used to study the factors that affect the mercury species distribution in typical coal-fired flue gas, to understand the reaction mechanism of mercury in flue gas and to provide a beneficial reference for mercury control methods.

4.3.1 Reaction Kinetic Model of Mercury and HCl in Coal-Fired Flue Gas

4.3.1.1 Transformation and Formation Mechanisms of Mercury in Coal-Fired Flue Gas

For better understanding the mercury transformation, the reaction kinetics mechanism of mercury should be clarified. Most studies about mercury reaction kinetics during coal combustion focused on the mechanism of mercury transformation in vapor using heat balance calculations. Although this approach could primarily estimate the main mercury speciation distribution in a coal-fired system under equilibrium, in practice the system is rarely balanced. Therefore, to understand the main reaction methods and illustrate accurately the concentrations of mercury reaction compounds in the system, kinetics experiments must be conducted in a coal-fired system. The description of the chemical kinetic mechanism is based on a comprehensive and accurate understanding of mercury and its different components and their elementary reaction kinetic parameters. This work is difficult.

Studies on the model establishing mercury oxidation have been conducted widely. Carpi studied the chemical form transformation of mercury emissions during the combustion process[2]. Widmer and West[3] proposed a two-step mechanism-based kinetic mechanism of mercury oxidation as the following Eq. (4-10). The model contained eight core elementary reactions, as shown in Table 4.4. The parameters were solved according to the modified Arrhenius Eq. (4-11). The model assumed that all reactions were reversible, and Arrhenius parameters were estimated using different methods. Almost all of the reactions involved those between radicals and molecular components, thus indicating that pre-exponential factors were close to the collision limit. Widmer and West[3] estimated the second and third activation energy E_a in the estimate sheet, and directly substituted the enthalpy value as the initial value because of the lack of relevant kinetic data, thus obtaining the coarse kinetic parameters of elementary reaction. This estimation often led to inconsistent collision frequency and a reaction constant.

$$\mathrm{Hg} \longrightarrow \mathrm{HgCl} \longrightarrow \mathrm{HgCl_2} \tag{4-10}$$

$$k = k_0 \cdot T^{\beta} \cdot \mathrm{e}^{-E_a/RT} \tag{4-11}$$

In Eq. (4-11), k_0 is the pre-exponential factor, β is the temperature index, and E_a is the activation energy.

Table 4.4 Kinetic mechanism of mercury oxidation

Reaction	k_0 (moles·cm^3·s)	β	E_a (cal/mol)
Hg+Cl+M=HgCl+M	9.00E+15	0.5	0
Hg+Cl_2=HgCl+Cl	1.39E+14	0	34000
Hg+HCl=HgCl+H	4.94E+14	0	79300
Hg+HOCl=HgCl+OH	4.27E+13	0	19000
HgCl+Cl_2=$HgCl_2$+Cl	1.39E+14	0	1000
HgCl+Cl+M=$HgCl_2$+M	1.16E+15	0.5	0
HgCl+HCl=$HgCl_2$+H	4.64E+03	2.5	19100
HgCl+HOCl=$HgCl_2$+OH	4.27E+13	0	1000

Lee[4] applied online analysis technology to study mercury reaction kinetics with the presence of chlorine-containing substances, obtaining an order of reaction of 1.55, an activation energy of 16.13 (kJ/mol), and a reaction rate constant of $5.07\times10^{-2}\exp(-1939.68/T)$ $[(\mu g/m^3)^{-0.55}\cdot s^{-1}]$. However, the quantitative impact of chlorine-containing substances on the reaction was not explored. Moreover, titanium-based catalysts were used in the reaction, which was quite different from actual flue gas. Dunham *et al.*[5] proposed a more comprehensive overview of mercury transformation into kinetics and analyzed kinetic models of homogeneous and heterogeneous reactions through comparisons using experiments. Sliger *et al.*[6] discussed the issue from the experimental and theoretical aspects.

Niksa[7] applied the homogeneous kinetics method to theoretically predict the importance of nitric oxide and water for mercury oxidation in coal-fired flue gas. Liu *et al.*[8] applied quantum chemistry to study the reaction mechanism of mercury and chlorine gas starting from the initiation of coal combustion. After the optimization, the reactants, transition states, intermediates and geometry of products were determined. Zheng also calculated the activation energy and heat effect on the reaction.

Studies on the oxidation of mercury in simulated flue gas have been conducted. Mamani-Paco *et al.*[9] studied the impact of the simultaneous presence of HCl and Cl_2 on mercury oxidation through experiments. In the experiments, the concentration of mercury was 50 μg/m^3. The experimental results showed that when the Cl_2 concentration was 50 ppm, 7% to 10% of the mercury was oxidized, when the Cl_2 concentration was 100 ppm, 36% to 45% of the mercury was oxidized, and when the Cl_2 concentration was 300 ppm, 66% to 69% of the mercury was oxidized. On the other hand, when HCl was added, the overall concentration of Cl_2 increased, but the oxidation rate of mercury was not significantly different from that with only the presence of Cl_2 at 50 ppm.

Dajnak and Lockwood[10] explored the transformation mechanism of mercury during combustion and summarized the possible oxidation and reduction reactions of mercury-containing substances during the combustion process (Tables 4.5 and 4.6).

Table 4.5 Possible oxidizing reactions of mercury in the coal combustion

$2Hg^0_{(g)} + 4HCl_{(g)} + O_{2\ (g)} \rightarrow 2HgCl_{2(g,s)} + 2H_2O$
$Hg^0_{(g)} + HCl_{(g)} \rightarrow$ Oxidized Products
$Hg^0_{(g)} + Cl_{2(g)} \rightarrow HgCl_{2(g,s)}$
$Hg^0_{(g)} + Cl_{(g)} \rightarrow HgCl_{(g)}$
$HgCl_{(g)} + Cl_{2(g)} \rightarrow HgCl_{2(g)}$
$HgCl_{(g)} + Cl_{(g)} \rightarrow HgCl_{2(g)}$
$HgCl_{(g)} + HCl_{(g)} \rightarrow HgCl_{2(g)}$
$2Hg^0_{(g,ads)} + O_{2(g,ads)} \rightarrow 2HgO_{(g,s)}$
$Hg^0_{(g)} + NO_{2(g)} \rightarrow HgO_{2(g,s)} + NO_{(g)}$
$Hg^0_{(s,g)} + NO_{(g)} \rightarrow HgO_{(s,g)}$

Table 4.6 Possible reduction reactions of mercury in the coal combustion

$HgO_{(s,g)} + SO_{2\ (g)} \rightarrow Hg^0_{(g)} + SO_{3(g)}$
$HgO_{(s,g)} + NO_{(g)} \rightarrow Hg^0_{(g)} + NO_{(g)}$
$HgO_{(s,g)} + CO_{(g)} \rightarrow Hg^0_{(g)} + CO_{2(g)}$
$HgCl_{(s,g)} + Cl_{(g)} \rightarrow Hg^0_{(g)} + Cl_{2(g)}$
$HgCl_{2(s,g)} + SO_{2(g)} \rightarrow Hg^0_{(g)} + SO_2Cl_{2(g)}$

Based on previous studies, various factors were taken into consideration and quantitative forecasting of major influencing factors was conducted. The apparent reaction kinetic model of the combination of mercury and HCl was established through experiments.

4.3.1.2 Establishment of the Kinetic Model

The mercury oxidization in coal-fired flue gas was main the result of the reaction between the chlorine-containing substance and mercury. Therefore, the Hg^{2+} in the flue gas was generally believed to be mainly $HgCl_2$. The direct reaction of HCl and mercury that generates $HgCl_2$ could be expressed as follows:

$$Hg^0(g) + 2HCl(g) \rightarrow HgCl_2(g) + H_2(g) \tag{4-12}$$

Thermodynamic calculations showed that the above reaction had a high energy barrier. At a temperature below 600 K, the reaction was very slow, and the direct reaction between mercury and HCl was restricted. No clear pathway of reaction was found, and there may be multiple elementary reactions. Theoretical and experimental studies[11] had shown that chlorine molecules (Cl_2) and chlorine atoms (Cl) were very active chloride media, and the following reaction pathways were proposed:

Pathway 1: $$Hg^0(g) + Cl_2(g) \rightarrow HgCl_2(g,s) \tag{4-13}$$

Pathway 2: $$Hg^0(g) + Cl(g) \rightarrow HgCl(s,g) \tag{4-14}$$

$$HgCl(s,g) + HCl(g) \rightarrow HgCl_2(s,g) + H \tag{4-15}$$

In Pathway 1, the formation of gaseous Cl_2 might be limited by reaction kinetics, and the generated Cl_2 was very small in quantity, making the approach inappropriate as a principal pathway of Hg^{2+} in flue gas[12]. In addition, the mercury oxidation reaction was accelerated with increasing temperature, which was also incompatible with the pathway because the concentration of Cl_2 decreases as the temperature increases. Senior and Morency[13] calculated that in the exterior of air pollution control devices (at about 24 to 190 °C), only about 1% of Cl turns into Cl_2. Moreover, at low temperatures and with a few particles, Cl_2 could be catalyzed by the following process:

$$2HCl+½O_2 \rightarrow Cl_2+H_2O \tag{4-16}$$

In Pathway 2, Cl was generated because radicals attack the HCl molecules and could be expressed as follows:

$$HCl+OH\cdot \rightarrow Cl+H_2O \tag{4-17}$$

According to thermodynamic principle, the above reaction could be conducted at higher temperatures. Cl might be the main substance for the oxidation of Hg^0 in flue gas. Pathway 2 might be the principal pathway of mercury oxidation.

The mercury oxidation reaction contained several elementary reactions, the existence of which could not be clarified by quantitative studies, making kinetics studies of the oxidation of mercury very difficult. However, kinetic parameters could be calculated using some simplest expressions. Based on the above discussion, the following formula was adopted:

$$3Hg+4HCl \rightarrow 2HgCl+HgCl_2+2H_2 \tag{4-18}$$

Based on the above mentioned formula, in the presence of HCl, the total reaction rate in the homogeneous gas-phase oxidation of mercury could be expressed as follows:

$$\frac{dC_{Hg}}{dt} = -k \times C_{Hg}{}^{\alpha} \times C_{HCl}{}^{\beta} \tag{4-19}$$

where C_{Hg} is the concentration of Hg^0 in simulated flue gas; C_{HCl} is the concentration of HCl in simulated flue gas; k is the total reaction rate constant; α is the reaction order relevant to the concentration of Hg^0 in simulated flue gas; and β is the reaction order relevant to the concentration of HCl in simulated flue gas.

In all experiments, C_{HCl} was excessive relative to C_{Hg} in the reaction Eq. (4-18). In the reaction process, the oxidation reaction of mercury turned into a pseudo α-level reaction. In this case, Eq. (4-19) became:

$$\frac{\mathrm{d}C_{Hg}}{\mathrm{d}t} = -k_1 \times C_{\mathrm{Hg}}{}^{\alpha} \tag{4-20}$$

where

$$k_1 = k \times C_{\mathrm{HCl}}{}^{\beta} \tag{4-21}$$

Natural logarithms were substituted on both sides, and the following formula was derived:

$$\ln\left(-\frac{\mathrm{d}C_{\mathrm{Hg}}}{\mathrm{d}t}\right) = \ln k_1 + \alpha \times \ln C_{\mathrm{Hg}} \tag{4-22}$$

Thus, a straight line could be drawn from $\ln\left(-\frac{\mathrm{d}C_{\mathrm{Hg}}}{\mathrm{d}t}\right)$ to $\ln C_{\mathrm{Hg}}$. And α could thus be obtained from the slope of the line. Also, k_1 could be obtained from the linear intercept. In order to obtain the dependence of the reaction rate on HCl, natural logarithms were substituted on both sides of Eq. (4-21) as follows:

$$\ln k_1 = \ln k + \beta \ln C_{\mathrm{HCl}} \tag{4-23}$$

During the experiment, with excessive HCl concentration, it was changed to obtain the values of $k_1 \sim C_{\mathrm{HCl}}$. A line could be drawn from $\ln k_1$ to $\ln C_{\mathrm{HCl}}$. Then, β could be obtained from the slope, and k could be obtained from the linear intercept. This approach was shown in the literature.

The overall reaction rate constant could be expressed using the Arrhenius formula as follows:

$$k = A\exp(-E_a / RT) \tag{4-24}$$

where E_a is the energy activation; A is the preexponential factor; R is the gas constant; and T is the gas temperature.

Natural logarithms were substituted on both sides and the following expression was derived:

$$\ln k = \ln A - \frac{E_a}{R} \times \frac{1}{T} \tag{4-25}$$

A line could be drawn from $\ln k$ to $1/T$ to obtain the energy activation E_a and the pre-exponential factor A of the adsorption reaction.

1) Reaction order α

Based on the kinetic model established in this section, the simulated flue gas in the experiment was close to that of the actual gas. It was because the oxidation of mercury in flue gas was mainly the reaction of Hg^0 with chlorine-containing substances, but also was affected by the other components. In the experiment, the HCl concentration and reaction temperatures were changed. Mercury reaction kinetic experiments in the simulated flue gas were conducted under experimental conditions as shown in Table 4.7.

Table 4.7 The simulated flue gas in the kinetic experiments

Name	Composition
O_2	7%
CO_2	13%
SO_2	1200 ppm
NO	800 ppm
HCl	20, 40, 60, 80, and 100 ppm
Hg	6.478 μg/m^3
N_2	Equilibrium gas
T	373, 573, 773, 973, and 1173 K

Mercury concentrations were measured for different flue gas components, including the HCl concentration, reaction temperature and residence time. Based on the experimental results, the reaction rates were obtained for different situations. Then, according to Eq. (4-22), a straight line could be drawn from the logarithm of the reaction rate to that of the mercury concentration. α could be obtained from the slope, and k_1 could be obtained from the linear intercept. The reaction rate constant at a given HCl concentration and reaction temperature, as well as the simulation results of the reaction order, are shown in Figs. 4.17 to 4.41, respectively.

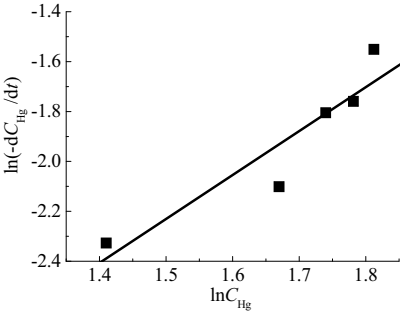

Fig. 4.17 α and K_1 when C_{HCl}=20 ppm and T=373 K (α=1.762; K_1=0.00765; r^2=0.931)

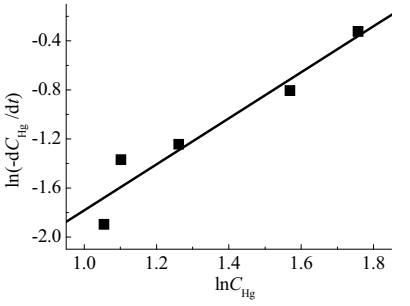

Fig. 4.18 α and K_1 when C_{HCl}=20 ppm and T=573 K (α=1.876; K_1=0.0258; r^2=0.961)

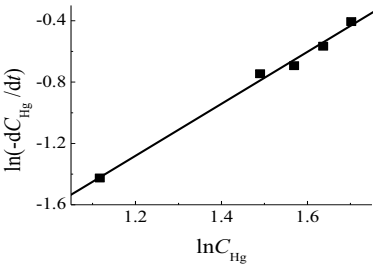

Fig. 4.19 α and K_1 when C_{HCl}=20 ppm and T=773 K (α=1.694; K_1=0.0364; r^2=0.996)

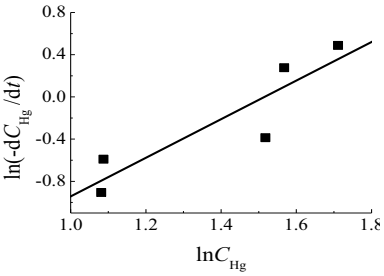

Fig. 4.20 α and K_1 when C_{HCl}=20 ppm and T=973 K (α=1.83; K_1=0.0624; r^2=0.904)

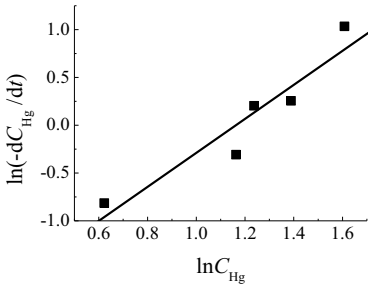

Fig. 4.21 α and K_1 when C_{HCl}=20 ppm and T=1173 K (α=1.779; K_1=0.1264; r^2=0.946)

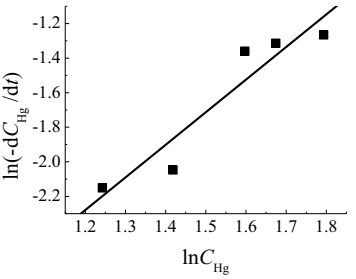

Fig. 4.22 α and K_1 when C_{HCl}=40 ppm and T=373 K (α=1.886; K_1=0.0107; r^2=0.945)

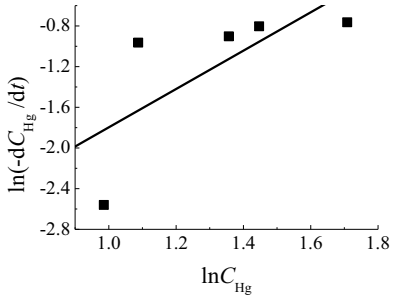

Fig. 4.23 α and K_1 when C_{HCl}=40 ppm and T=573 K (α=1.886; K_1=0.02514; r^2=0.713)

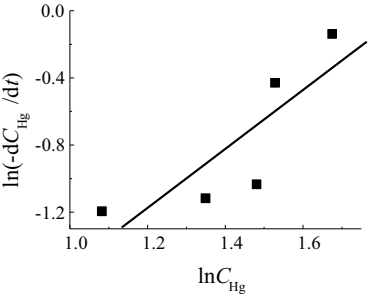

Fig. 4.24 α and K_1 when C_{HCl}=40 ppm and T=773 K (α=1.756; K_1=0.03759; r^2=0.834)

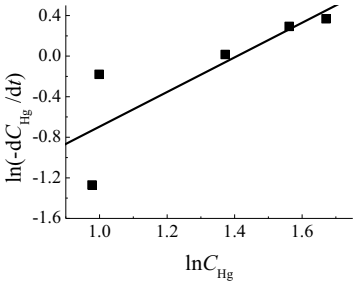

Fig. 4.25 α and K_1 when C_{HCl}=40 ppm and T=973 K (α=1.707; K_1=0.09049; r^2=0.821)

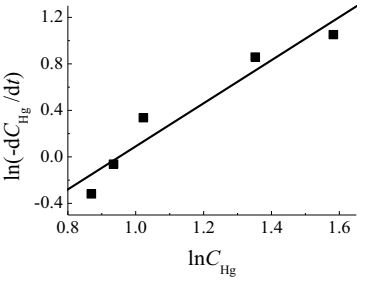

Fig. 4.26 α and K_1 when C_{HCl}=40 ppm and T=1173 K (α=1.853; K_1=0.1715; r^2=0.964)

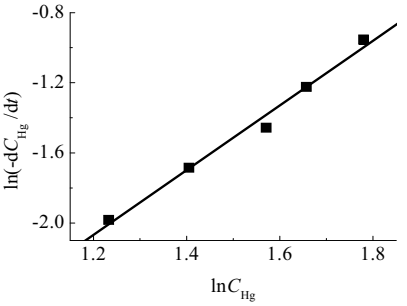

Fig. 4.27 α and K_1 when C_{HCl}=60 ppm and T=373 K (α=1.847; K_1=0.01378; r^2=0.994)

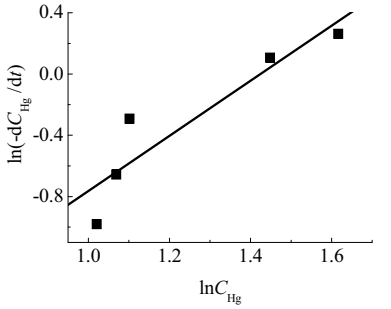

Fig. 4.28 α and K_1 when C_{HCl}=60 ppm and T=573 K (α=1.8; K_1=0.07694; r^2=0.923)

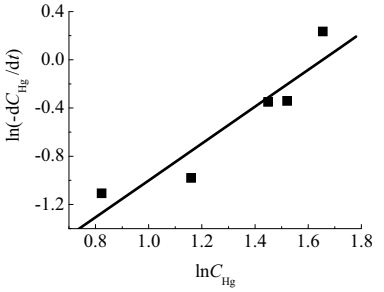

Fig. 4.29 α and K_1 when C_{HCl}=60 ppm and T=773 K (α=1.531; K_1=0.07951; r^2=0.934)

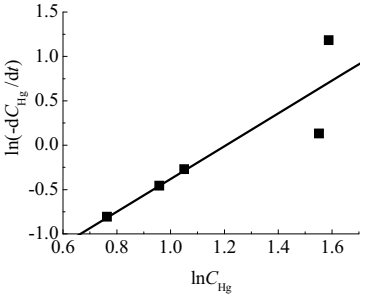

Fig. 4.30 α and K_1 when C_{HCl}=60 ppm and T=973 K (α=1.85; K_1=0.1078; r^2=0.8901)

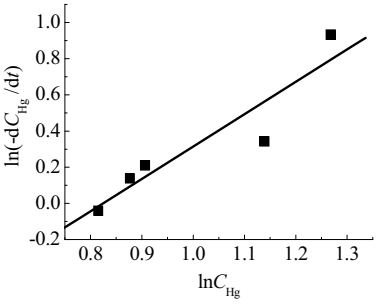

Fig. 4.31 α and K_1 when C_{HCl}=60 ppm and T=1173 K (α=1.789; K_1=0.2290; r^2=0.931)

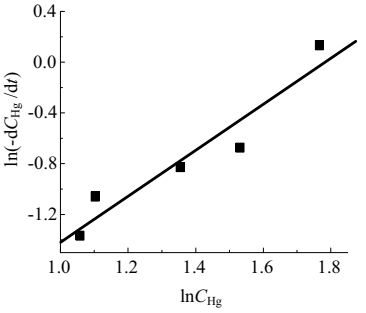

Fig. 4.32 α and K_1 when C_{HCl}=80 ppm and T=373 K (α=1.814; K_1=0.03939; r^2=0.956)

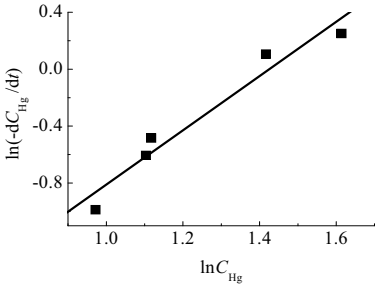

Fig. 4.33 α and K_1 when C_{HCl}=80 ppm and T=573 K (α=1.91; K_1=0.066; r^2=0.975)

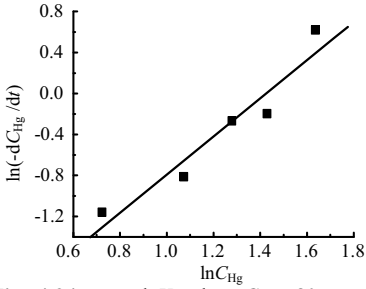

Fig. 4.34 α and K_1 when C_{HCl}=80 ppm and T=773 K (α=1.86; K_1=0.07024; r^2=0.961)

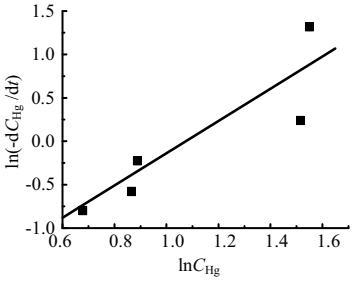

Fig. 4.35 α and K_1 when C_{HCl}=80 ppm and T=973 K (α=1.86; K_1=0.1280; r^2=0.894)

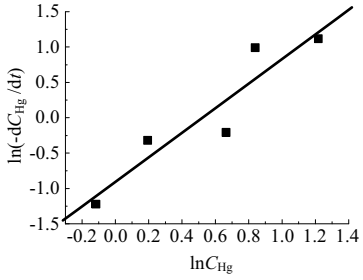

Fig. 4.36 α and K_1 when C_{HCl}=80 ppm and T=1173 K (α=1.74; K_1=0.4034; r^2=0.935)

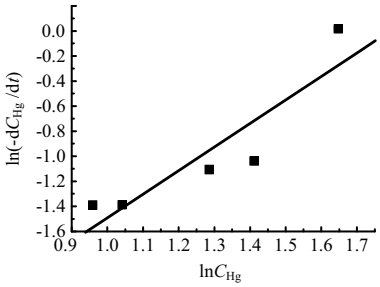

Fig. 4.37 α and K_1 when C_{HCl}=100 ppm and T=373 K (α=1.88; K_1=0.03434; r^2=0.905)

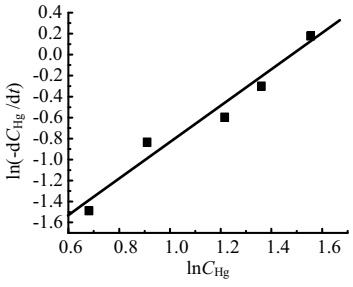

Fig. 4.38 α and K_1 when C_{HCl}=100 ppm and T=573 K (α=1.74; K_1=0.0743; r^2=0.98)

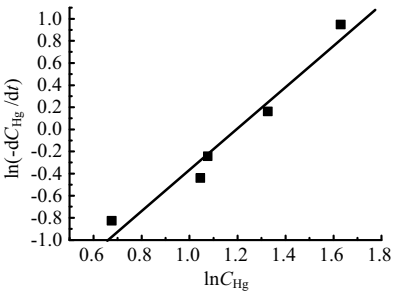

Fig. 4.39 α and K_1 when C_{HCl}=100 ppm and T=773 K (α=1.87; K_1=0.1073; r^2=0.98)

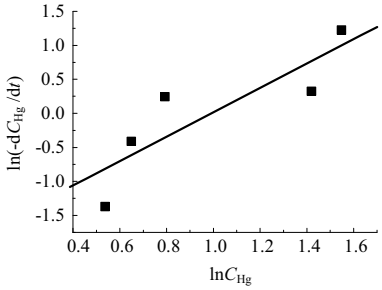

Fig. 4.40 α and K_1 when C_{HCl}=100 ppm and T=973 K (α=1.79; K_1=0.1691; r^2=0.86)

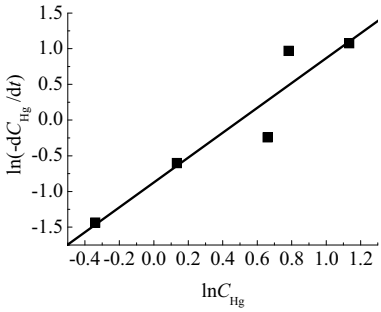

Fig. 4.41 α and K_1 when C_{HCl}=100 ppm and T=1173 K (α=1.74; K_1=0.4173; r^2=0.943)

From the simulation results shown in Figs. 4.17 to 4.41, the value of α was between 1.53 and 1.91, and the average was 1.78. This value is similar to that given in the literature[14, 4].

2) Reaction order β and reaction rate constant K

The results shown in Figs. 4.17 to 4.41 determined the reaction rate K_1 of the pseudo α-level at a given HCl concentration and reaction temperature, which were summarized and shown in Table 4.8. The reaction order β of reaction rate to HCl and the apparent reaction rate constant K between mercury and HCl could be obtained from these results.

Table 4.8 Reaction rate K_1 of the pseudo α-level at a given HCl concentration and reaction temperature

T (K)	C_{HCl} (ppm)	K_1	T (K)	C_{HCl} (ppm)	K_1
373	20	0.00765	773	80	0.07024
373	40	0.0107	773	100	0.1073
373	60	0.01378	973	20	0.0624
373	80	0.03939	973	40	0.09049
373	100	0.03434	973	60	0.1078
573	20	0.0258	973	80	0.1280
573	40	0.02514	973	100	0.1691
573	60	0.07694	1173	20	0.1264
573	80	0.066	1173	40	0.1715
573	100	0.0743	1173	60	0.2290
773	20	0.0364	1173	80	0.4034
773	40	0.03759	1173	100	0.4173
773	60	0.07951			

Based on the kinetic model, a straight line could be drawn from the logarithmic of the pseudo α-level reaction rate constant K_1 to the logarithmic of HCl concentration. β could be obtained from the slope, and K could be obtained from the linear intercept. The results are shown in Figs. 4.42 to 4.46.

From the simulation results shown in Figs. 4.42 to 4.46, the range of β was between 0.76 and 0.88, and the average was 0.79. In this way, the specific form of the kinetics formula of the total combination reaction of mercury and HCl in the flue gas with other compositions was established.

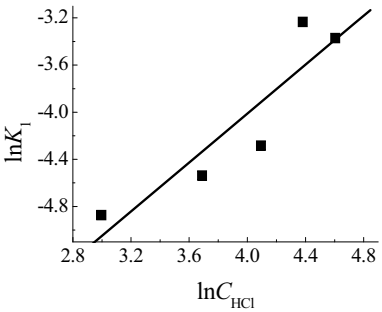

Fig. 4.42 β and K when T=373 K (β=0.88; K=0.000499; r^2=0.861)

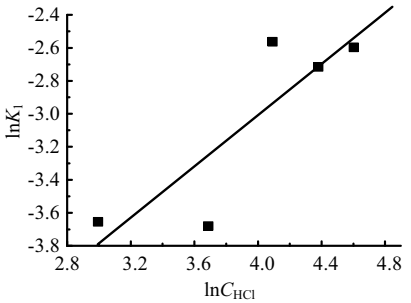

Fig. 4.43 β and K when T=573 K (β=0.78; K=0.002217; r^2=0.859)

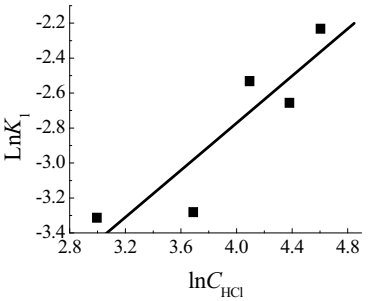

Fig. 4.44 β and K when T=773 K (β=0.76; K=0.003198; r^2=0.887)

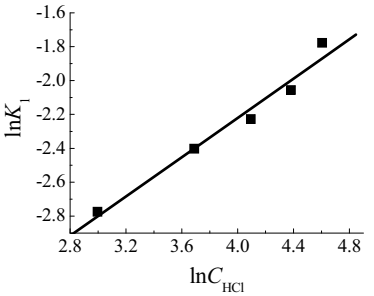

Fig. 4.45 β and K when T=973 K (β=0.79; K=0.005312; r^2=0.896)

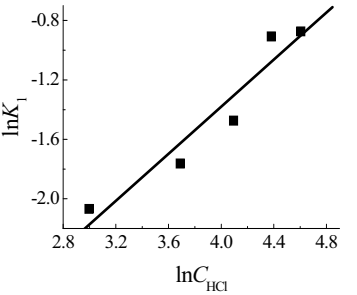

Fig. 4.46 β and K when T=1173 K (β=0.80; K=0.010584; r^2=0.959)

● *Energy activation and pre-exponential factor*

The reaction rate K of mercury and HCl at various reaction temperatures has been obtained as shown in Figs. 4.42 to 4.46. The results are summarized and shown in Table 4.9. With the use of K at different temperatures, the energy activation and pre-exponential factor of the chemical reaction were calculated to derive the specific reaction rate equation.

Table 4.9 Reaction rate K of mercury and HCl at various reaction temperatures

K	ln$K$	T (K)	1/T
0.000499	–7.6029	373	0.002680965
0.002217	–6.1116	573	0.001745201
0.003198	–5.74523	773	0.001293661
0.005312	–5.23779	973	0.001027749
0.010584	–4.54841	1173	0.000852515

Based on the kinetic model, a straight line could be drawn from the logarithmic of the reaction rate constant K to 1/T. E_a could be obtained from the slope, and A could be obtained from the linear intercept. The results are shown in Fig. 4.47.

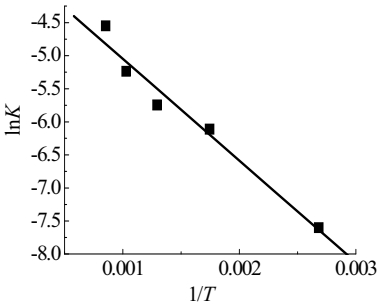

Fig. 4.47 Energy activation and pre-exponential factor (E_a=12787.54 J/mol, A=0.029858 $(\mu g/m^3)^{-0.78}\cdot ppm^{0.21}\cdot s^{-1}$, r^2=0.985)

Based on the simulated results shown in Fig. 4.47, E_a=12787.54 J/mol and A=0.029858 $(\mu g/m^3)^{-0.78}\cdot ppm^{0.21}\cdot s^{-1}$. This value was similar to the literature, and the values were in the same order of magnitude. Senior[1] applied reaction rate constants for two temperatures to derive an energy activation of 15 kJ/mol for mercury and HCl.

● *Error analysis between experimental and model simulated results*

To examine the accuracy, model simulated results were compared with the experimental results in the same conditions with 40 ppm HCl, 6.478 $\mu g/m^3$ mercury, 7% O_2, 13% CO_2, 1200 ppm SO_2, 800 ppm NO, and N_2 balance gas at a temperature of 300 °C. The comparison result is shown in Fig. 4.48 and Table 4.10.

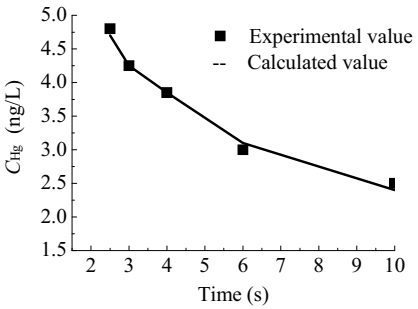

Fig. 4.48 Error analysis between the experimental and simulated results (C_{HCl}=40 ppm and T=300 °C)

The small differences between the simulated and experimental results might be attributed to two aspects. First, the uncertainty of experimental data meant that there were complex procedures for gas distribution and instrument adjustment during the test. Thus, a variety of experimental errors and manual errors might have been generated. Second, the model analysis was only a total combination experimental dynamic model, and a variety of errors were included, thereby causing the difference between calculated and experimental results. However, based on the comparison of the calculated and experimental values, both results showed a high degree of similarity.

Table 4.10 Error analysis between the experimental and simulated results

Residence time	Experimental results C_{Hg} (ng/L)	Simulated results C_{Hg} (ng/L)	Errors (%)
2.36	4.8212	4.641028	–3.74
3.06	4.2502	4.26598	0.37
4.02	3.8842	3.832197	–1.34
6.07	2.9669	3.128889	5.46
9.8	2.4787	2.312036	–6.72

Experimental errors could lead to significant deviations to the results of the proposed model. The stability of the entire experimental system was analyzed. Four different groups of experimental data were used as examples for the calculation of the total experimental errors. The results are shown in Table 4.11. The results showed that the total experimental error was insignificant, indicating the credibility of the experimental results in this section as well as the reliability of the proposed model were reliable.

Table 4.11 Calculation of the overall error in the experimental system

Measurement condition	No. 1 (ng/min)	No. 2 (ng/min)	No. 3 (ng/min)	Arithmetic mean value	Standard error
Condition 1	10.75	11.35	9.28	10.46	1.06
Condition 2	14.67	16.71	16.02	15.80	1.04
Condition 3	18.18	20.80	23.21	20.73	2.52
Condition 4	27.32	27.54	25.81	26.89	0.94

4.3.2 Reaction Kinetics Equation of Mercury in the Flue Gas

Based on the above results, the value of α was 1.78, and the value of β was 0.79. Therefore, in the presence of HCl, the total reaction rate of the homogeneous gas-phase oxidation of mercury could be expressed as

$$\frac{\mathrm{d}C_{\mathrm{Hg}}}{\mathrm{d}t} = -k \times C_{\mathrm{Hg}}{}^{1.78} \times C_{\mathrm{HCl}}{}^{0.79} \tag{4-26}$$

As E_a=12787.54 J/mol, A=0.029858 $(\mu g/m^3)^{-0.78} \cdot ppm^{0.21} \cdot s^{-1}$, the overall reaction rate constant could be expressed using the Arrhenius formula given by

$$k = 0.029858 \exp(-12787.54 / (RT)) \tag{4-27}$$

4.3.3 Model Simulation of Mercury Reaction in the Flue Gas

The model established in this section presents the quantitative mathematical model of Hg^0 to Hg^{2+} in the simulated flue gas. Through the model, the degree of the transformation from Hg^0 to Hg^{2+} under different reaction conditions, such as concentration, temperature, could be gained.

4.3.3.1 Comparison Between Simulated and Experimental Results

In the specified reaction conditions, it simulated the transformation process of Hg^0 to Hg^{2+}. The simulated results were compared with the experimental results. The results are presented from Figs. 4.49 to 4.52. The basic reaction flue gas concentrations consisted of 6.478 μg/m^3 Hg^0, 7% O_2, 13% CO_2, 1,200 ppm SO_2, and 800 ppm NO. High-purity N_2 was used as the balance gas.

Figs. 4.49 and 4.51 show the comparison between the simulated and the experimental results with 20 and 60 ppm HCl at 100 °C reaction temperature, respectively. Figs. 4.50 and 4.52 show the comparison between the simulated and the experimental results with 20 and 100 ppm HCl at 900 °C, respectively. Figs. 4.49 – 4.52 show that the simulated results were very close to the experimental results.

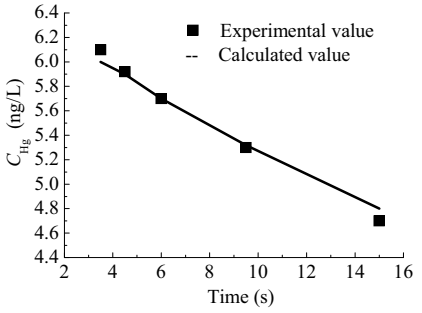

Fig. 4.49 Comparison between the experimental and simulated results (C_{HCl}=20 ppm, T=100 °C)

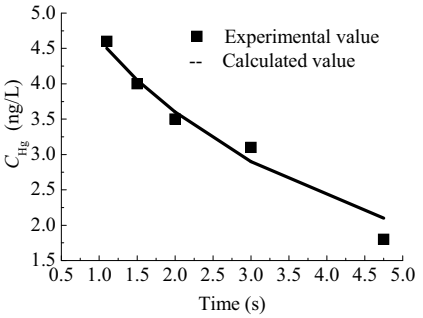

Fig. 4.50 Comparison between the experimental and simulated results (C_{HCl}=20 ppm, T=900 °C)

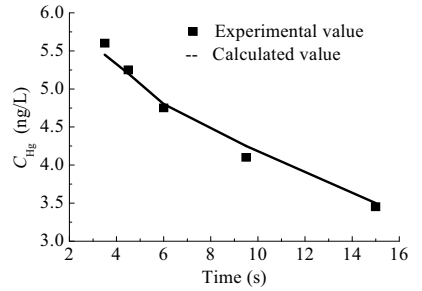

Fig. 4.51 Comparison between the experimental and simulated results (C_{HCl}=60 ppm, T=100 °C)

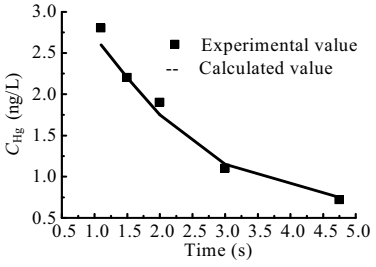

Fig. 4.52 Comparison between the experimental and simulated results (C_{HCl}=100 ppm, T=900 °C)

4.3.3.2 Prediction of Mercury Oxidation using Established Model

The established model could be used to predict the degree of transformation from Hg^0 to Hg^{2+} in coal-fired flue gas. The prediction results are affected by the following factors: HCl concentration, residence time, reaction temperature, other gas components, and so on. The model mainly considered the reaction between mercury and HCl which could be applied to predict the impact of HCl concentration, residence time, reaction temperature, Hg/Cl, etc. on the oxidation of Hg^0 to Hg^{2+}. The results are shown in Figs. 4.53 to 4.62.

Figs. 4.53 and 4.54 show the impact of HCl on the transformation of mercury speciation under different conditions, which considered the parameters including Hg^0 inlet concentration (6.478 μg/m^3), reaction temperatures (100 and 900 °C), residence time (3.63 – 15.05 and 1.15 – 4.79 s), and HCl concentrations (20 – 100 ppm). With increasing HCl concentration during the same residence time, the Hg^0 concentration reduced. It was because increasing HCl was equivalent to increasing Cl as the mercury oxidant. In addition, with a low HCl concentration, the impact of mercury transformation from increased HCl concentration was relatively significant. When HCl concentration increased from 20 to 40 ppm, the maximum distance between the two curves was observed, indicating that the Hg^0 concentration dropped sharply. Niksa[7] predicted the impact of chlorine on mercury transformation.

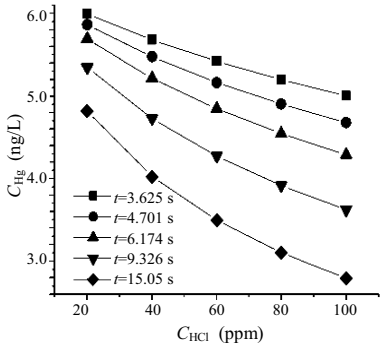

Fig. 4.53 Impact of HCl on Hg^0 oxidization at 100 °C, residence time from 3.63–15.05 s

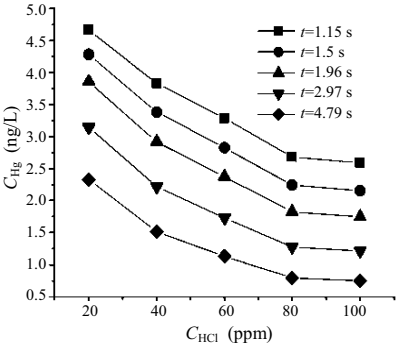

Fig. 4.54 Impact of HCl on Hg^0 oxidization at 900 °C, residence time from 1.15 to 4.79 s

Fig. 4.55 and Fig. 4.56 show the impact of temperature on the transformation of mercury speciation with the reaction condition of 6.478 μg/m^3 Hg^0 inlet concentration, 20 or 40 ppm HCl concentrations, and 1.15 – 4.79 s or 3.63 – 15.05 s residence time, respectively. As results show, the reaction temperature increased while the Hg^0 concentration dropped, indicating that a higher temperature in a certain temperature range promoted the oxidation of Hg^0. In addition, at lower HCl concentration, when the residence time was shorter, the transformation of mercury speciation was less affected by temperature; when the residence time was longer, the impact became more significant. Using CHEMKIN, it was found that when the

temperature was close to 1,000 K, the final product was 2% Hg^0, 20% HgCl, and 78% $HgCl_2$ [15]. These values were higher than the predicted results in this section. The difference could be attributed to the parameter options in the calculation and the differences in experimental and calculation conditions in the current work.

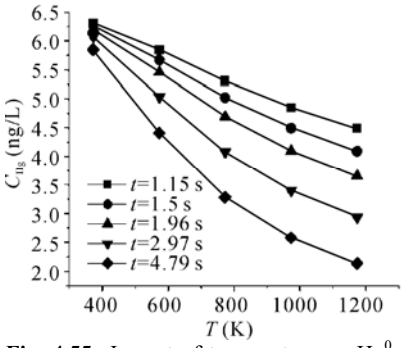

Fig. 4.55 Impact of temperature on Hg^0 oxidization at 20 ppm HCl, residence time from 1.15 to 4.79 s

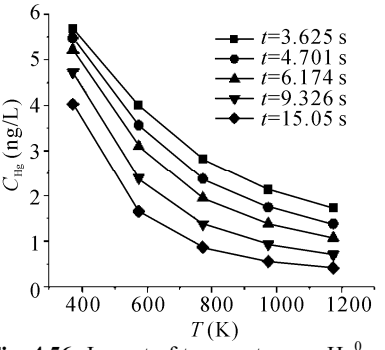

Fig. 4.56 Impact of temperature on Hg^0 oxidization at 40 ppm HCl, residence time from 3.63 to 15.05 s

Fig. 4.57 and Fig. 4.58 present the impact of residence time on the transformation of mercury speciation with the reaction conditions of 6.478 μg/m^3 Hg^0 inlet concentration, 60 or 20 ppm HCl concentration, and 373–1173 K reaction, respectively. When all other conditions were unchanged, the increase in gas residence time decreased the amount of Hg^0. It meant that a longer retention period increased the oxidation of Hg^0, and that mercury oxidation in flue gas usually was far from a theoretically balanced state because residence time was usually less than reaction time in theory.

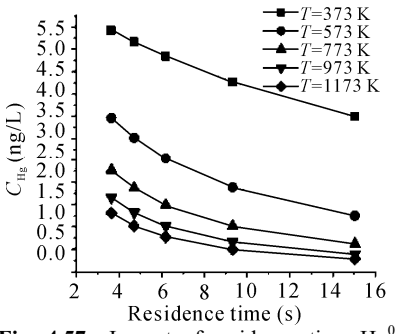

Fig. 4.57 Impact of residence time Hg^0 oxidization at 60 ppm HCl, temperatures from 373 to 1173 K

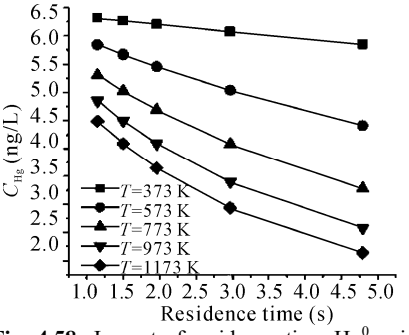

Fig. 4.58 Impact of residence time Hg^0 oxidization at 20 ppm HCl, temperatures from 373 to 1173 K

Fig. 4.59 and Fig. 4.60 present the impact of Hg^0 inlet mercury concentration on the transformation of mercury speciation with the reaction conditions of 20 or 80

ppm HCl concentrations, 373 or 1,173 K reaction temperatures, 1.15 – 4.79 s or 3.63–15.05 s residence time, respectively. With the increasing concentration of Hg^0 inlet mercury in the same residence time, the concentration of Hg^0 gradually increased, thus leading to reduced transformation rate.

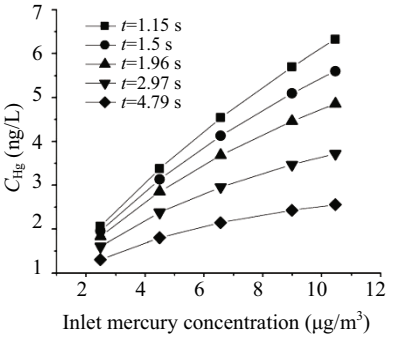

Fig. 4.59 Impact of inlet mercury concentration on Hg^0 oxidization, at 20 ppm HCl, 1173 K, different residence time from 1.15 to 4.79 s

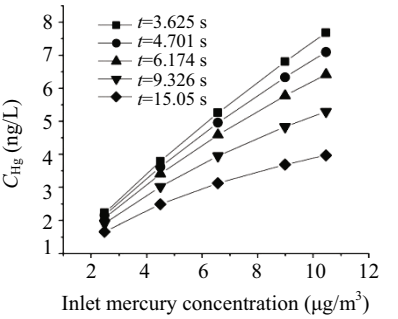

Fig. 4.60 Impact of inlet mercury concentration on Hg^0 oxidization, at 80 ppm HCl, 373 K, different residence time from 3.63 to 15.05 s

Figs. 4.61 and 4.62 present the impact of Cl/Hg on the transformation of mercury speciation with the reaction condition of Hg^0 inlet concentration of 6.478 μg/m³, reaction temperatures of 373 or 1173 K, and HCl concentrations of 20 or 60 ppm, residence time of 3.63 – 15.05 s or 1.15 – 4.79 s, respectively. As shown in the figures, Cl/Hg increased while the concentration of Hg^0 dropped. It meant that higher Cl/Hg increased the oxidation of Hg^0 under certain conditions. Cl/Hg could be considered a parameter in the discussion of regulating mercury oxidation in coal-fired flue as.

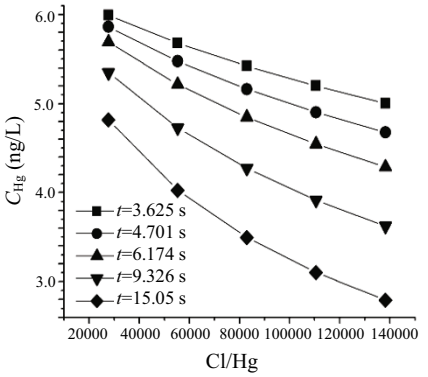

Fig. 4.61 Impact of Cl/Hg on Hg^0 oxidization at 60 ppm HCl, 373 K, different residence time from 3.63 to 15.05 s

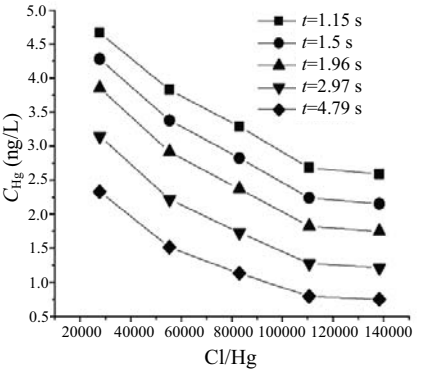

Fig. 4.62 Impact of Cl/Hg on Hg^0 oxidization, at 20 ppm HCl, 1173 K, different residence time from 1.15 to 4.79 s

4.4 Thermochemical Equilibrium Analysis of Mercury Speciation Transformation After Coal Combustion

The significant amount of mercury emissions from coal-fired power plants was found to depend on the mercury content of coal, temperature, composition, and the unburned carbon in flue gas, as well as the air pollution control devices (APCD) used. Also, it is strongly determined by the speciation of the mercury in flue gas[2]. In general, in coal-fired flue gas, gaseous mercury exists predominantly in Hg^0, Hg^{2+}, along with the +1 oxidation state, although this state is very rare. As stated from the real experimental results statistically, the Hg^0 was 52% – 83% of the total $Hg_{(g)}$, Hg^{2+} was 17% – 48% emitted from coal-fired flue gas[16]. Cost-effective methods for removing mercury from coal-fired flue gas has received increased attention because of recent limitations placed on mercury emissions by the Protection Agency[17]. Therefore, a variety of possible options to reduce mercury emissions were proposed and discussed while a more efficient utilization of already existing air pollution control devices (APCD) for mercury removal purposes was considered as a reliable and cost-effective alternative to the development of new and mercury specific removal technologies.

The speciation of mercury in the flue gas of a coal-fired power plant affects the amount of mercury retained in the air pollution control devices (and not emitted from the stack) due to the chemistry of Hg^0 in flue gas being different from that of Hg^{2+}. Hg^0 is difficult to capture by typical APCD because it is highly volatile and nearly insoluble in water. Whereas Hg^{2+} can be removed in the wet flue gas desulfurization (WFGD) facilities of coal combustion processes due to its high solubility in aqueous solutions. So a promising approach for mercury removal from coal-fired flue gas is to achieve oxidation of Hg^0 to Hg^{2+}, subsequently captured by WFGD[18]. Thus, the mercury speciation, no matter whether the mercury is Hg^0 or Hg^{2+}, has an extreme impact on mercury removal by WFGD.

Whereas the speciation was considerably correlated to the flue gas temperature and particularly the flue gas species including HCl, SO_2, NO_x, Cl, O_2, H_2O etc.[19,20].

Some literature on the impact of flue gas composition on the mercury speciation transformation was reported. Hall *et al*.[11,21,26] studied the reaction characteristics between $Hg^0_{(g)}$ and the flue gas components, including CO_2, HCl, Cl_2, SO_2, NO_2, N_2O, NO, NH_3, H_2S. It was shown that Hg^0 was reacting with NO_2 at a very low rate, hardly with N_2O, NH_3, H_2S, SO_2, but sensitive to HCl, Cl_2 and O_2[21]. Frandsen[22] focused on the thermodynamic equilibriums of trace elements such as mercury, selenium, arsenic, using the MINGSYS program and DGFBASE database. Hall *et al*.[21] concluded that Cl played a key role in mercury speciation transformation, instead of HCl, Cl_2, NO_x, O_2. Senior *et al*.[1] conducted a simple model of mercury transformation in flue gas, which was devised so that an importance was attached to Cl in flue gas in mercury transformation, whereas, H_2O, SO_2, NO_2 were also influenced slightly by the homogeneous reaction rate with mercury. Qiao Yu proposed a kinetic model of the Hg/O/H/Cl reaction system, and the modeling results agreed well with experimental data by Mamani-Paco *et al*.[9].

So far, critical information as to which key parameter is the most sensitive to mercury speciation and transformation among the flue gas species, was missing from the literature. Maybe it is a good approach to obtain such information as above with the aid of a thermochemical equilibrium calculation.

However, modeling the impact on mercury transformation by the gas species at the inlet of the web scrubber predicted from a thermochemical equilibrium calculation is rarely observed in practice. If only to measure the formation of mercury, it is vital to conduct the mercury absorption experiments in a pilot-scale web scrubber. With the assistance of the thermochemical equilibrium calculation, a subtle reaction between gas components and mercury compounds will be shown. The reaction products of both will be represented as well.

4.4.1 Introduction

The equilibrium product amounts are positive, satisfy the mass balance constraints with respect to the system components and correspond to the lowest possible Gibbs energy for this particular selection of possible products.

The Equilib module is the Gibbs energy minimization workhorse of FactSage and the most popular program. It calculates the concentrations of chemical species when specified elements or compounds react, or partially react, to reach a state of chemical equilibrium. Equilib employs the Gibbs energy minimization algorithm and thermochemical functions of ChemSage and offers great flexibility in the way the calculations may be performed. For example, the following are permitted: a choice of units (K, C, F, bar, atm, psi, J, cal, BTU, kW·h, mol, wt.%, ...); dormant phases in equilibria; equilibria constrained with respect to T, P, V, H, S, G, U or A or changes thereof; user-specified product activities (the reactant amounts are then computed); user-specified compound and solution data; and much more. Phase targeting and one-dimensional phase mappings with automatic search for phase transitions are possible. For example, you can calculate all equilibrium (or Scheil-Gulliver non-equilibrium) phase transitions as a multicomponent mixture is cooled.

Chemical thermodynamics is the study of the interrelation of heat and work with chemical reactions or with physical changes of state within the confines of the laws of thermodynamics. The primary objective of chemical thermodynamics is the establishment of a criterion for the determination of the feasibility or spontaneity of a given transformation. In this manner, chemical thermodynamics is typically used to predict the energy exchanges that occur in the reactions assumed to be at equilibrium.

The chemical thermodynamics model, which is of homogeneous zero-dimensional, only takes account of global parameters, i.e. pressure and temperature, instead of those of gradient. In a boiler case, the equilirium will be met in the high temperature zone where the reaction rate is fast enough, whilst the reactions in the low temperature zone can barely reach equilibrium states even with long

residence time.

Due to the complex operational conditions in a coal-fired power plant, the reaction system may not be well at perfect equilibrium. The causes could be, for example, the catalysis effects of fly ash components on the mercury reactions, or the mercury adsorption on the particles, unimaginative enough for a lower reaction rate in the lower temperature zone. Nevertheless, the chemical thermodynamics analysis will give reasonable and valuable results of the mercury speciation distribution in the boiler and the sulfur removal unit, and the products from the mercury reactions.

So far, the chemical thermodynamics analysis is a good approach for calculation. The equilibrium will be reached at minimized Gibbs free energy. Gibbs energy (also referred to as ΔG) is the chemical potential that is minimized when a system reaches equilibrium at constant pressure and temperature, that is $(\delta G)_{T,P} \geq 0$, so the problem of solving the chemical equilibrium comes to be calculated for certain agents composition n_i at minimized Gibbs free energy.

FactSage, one of the largest fully integrated database computing systems in chemical thermodynamics in the world, was introduced in 2001 and is the fusion of the FACT-Win/F*A*C*T and ChemSage/SOLGASMIX thermochemical packages. FactSage is the result of over 20 years of collaborative efforts between Thermfact/CRCT (Montreal, Canada; www.crct.polymtl.ca) and GTT-Technologies (Aachen, Germany; www.gtt-technologies.de).

FactSage 5.2 (Facility for the analysis of Chemical Thermodynamics) package was developed both by GTT lnc. Germany and CRCT lnc. Canada.

The Equilib module is the Gibbs energy minimization workhorse of FactSage and the most popular program. It calculates the concentrations of chemical species when specified elements or compounds react or partially react to reach a state of chemical equilibrium.

Equilib employs the Gibbs energy minimization algorithm and thermochemical functions of ChemSage and offers great flexibility in the way the calculations may be performed. For example, the following are permitted: a choice of units (K, C, F, bar, atm, psi, J, cal, BTU, kW·h, mol, wt.%, ...); dormant phases in equilibria; equilibria constrained with respect to T, P, V, H, S, G, U or A or changes thereof; user-specified product activities (the reactant amounts are then computed); user-specified compound and solution data; and much more. Phase targeting and one-dimensional phase mappings with automatic search for phase transitions are possible. In this work, this Equilib module is employed to simulate the chemical reactions.

4.4.2 Comparison Between Calculation and Experimental Results

Based on the Gibbs energy minimization, the Equilib module of FACTsage5.2 software package provides a multi-element, multi-phase thermodynamic equilibrium model, mercury compounds in gas phase, liquid phase or solid phase which react or partially react also taking everything into account. Chemical thermody-

namics analysis on mercury transformation is to be performed if possible, if the typical gas components, initial concentration of mercury and reaction condition (pressure, temperature) are input into the Equilib module.

Table 4.12 shows mercury compound included in the model, which comprises the mercury chemical species in gas/liquid/solid phases when specified elements or compounds react or partially react to reach a state of chemical equilibrium. In fact, most of them are intermediate products which are unstable, liable to decompose with a temperature increase.

Table 4.12 Mercury compound included in the model

Gas phase	Hg, Hg[+], Hg_2, HgH, HgCl, $HgCl_2$, $Hg(CH_3)_2$, HgO, HgS
Liquid phase	Hg, $HgCl_2$, $Hg(CH_3)_2$
Solid phase	HgO, HgS, $HgSO_4$, Hg_2SO_4, Hg_2CO_3, $Hg_2C_2O_4$, $Hg_2(N_3)_2$, $Hg_2(N_3)_2$, $Hg_2(CNS)_2$, $Hg_2(C*N*S)_2$

During calculation, four cases with various initial conditions are given here (Table 4.13). A typical coal-fired flue gas such as O_2 (0 – 7%), CO_2 (fixed at 13%), N_2 as balance gas (80% – 87%), were considered firstly. Other cases involved 4% O_2, 13% CO_2, 83% N_2, HCl (0 – 1000 ppm), NO (0 – 900 ppm), SO_2 (0 – 1200 ppm) simultaneously. The initial mercury concentration in the flue gas was 18.75 μg/m^3, equivalent to 9.3E – 08 by mole fraction. The flue gas temperature was arranged at 300 – 900 K, ambient pressure. In general, mercury tended to be oxidized with the assistance of an oxidizing agent, such as chlorine, oxygen, nitrogen oxide, sulfur oxide. The mercury transformation was defined as mercury oxidization, as

$$\text{mercury transformation}\% = \frac{\text{mass of mercury oxide in the flue gas}}{\text{mass of mercury oxide} + \text{mass of elemental mercury}} * 100\% \quad (4\text{-}28)$$

Table 4.13 Initial condition during the calculation

Case 1						Case 2	Case 3	Case 4
O_2		N_2		CO_2		4%O_2-13%CO_2-83%N_2		
O_2 (%)	Mole fraction	N_2 (%)	Mole fraction	CO_2 (%)	Mole fraction	HCl (ppm)	NO (ppm)	SO_2 (ppm)
0	0	87	1.214	13	0.181	0	0	0
0.2	0.002	86.8	1.212	13	0.181	20	100	100
0.5	0.007	86.5	1.207	13	0.181	50	300	500
1	0.014	86	1.200	13	0.181	100	600	1200
2	0.028	85	1.186	13	0.181	150	900	-
4	0.056	83	1.158	13	0.181	500	-	-
7	0.098	80	1.117	13	0.181	1000	-	-

The influence of temperature on the conversion was analyzed in the identical flue gas reaction system. The comparison between calculation and experimental results was shown, with a temperature range of 300 – 900 K in Fig. 4.63. Mercury transformation definitely shifted with temperature decrease. Hg^0 occupied 90% percent of the total mercury, which means that Hg^0 is the thermal steady state in the high temperature area of a furnace. Hg^0 converted into Hg^{2+} as the temperature decreased, and the mercury conversion reached 50% at 473 K finally. The reaction between Hg^0 and oxygen was specifically as follows:

$$Hg_{(g)} + \frac{1}{2}O_{2(g)} \rightarrow HgO_{(s,g)} \tag{4-29}$$

The thermodynamic equilibrium simulation results were in accord with the experimental results in Fig. 4.63, but the simulation curve was mostly lower than experimental results. The reason stemmed from the fact that the temperature variation in the heating system was not an isothermal reaction process but a parabola, and the quenching process of 1 – 2 s exists in the sampler tube as well. The rapid cooling of the flue gas assisted the production of Hg^{2+} as reported by Wang[25], and the production of Hg^{2+} increased as the temperature decreased. The thermodynamic equilibrium model did not take the mixing, dispersion and inhomogeneity of temperature into consideration, thus the simulation results were lower than experimental results, while the existing simulation error coincided with experimental results considerably. The results demonstrated that chemical thermodynamic equilibrium analysis could be pretty feasible in research on mercury transformation in complicated flue gas conditions.

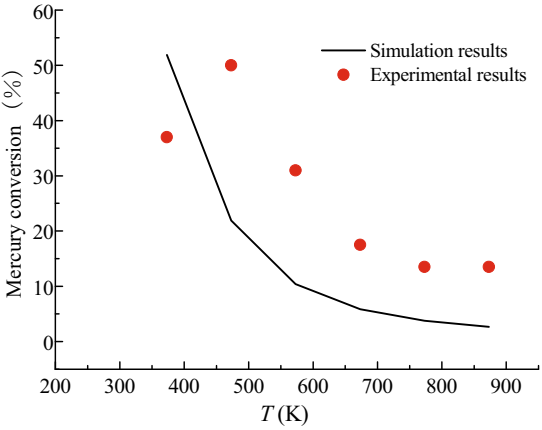

Fig. 4.63 Comparison between chemical thermodynamic simulation with experimental results

4.4.3 Thermochemical Equilibrium Calculation Results

4.4.3.1 Influence of Temperature

To explore the elements affecting mercury speciation transformation from coal-fired flue gas, the typical flue gas temperature was firstly considered. The simulated flue gas temperature was set at 300–2,000 K as in a real power plant, along with the flue gas components consisting of 7% O_2, 13% CO_2, 80% N_2, Hg (real working case 1). Table 4.13 shows mole fractions of the input flue gas components and Table 4.12 provides the various mercury compounds concerned. From Fig. 4.64(b), as the temperature went down, the mercury conversion rate increased definitely, which was in line with the general law shown in Fig. 4.63. At 1,200 K, only a small amount of mercuric oxide gas was detected and a large amount of mercuric oxide (HgO) gas-solid mixture at 473 K, while at 300 K mercuric oxide existed in the form of a solid phase in Fig. 4.64(a). The conclusion could be drawn that Hg^0 tended to react with oxygen molecules to form mercuric oxide, which was observed by Hall and his colleagues as well[21].

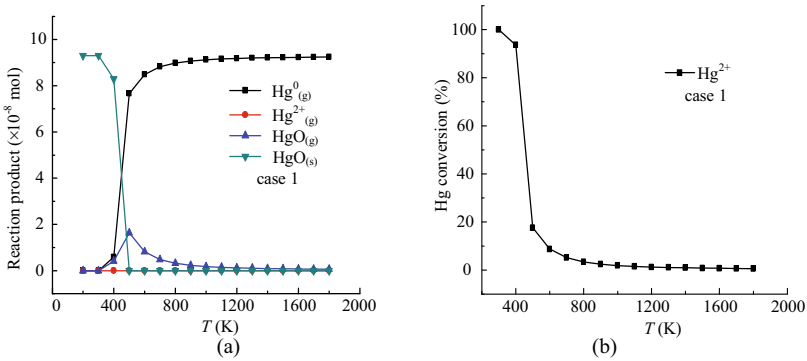

Fig. 4.64 Effect of temperature on mercury speciation transformation

From the chemical and thermodynamics equilibrium discussed above, it is inferred that most of the mercury evaporates and exists dominantly in the form of Hg^0. As the flue gas entered the convection pass and temperature decreased gradually, Hg^0 reacted with the oxygen molecules to form a mercuric oxide gas-solid mixture in the oxidizing atmosphere.

4.4.3.2 Influence of Oxygen Concentration

From Case 1 above, it was concluded that oxygen was the key factor in promoting mercuric oxide generation. Upon consideration of the variability of oxygen concentration in the flue gas in an actual power plant, the influence of oxygen concentration changes on mercury speciation transformation was simulated. The result

is shown in Fig. 4.65, which indicated that Hg^0 did not take part in the oxidizing reaction when there was no oxygen. With 0.2% of oxygen added into the flue gas, mercury oxidized rapidly, which was in accordance with the report on rapid reaction between Hg and oxygen proposed by Hall *et al.*[26]. While under a high-temperature-burning condition, oxygen concentration almost had no effect on mercury transformation. With the temperature decreasing, the mercury conversion rate began to increase. At 300 – 1,400 K, mercury would transform into another speciation and the reaction was extremely vigorous at 600 – 800 K. As the oxygen concentration increased from 0.5% to 7%, this extended the range of the mercury transformation temperature. When the oxygen concentration was set at 7%, Hg^0 began to convert at 1,400 K; at 300 K, nearly all the Hg^0 transformed into Hg^{2+}. Actually, due to the limitation of the chemical reaction rate, the mercury conversion rate was not as high as expected. When the oxygen concentration in flue gas was relatively low, the mercury transformation temperature and the mercury conversion rate were relatively low too. It was clear that high oxygen concentration in flue gas could promote the oxidation of mercury from the above analysis.

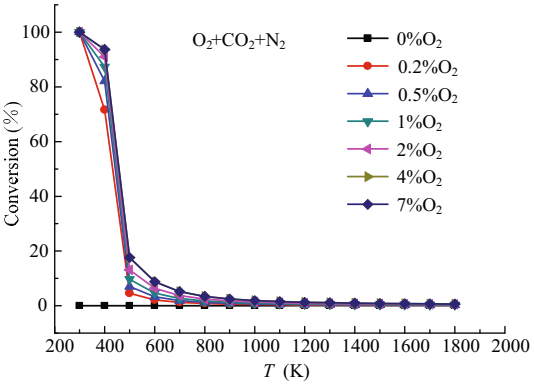

Fig. 4.65 Effect of O_2 content on Hg transformation

4.4.3.3 Influence of HCl

Fig. 4.66 is for observing the impact of HCl on mercury transformation by changing the concentration of $HCl_{(g)}$. After increasing HCl concentration (Case 2), we can concluded that mercury begins to transform at higher temperatures with the existence of HCl. At the same time, there will be plenty of products within the mercuric species, i.e. Hg^0, Hg^{2+}, HgH, $Hg(CH_3)_2$, HgO, HgCl, $HgCl_2$ in a gaseous phase from Fig. 4.66(a), while gaseous $HgCl_2$ is the dominant form according to the calculation result. Because coal consists of chlorine, generally 60 ppm, when it burns HCl will be released from coal and into the flue gas. HCl gas tends to decompose into a more active chlorine atom at high temperature, which swiftly reacts with Hg^0 to form $HgCl_2$, sometimes oxidizing into HgCl first and then into $HgCl_2$. The possible reactions list is as follows:

$$HCl_{(g)} \rightarrow Cl_{(g)} + H \tag{4-30}$$

$$OH + HCl_{(g)} \leftrightarrow Cl_{(g)} + H_2O \tag{4-31}$$

$$Hg^0_{(g)} + 2Cl_{(g)} \longrightarrow HgCl_{2(g)} \tag{4-32}$$

$$2HCl_{(g)} + \frac{1}{2}O_{2(g)} \rightarrow Cl_{2(g)} + H_2O_{(g)} \tag{4-33}$$

$$2Cl_{(g)} \longrightarrow Cl_{2(g)} \tag{4-34}$$

$$Hg^0_{(g)} + Cl_{2(g)} \rightarrow HgCl_{2(g)} \tag{4-35}$$

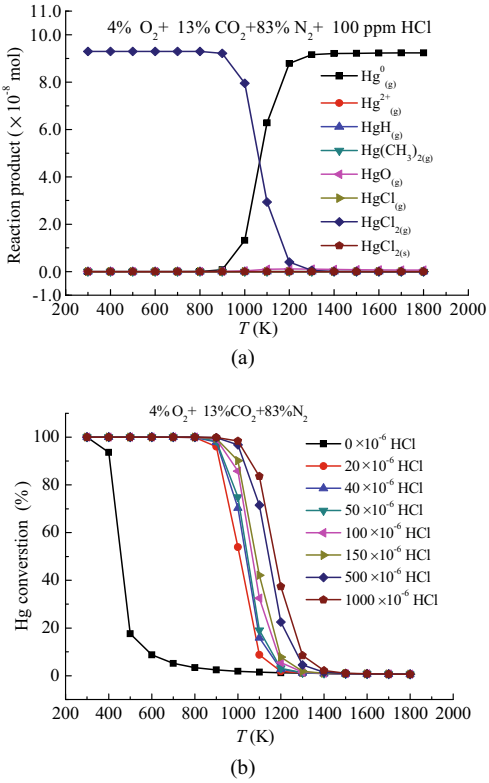

Fig. 4.66 Effect of HCl concentration on Hg transformation and reaction product

From Fig. 4.66, HCl had a significant impact on mercury oxidization. The more the HCl content in the flue gas, the more $HgCl_2$ appeared. Possibly chlorine might lead to Hg^0 oxidization by a homogeneous or heteogeneous, catalytic oxidization process.

We introduce two parameters here: the initial temperature and cut-off temperature of mercury. The initial temperature (T_{ts}) of mercury is defined as the temperature point at which Hg^0 starts to transform to Hg^{2+}. The cut-off temperature (T_{te}), is the point at which Hg^0 converts into Hg^{2+} completely. Fig. 4.67 shows the

of HCl concentration on T_{ts} and T_{te} in mercury transition. The higher the concentration of HCl gas, the higher the initial and cut-off temperature of mercury conversion. Without HCl, T_{ts} and T_{te} were 900 K and 300 K, respectively. With the assistance of a small amount of hydrogen chloride gas, T_{ts} and T_{te} in mercury conversion were significantly higher. When the HCl concentration was 100 ppm, both temperatures were 1,350 K and 800 K, respectively. Musmarra *et al.*[27] reported that when the HCl concentration increased from 10 to 1,000 ppm in the incinerator flue gas, the compounds of mercury had the same distribution. Sliger *et al.*[28] reported 50% equilibrium conversion to $HgCl_2$ occurred at approximately 950 K in the presence of 500 ppm HCl. Some equilibrium calculations declared that the 50% conversion point depended on chlorine content in the flue gas[1]. Other investigators proposed conversion points in the same general 800 – 900 K range[29].

The existence of HCI could effectively improve the mercury transition temperature, and the oxidation of mercury worked easily within a wide temperature range. The calculation suggested that a higher concentration of HCl gas in the flue would help Hg^0 convert to Hg^{2+} at a higher temperature.

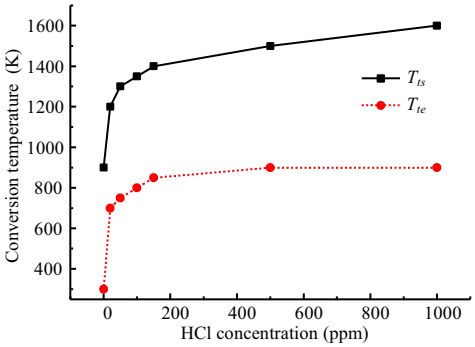

Fig. 4.67 Effect of HCl on the initial and cut-off temperature of mercury conversion

4.4.3.4 Influence of NO

In consideration of the actual coal-fired boiler flue gas components generally containing NO of 300 – 600 ppm, case 3 (Table 4.11) was employed to analyze the influence of NO on the transformation of mercury species by changing the concentration of NO. The simulation results are shown in Fig. 4.68.

By comparing Fig. 4.64(a) and Fig. 4.68(a), it could be seen that the reaction of mercury trends and reaction products were the same with or without NO in flue gas. That means the components of NO were insensitive to the homogenous conversion to mercury. There was not any change happening even with an increase or decrease in the concentration of NO. It was deduced by the simulation results that NO neither promotes nor hinders the conversion of mercury, which plays a neutral role in the homogenous reaction.

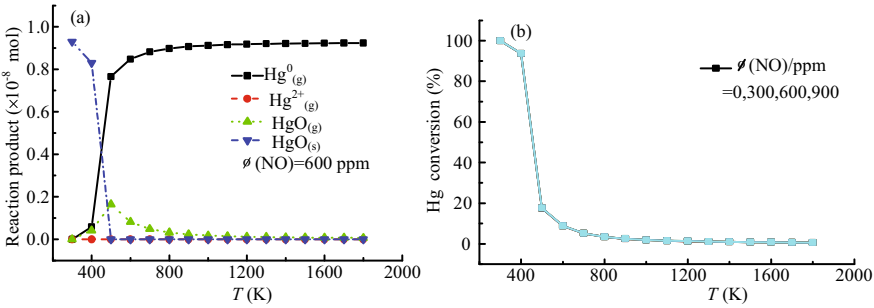

Fig. 4.68 Influence of NO on mercury speciation transformation

4.4.3.5 Influence of SO_2

To investigate the impact of SO_2 on mercury speciation transformation, Case 4 condition was designed. The results are displayed in Fig. 4.69. When the concentration of SO_2 was 500 ppm in the flue gas, compared with no SO_2, it was obvious that $HgS_{(g)}$, $HgSO_{4(g)}$ and $Hg_2SO_{4(g)}$ appeared in the reaction product of mercury.

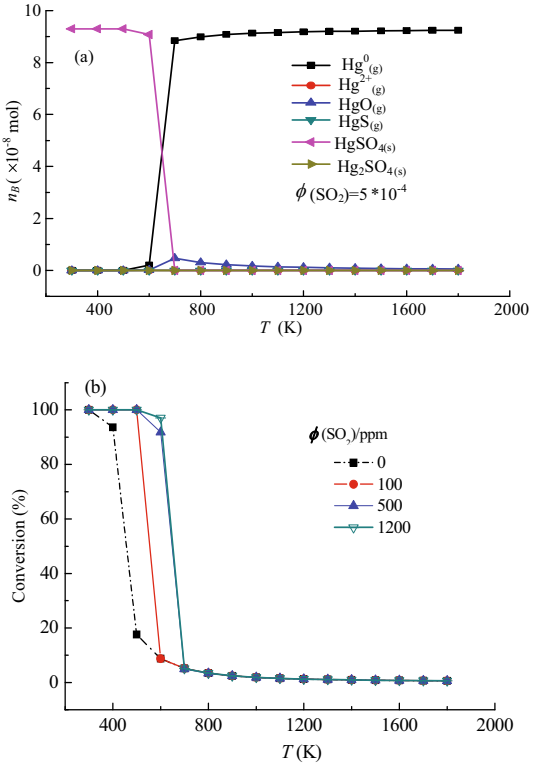

Fig. 4.69 Influence of SO_2 on mercury speciation transformation

When the temperature is higher than 1,000 K, mercury exists mainly in the form of gaseous Hg^0. As the temperature reduces, Hg^0 slowly decreases, while Hg^{2+} generally increases (Eq. (4-36)). A small part of Hg^{2+} is produced from 600 K to 1,000 K. With the temperature decreases further, the conversion reaction intensifies so that the reactions between SO_2 and Hg^0 produce solid mercuric sulfate ($HgSO_4$) (Eq. (4-37)). When the temperature is down to 500 K, 100% of the mercury exists in the solid form of $HgSO_4$ in the flue gas.

$$Hg_{(g)} + \frac{1}{2}O_{2(g)} \rightarrow HgO_{(g)} \tag{4-36}$$

$$2SO_{2(g)} + 2HgO_{(g)} + O_{2(g)} \longrightarrow 2HgSO_{4(s)} \tag{4-37}$$

When SO_2 concentration was set at 100, 500, 1,200 ppm respectively, the result is depicted in Fig. 4.69(b). The impact of SO_2 concentration on conversion of the mercury temperature curve is shown in Fig. 4.70. It shows that different SO_2 concentration had hardly any effect on T_{ts}, but a bad effect on T_{te} of Hg^0 transformation into Hg^{2+}. T_{te} was 300 K in the flue gas without SO_2. When SO_2 concentration was 100, 500, 1,200 ppm, T_{te} was 500, 550, 600 K respectively. It was obvious that T_{te} increased as the SO_2 concentration was enhanced.

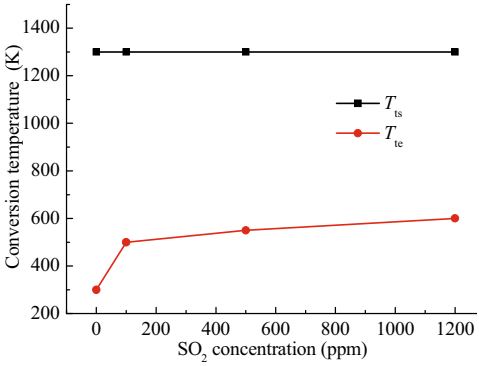

Fig. 4.70 Influence of SO_2 on mercury speciation conversion temperature

This conveyed the information that SO_2 contributed to the conversion of mercury, and especially that SO_2 had stronger activity than O_2 at low temperature. When SO_2 concentration was higher, Hg^0 could be converted into Hg^{2+} at higher temperatures.

4.4.3.6 Co-influence of Typical Gas Components

With regard to the real case, it is highly important to investigate the comprehensive effects of the typical gas components in the flue gas. When the flue gas includes 7%

O_2, 13% CO_2, 80%, N_2, 800 ppm NO, 1,200 ppm SO_2, 600 ppm NO, 60 ppm HCl, the results are displayed in Fig. 4.71.

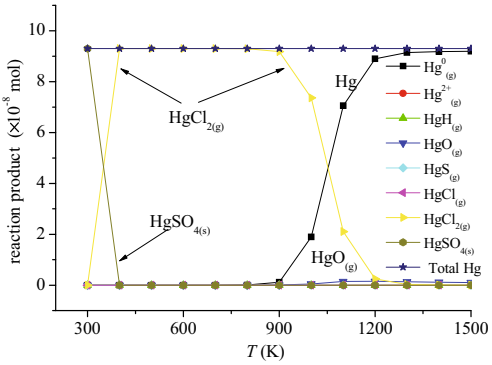

Fig. 4.71 Co-influence of typical gas components on mercury speciation

In general, during the pulverized coal combustion process, mercury in coal exists as Hg^0 in the flue gas in principle. The furnace temperature is around 1200–1500 °C, most of the mercury compound (organic or inorganic form) is in a non-steady state, and tends to decompose into Hg^0 in a stable thermal state. With the temperature falling gradually, the Hg^0 will be oxidized into Hg^{2+} with the assistance of oxidizing agents, chlorine, sulfur, iodine, oxygen, bromine, etc.

Conclusively, it was quite a little different from the previous result. As shown in this figure, mercury started to exist in Hg^0 above 900 K, in particular. Within a high-temperature region at about 1,500 K, mercury evaporated and Hg^0 was the dominant form at that time. With the temperature cooling, mercury was oxidized into HgO in a gaseous phase gradually, similar to the investigation result reported that above temperature 1,073 K, mercury existed as Hg^0 primarily and HgO in a very small amount[30]. At the same time, $HgCl_{2(g)}$ was converted into a big amount swiftly, due to the fact that Cl_2 was rather more sensitive than O_2. Accordingly, at a temperature from 873 K to 1,273 K, gaseous Hg^0, $HgCl_2$ and HgO co-exist at the same time. At 873 K, $HgCl_2$ had completed 100% conversion. Almost all $HgCl_2$ conversion took place in this zone between 873 K and 373 K.

Up to 373 K, $HgSO_4$ in a solid phase would be formed and separated out from the gas phase system. With the shift in chemical equilibrium, mercury will transfer from $HgCl_2$ into $HgSO_{4(s)}$.

Definitely, while in the low temperature region below 400 K, just as for ESP and the WFGD tower entrance, mercury may exist in a gas-solid compound, i.e. solid $HgSO_4$, gaseous $HgCl_2$, gaseous Hg^0. As is known, $HgCl_2$ is highly soluble in water, and small particles of $HgSO_4$ can be removed in the desulfurization tower. Therefore, the utilization of the already existing WFGD tower for mercury removal purposes is considered as a cost-effective, high-efficiency alternative.

The chemical thermodynamic equilibrium model is the ideal system response to the results over an unlimited time. However, the residence time of the flue gas is limited to only 3 – 5 s in the actual operation of the desulfurization tower. So the

mercury removal efficiency in the desulfurization tower is strongly dependent on the mercury species, reaction time (retaining time), other flue gas components, temperature, etc.

4.5 Modeling Research of Mercury Speciation Transformation During Coal Combustion

4.5.1 Introduction

Field test studies showed 5% to 95% of the mercury emitted in gaseous form from coal-fired plants[31,32]. At present, with the inconvenience of sampling mercury at higher temperature conditions (over 400 °C), it is difficult for us to determine how mercury is escaping from coal, what is the mercury concentration and speciation in the emissions, i.e. gaseous Hg^0 or Hg^{2+} is not quantitatively known during the coal combustion process. The field test for mercury formation and oxidation at high temperature was seldom reported. Sliger *et al*. [6] observed and measured mercury oxidation from a furnace operating between 860 °C and 1,171 °C. In this work, the possible elementary reactions that may lead to oxidation were reviewed and a chemical kinetic model was proposed as well. As the model indicated, Cl was the key oxidizing species and the oxidation was limited to a temperature between 700 °C and 400 °C. The oxidation was governed primarily by HCl concentration, quench rate and other gas composition. The mercury distribution at a higher temperature requires further observation and the mercury oxidation mechanism has also been a query up till now.

Hou *et al*.[33] reported that mercury oxidation was simulated in the atmosphere with different concentrations of Cl_2 and HCl using CHEMKIN3.7 coupled with FLUENT6.2 software. The three dimensional concentration distribution of mercury within the cylindrical stack and the impact of the temperature on mercury oxidation were also obtained. Further, the simulation result showed that even a small amount of Cl_2 is much more effective in oxidation of Hg^0 than HCl, the temperature for the higher oxidizing rate of the Hg^0 focused on 950 – 1,150 K. Although the simulation trial seemed successful, the simulation of mercury is limited to within the cylindrical stack, just a beginning of simulation work. The operating condition has much greater discrepancy in a real coal-fired power plant, while this simulation work above indicates that the coupling calculation can solve the problem of the combination of computational fluid dynamics (CFD) with the complex kinetic mechanism.

With the increasing maturity of the CFD technique and computing power, it is possible to have a numerical simulation of the field of application, such as distribution of temperature, velocity and formation of pollutants available in 3-D. This study was employed to demonstrate the mechanism of formation, distribution,

transformation of mercury species (limited to gaseous mercury compound) during the coal combustion process, based on the CFD model-FLUENT6.2 as a platform, incorporated with a mercury species sub-model. Initially, 3-D distributions of temperature, velocity and components were to be simulated as a basis, mercury simulation would be given accordingly, coupled with the mercury sub-model. This self-developed empirical model was validated for mercury simulation in the furnace. The result was to be stretched, in combination with a 1-D kinetics model of the heating surface after the furnace, as well as CEM *in-situ* measurement of mercury species concentrations at a real 250 MW pulverized coal boiler.

4.5.1.1 CFD Introduction

The development of modern CFD began with the advent of the digital computer in the early 1950s. It is one of the branches of fluid mechanics that uses numerical methods and algorithms to solve and analyze problems that involve fluid flows. Computers are used to perform the millions of calculations required to simulate the interaction of liquids and gases with surfaces defined by boundary conditions. Even with high-speed supercomputers only approximate solutions can be achieved in many cases.

The essence of CFD is to discretize the governing equations at a fixed computational domain based on point (for example, finite difference method) or volume (for example, finite element and finite volume methods), convert them to algebraic equations defined at each computational grid and volume, and then solve these algebraic equations by way of iteration.

The simulation work was conducted with the aid of FLUENT6.2 code. For over twenty years, Fluent has been a leader in the development of CFD software for simulating fluid flow, heat and mass transfer, and a host of related phenomena involving turbulence, reactions, and multiphase flow. But with the acquisition of Fluent by ANSYS, Inc. (NASDAQ: ANSS), additional state-of-the-art computational fluid dynamics (CFD) technology will be incorporated into the impressive ANSYS suite of CAE simulation solutions. The finite volume method (FVM) is the classical or standard approach used most often in commercial software and research codes, including in FLUENT.

The design of FLUENT6.2 is based on the concept of a computer software cluster, which aims to solve problems with suitable computational speed, stability and accuracy according to the characteristics of the problem.

A CFD software cluster is composed of different software from different fields. The construction of a CFD software cluster solves the problems involved in the computation of complicated flow in each field and makes data exchange more efficient and convenient due to the unified fore-end and rear-end treatment tools. This forms the basis for the general utilization of FLUENT. ANSYS FLUENT software contains the broad physical modeling capabilities needed to model flow, turbulence, heat transfer, and reactions for industrial applications ranging from air flow over an aircraft wing to combustion in a furnace, from bubble columns to oil

platforms, from blood flow to semiconductor manufacturing, and from clean room design to wastewater treatment plants. Special models that give the software the ability to model in-cylinder combustion, aeroacoustics, turbo machinery and multiphase systems have served to broaden its reach.

Although FLUENT6.2 code was quite successful in respect of simulating flow, heat transfer, combustion and so on, it was incapable of modelling trace elements in the furnace, such as Hg. To model Hg reaction and distribution in a furnace, there are a series of challenges: first, it is very difficult to accurately describe the reaction process between Hg and various gas species; second, the devolatilization process of Hg accompanied by carbon has not been deeply understood; finally, because the magnitude of Hg concentration is very low, normally in the order of parts per billion, the numerical error in the computational process can largely degrade the accuracy of results. Additionally, currently the species database of FLUENT6.2 does not include the relevant species parameters of Hg. All these factors should be considered in the simulation work.

The calculation steps mainly include grid meshing, turbulence model choice, combustion model choice, particle phase treatment, boundary condition setting, Hg computational model treatment, iteration solving and simulation results treatment.

4.5.1.2 Furnace Introduction

Nowadays, the tangentially fired pulverized coal boiler is popular, specifically accounting for 95% of the total of utility boilers in China. A CFD investigation has been applied to the performance of a typical 410 tons/h tangentially coal-fired boiler with high volatility coal, at full load. Combined bituminous coals of 70% Shenhua coal and 30% Zhungeer coal were used here and the composition inputs were determined using proximate and ultimate analysis data (dry basis) provided in Table 4.14. Concentrations of mercury and chlorine in coal were given as well, mercury was 0.077 μg/g, chlorine was 0.02 μg/g, respectively.

Table 4.14 Proximate and ultimate analysis of coal

C_{ar}	H_{ar}	O_{ar}	N_{ar}	S_{ar}	M_{ar}	A_{ar}	V_{ar}	FC_{ar}	$Q_{ar,\,dw}$ (kJ/kg)
54.57%	3.43%	9.62%	0.8%	0.36%	18.21%	12.71%	23.53%	45.55%	20993

The boiler was made by Haerbin Boiler Co. Ltd., and was a single drum natural circulation, solid slag, square spray combustion, high-pressure pulverized coal boiler, and an intermediate warehouse ball mill pulverizing system was adopted.

As designed here, the furnace is square, 9980 mm×9980 mm, arranged as single-chamber, Π-type, 39 m high from the platform, 42.6 m high from the drum centerline, with membrane wall all around, super-heaters in the flue and two-stage super-heaters in the stack flue, well-decorated as well. The two-stage economizer

and two-stage air-heater are laid out alternatively. The designed parameters of the boiler are as in Table 4.15.

Table 4.15 Main designed operating parameters of boiler

Name	Data
Number	HG-410/9.8-YM15
Rated evaporation capacity	410 tons/h
Rated steam temp.	540 °C
Rated steam temp.	9.81 MPa
Steam drum operating pressure	11.28 MPa
Water temp.	220 °C
Cold temp.	20 °C
Air temp.	330 °C
Inlet temp. of air heater	30 °C
Exhaust gas temperature	134 °C
Excess air coefficient (the furnace exit)	1.2
Excess air coefficient (airheater exit)	1.39
Annual operational time	6000 h
Operational time at full load	5000 h
Boiler effeciency	92.07%
Furnace (width×depth)	9,980 mm×9,980 mm
Height from platform	39,000 mm
Height from drum centerline	42,600 mm
Furnace volumetric heat load	122 kW/m^3
Sectional heat load	3.1 MW/m^2

In general, the tangentially fired pulverized coal boiler is a typical case in China. The tangential combustion system used here is to create well-arranged air circulation and an even layout of the burning nozzle from up to down as follows: downdraft secondary air, downdraft primary air, mid-downdraft secondary air, mid-downdraft primary air, mid-updraft secondary air, updraft primary air, updraft secondary air, OFA and tertiary air. As requested, the rotation of primary air keeps in consistent rotation with the secondary air. Thus the imaginary tangential circle diameter is 800 mm obtained accordingly. Exhaust gas from milling, considered as tertiary air only, is injected from the upper side of the burner. The adjustable horizontal bias burner with blunt body is adopted for use in primary air. As is well-known, the parameters of air distribution in a furnace including primary, secondary, tertiary air are necessary to do the simulation work equivalent to realistic operational conditions. Other parameters involved in the ratio, temperature, velocity and height vary with the different kinds of air, and are described in detail in Table 4.16, which is substantially important for simulation investigation of mercury

formation, transformation and emission during the combustion process in the furnace as well.

Table 4.16 Parameters of air distribution in furnace for simulation as needed

Item	Ratio (%)	Temp. (K)	Velocity (m/s)	Standard height (mm)
Tertiary air	24.7	333	60	17,355
OFA	12	588	48	16,590
Updraft secondary air	8.76	588	48	15,892
Updraft primary air	8.34	433	30	15,378
Mid-draft secondary air	8.76	588	48	14,864
Mid-draft primary air	8.34	433	30	14,350
Mid-downdraft secondary air	8.76	588	48	13,836
Downdraft primary air	8.34	433	30	13,297
Downdraft secondary air	12	588	48	12,670

4.5.1.3 Meshing and Model Establishment

Generally, it's the first basic step to do good meshing for simulation work. Meshing quality has a positive effect on the convergence and accuracy of simulation results. In view of the complex multi-phase flow, heat transfer and combustion simultaneously happening in the furnace, an empirical unstructured grid is employed to do the simulation work here.

● *Model set-up*

Firstly, we utilized software-Gambit to establish a model for a full-size furnace. It was so hard to take into account the detailed structure of whole furnace beyond controversy so we simplified some of the detailed structure during the modeling process. For instance, to meet the demand of model simplification, the membrane wall was replaced by a plane, a pendant super-heater was omitted and a jet plane was a proper substitute for a burner. Even the perimeter air of the furnace was spread apart into secondary air.

Furthermore, in order to obtain reasonable meshing, the whole furnace was considered as one volume and divided into a number of zones which comprised the complex burner area, hopper, pendant super-heater etc. In particular, the burning zone with the characteristics of a large flow gradient, was meshed rather more densely than other parts, which was of significance for precise simulation work. Therefore, as shown clearly in Fig. 4.72, the simulation domain of the furnace was 9,980 mm×9,980 mm×39,000 mm (width×depth×height), nearly equal to the realistic size.

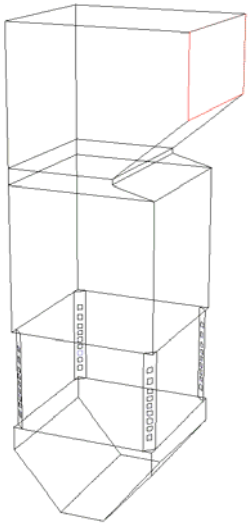

Fig. 4.72 The simulation domain of furnace

● *Mesh generation*

Mesh generation was the next step in carrying out the simulation, which was an essential as well. Paving was introduced into the furnace cross-section grid. A further stretch from the vertical direction, a hexahedral mesh of the whole furnace using cooper method and finally 720 thousand grids in total were shown in Fig. 4.73, which manifest perfectly, high efficiently, fewest grid-maker. The grid was at the base of the furnace hopper, the grid height was a real height (−10,112 mm) in the result.

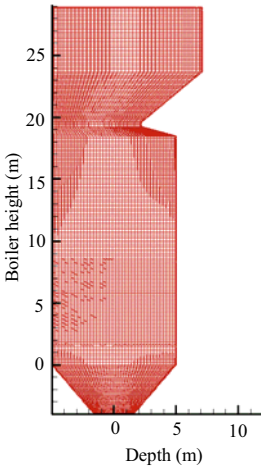

Fig. 4.73 Mesh of boiler

The power grid distortion performed well. All the grid distortions were lower than 0.9, less than 0.5 in general, except for the specific areas such as furnace hopper and arch.

● *Mathematical models*

Pulverized coal combustion is very complex process, including water evaporation, coal devolatilization, homogenous combustion of volatiles and heterogenous combustion of char. A lot of physical and chemical models are needed to simulate the combustion of pulverized coal. Gas phase flow, gas-solid two-phase flow, gas-solid heat transfer, devolatilization, char combustion, radiative heat transfer, etc. should be taken into account. The following models were chosen in this simulation work: K-ε standard turbulence flow model for gas flow, DPM (Discrete Phase Model) for char combustion, single rate devolatilization model for coal devolatilization, non-premixed combustion model for volatile combustion and kinetic/diffusion limited model for char combustion, P-1 radiation model, Langrange discrete phase model for particle traces in the furnace, stochastic trajectory model for particle turbulent diffusion and PDF (Probability Density Function Model) for turbulent and chemical interactivity.

● *Governing equation*

The mathematical model used here was based on the commercial CFD code, FLUENT6.2, where gas flow was described by the time averaged equations of global mass, momentum, enthalpy and species mass fraction. The base gas phase conservation equations for mass, momentum, energy, turbulence, quantities and species concentration can be expressed, in an Eulerian rectangular framework, as

$$\frac{\partial(\rho\varphi)}{\partial t}+\nabla\cdot(\rho\boldsymbol{u}\varphi)=\nabla\cdot(\Gamma_{\varphi}\nabla\varphi)+S_{\varphi} \tag{4-38}$$

In the above equation, Φ stands for general dependent variables expressed as a physical quantity per unit mass. ρ, Γ_{ϕ}, S_{ϕ} stand for density, diffusion coefficient and source term corresponding to Φ, respectively.

● *Equation of motion*

The equation of motion obeys following equations:

$$\frac{\mathrm{d}u_p}{\mathrm{d}t}=\alpha(u_g-u_p),\frac{\mathrm{d}v_p}{\mathrm{d}t}=\alpha(v_g-v_p)+\frac{w_p^2}{r_p}, \tag{4-39}$$

$$\frac{\mathrm{d}w_p}{\mathrm{d}t}=\alpha(w_g-w_p)-\frac{w_p v_p}{r_p}... \tag{4-40}$$

where $\alpha=\dfrac{18\mu_g C_D \mathrm{Re}_p}{24\rho_p d_p^2}$.

● *Reaction mercury model*

The reaction mercury model was not excluded in the FLUENT6.2 software. It was imperative to introduce a sub-model to FLUENT6.2 by providing the database of mercury components concerned. General speaking, the main forms of mercury during coal combustion were gaseous Hg^0, $HgCl_2$, HgO and HgCl. According to US-NIST and the NASA database, the thermodynamic parameters such as thermal conductivity, specific heat volume, enthalpy, entropy, viscosity were calculated and generated from the thermo.db database by FITDAT tool of CHEMKIN3.7. Flow and energy processes in the furnace had been simulated by standard CFD techniques, incorporating a sub-mercury model. Predictions had been validated to a reasonable degree of agreement against real data taken at the full-scale boiler. Then thermo.db as sub-model was injected into the turbulence reaction model. The numerical simulation of the 410 tons/h tangentially coal-fired furnace was presented using a combined simulation method with the sub-reaction mercury model.

```
                HG              HG  1         G   300.000  1500.000 1500.00                1
 0.24511171E+01  0.00000000E+00  0.00000000E+00  0.00000000E+00  0.00000000E+00    2
  -0.38972327E+03-0.41051658E+01   0.13584232E+01 0.14054719E-01-0.31908790E-04    3
          0.26032205E-07-0.71216394E-11-0.79587207E+03-0.15716494E+01                4
               HGCL            HG  1CL  1    G   300.000   1500.000 1500.00          1
 0.46327644E+01  0.00000000E+00   0.00000000E+00   0.00000000E+00   0.00000000E+00    2
 0.79568299E+04   0.46911341E+01   0.39866342E+01   0.19907714E-02-0.27720864E-05    3
            0.18025373E-08-0.43188065E-12   0.81795871E+04   0.80676115E+01          4
              HGCL2         CL  2HG  1    G  0300.00   5000.00  1000.00               1
 0.07251461E+02   0.03082143E-02-0.14475549E-06   0.02958294E-09-0.02201214E-13     2
-0.01981231E+06-0.06061846E+02   0.06249130E+02   0.03221572E-01-0.02109668E-04     3
      -0.07713536E-08   0.08526178E-11-0.01958242E+06-0.10156133E+01                4
               HGO          HG  1O   1      G  0300.00   5000.00  1000.00            1
 0.04192035E+02   0.04176083E-02-0.16589761E-06   0.03318184E-09-0.02429647E-13     2
0.03713109E+05   0.04621457E+02   0.03235991E+02   0.03067170E-01-0.01992628E-04     3
      -0.04378690E-08   0.06018340E-11   0.03950193E+05   0.09495331E+02          4
```

The thermo.db was provided from CHEMKIN3.7 and injected into FLUENT6.2 code, which included a series of thermodynamic coefficients, the thermal conductivity $\lambda(T)$, the specific heat capacity $Cp(T)$, the enthalpy $H(T)$, the entropy $S(T)$, the viscosity $\mu(T)$ and the other thermodynamic parameters, which were fitted polynomially from the standard thermodynamic databases from NIST and NASA. The coefficients could be generated by FITDAT tool of CHEMKIN3.7. Several major forms of mercury, Hg, HgCl, $HgCl_2$, HgO were taken into account. The reaction model was, as with pulverized coal combustion, the equilibrium reaction model. The typical simulation of temperature, velocity, component distributions of pulverized coal combustion in a three dimensional model at full scale were presented at first, regardless of Hg and Cl species contained in the coal. Because both are trace elements, mercury concentration in the furnace is at a magnitude of 1×10^{-9} at the most, chlorine is about 500 ppm. Unfortunately, the mercury sub-model could not cope with the FLUENT6.2 code after the initial simulation converged. This led to a severe truncation error resulting from the limitation of memory in the computer. There was an effective alternative way to have the Hg

concentration in the model increased 100 times, thus avoiding the truncation error. Correspondingly, Hg concentration distribution was only 1% of the simulation results.

4.5.2 Three-Dimensional Simulation Results in a Furnace

4.5.2.1 Temperature Fields

The input parameters for simulation (including boiler operational condition) were selected in accordance with data from the experimental tests of a boiler. The simulation was conducted as if the boiler had a full load.

Flow and energy processes in the furnace had been simulated by standard CFD techniques, incorporating a sub-mercury model. Predictions had been validated to a reasonable degree of agreement against real data taken at the full-scale boiler. The formation and distribution of gaseous Hg^0 were simulated in the furnace during coal combustion. In general, mercury belongs to the easily volatile metals. Mercury mainly exists in elemental form. That is because when the temperature in the furnace is higher than 973–1,073 K, mercury composition will decompose into Hg^0.

Fig. 4.74 shows the temperature field of the longitudinal plan in the boiler. As shown, the area near the burners had the highest temperature, which could reach 1,618 °C, which also contained alternate temperature bands as a result of the alternate primary air and secondary air. Primary air had low temperature. The combustion was enhanced with the inlet of secondary air, which made the temperature increase rapidly in some areas. After the incoming tertiary air, the flame was close to the center, due to the low temperature (60 centigrade) and high momentum (60 m/s) of the tertiary air. The flow was high in rigidity, so it condensed the center of the flame. All this matched with the facts, and is well shown in CFD. Fig. 4.75 is the comparison of CFD results and measured results. The figure shows the average temperature, the maximum temperature and their curves with the height increasing. The measured data at a height of 3 m was as shown by the stars. From the figure, we can see that at a height of 25 m, the difference between the temperatures of the CFD result and measured data is within 3 °C, and it is within 20 °C at a height of 34 m. The CFD results in a thermal state were extremely credible.

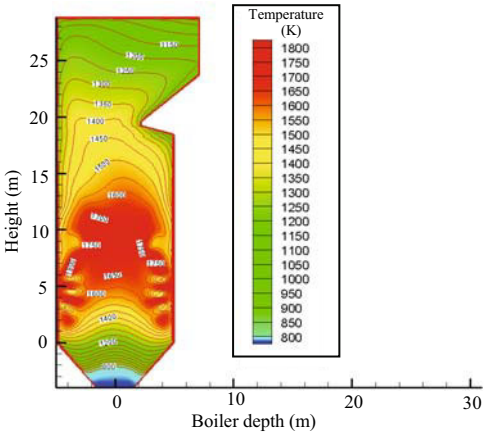

Fig. 4.74 Temperature distribution in the furnace (K)

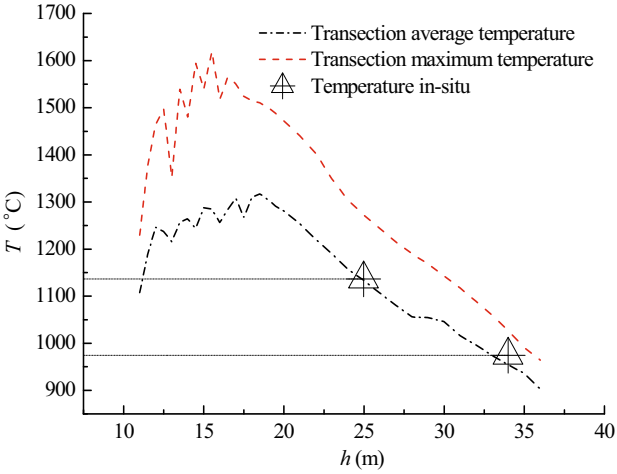

Fig. 4.75 Comparison results between CFD and in-situ

4.5.2.2 Gas Components and Hg Distribution Fields

Figs. 4.76 and 4.77 show the concentration of gas components and Hg distribution in the furnace. The temperature, velocity and the densities of O_2, CO, HCl, H_2S, Cl, Cl_2, Hg, $HgCl_2$, HgO in the lower secondary air section are shown in Fig. 4.76. The high temperature area and the high speed area almost coincide, which is outside the rotating flame ball, as shown in Figs. 4.76(a) and (b). The concentration of O_2 and CO is shown in Figs. 4.76(c) and (d). The former represents the oxidizing atmosphere and the latter the reducing atmosphere. The oxygen with high concentration from the secondary air inlet has a deflection because of the brush from upstream.

The oxygen will be consumed with the flow, which is shown in Fig. 4.76(c). In Fig. 4.76(d), due to the hardness of the diffusion of the oxygen and the combustion of the fuel, there is an area with a high concentration of CO in the center of the furnace and the circle of contact. Most CO is generated in the center of the furnace, and the

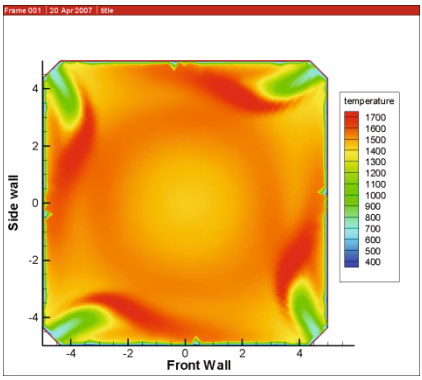

(a) Temperature field

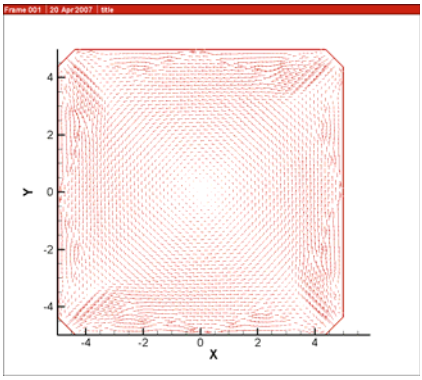

(b) Velocity field

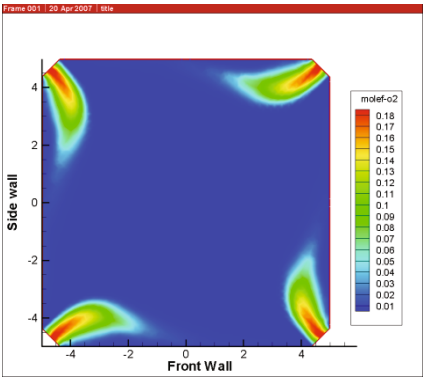

(c) Oxygen concentration profile

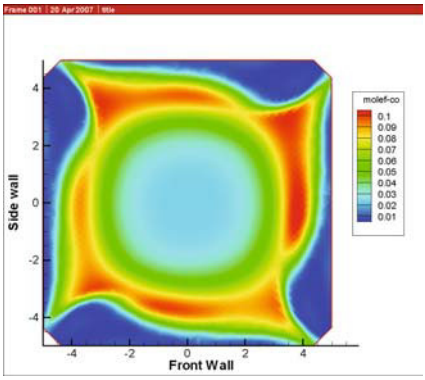

(d) CO concentration profile

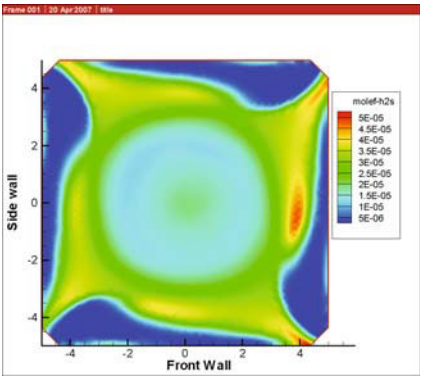

(e) H_2S concentration profile

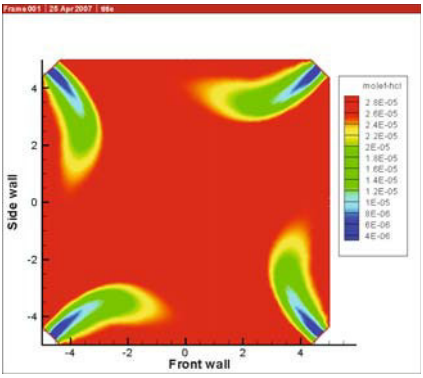

(f) HCl concentration profile

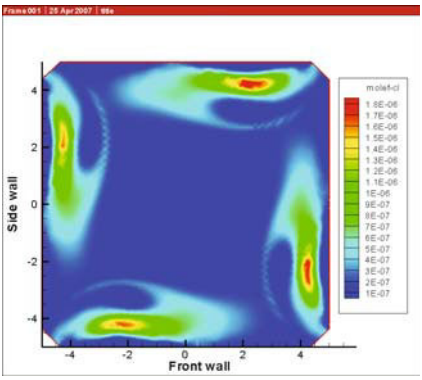

(g) Cl concentration profile

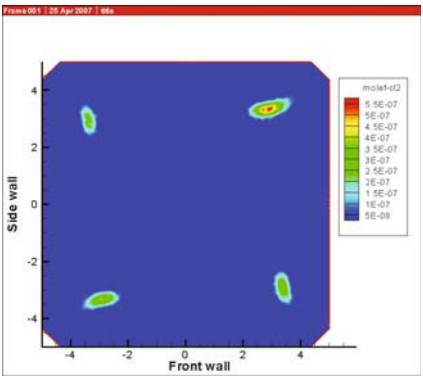

(h) Cl_2 concentration profile

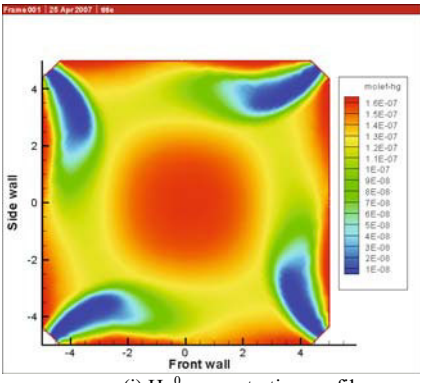

(i) Hg^0 concentration profile

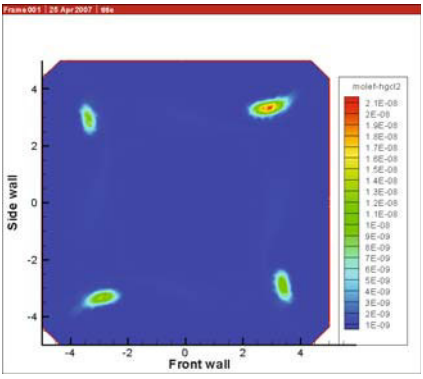

(j) $HgCl_2$ concentration profile

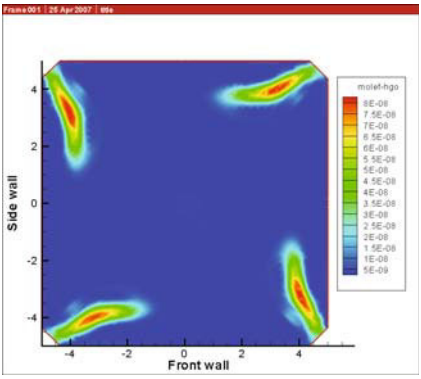

(k) HgO concentration profile

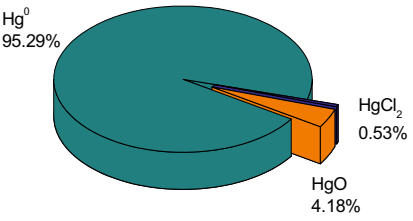

(l) Mercury species distribution at horizontal level of downdraft secondary air

Fig. 4.76 Gas components and mercury species distribution at downdraft secondary air

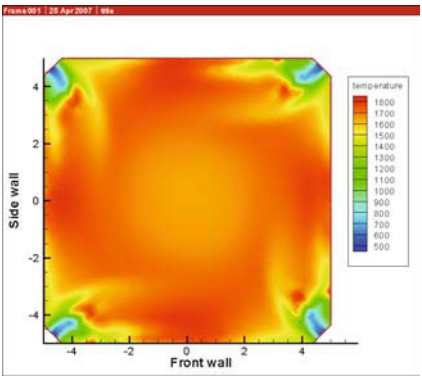

(a) Temperature field

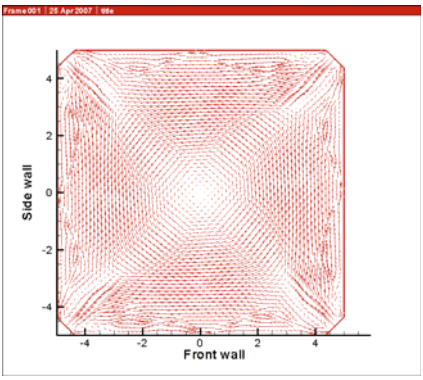

(b) Velocity field

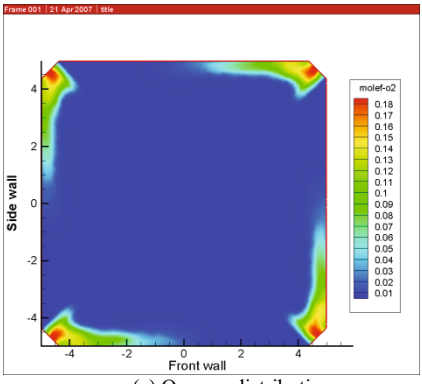

(c) Oxygen distribution

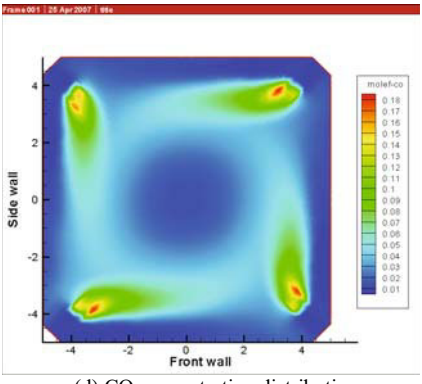

(d) CO concentration distribution

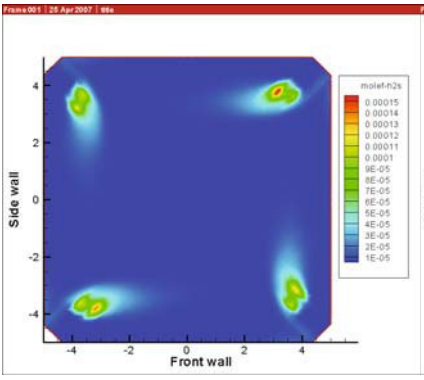

(e) H_2S concentration distribution

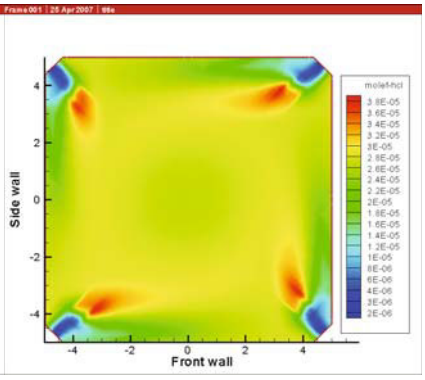

(f) HCl concentration distribution

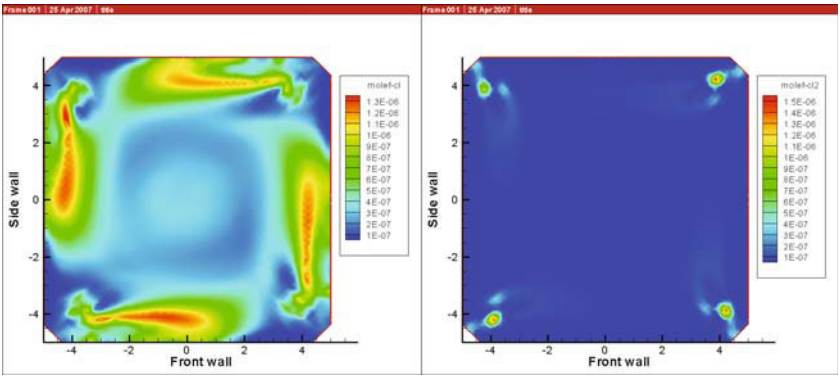

(g) Cl concentration distribution (h) Cl_2 concentration distribution

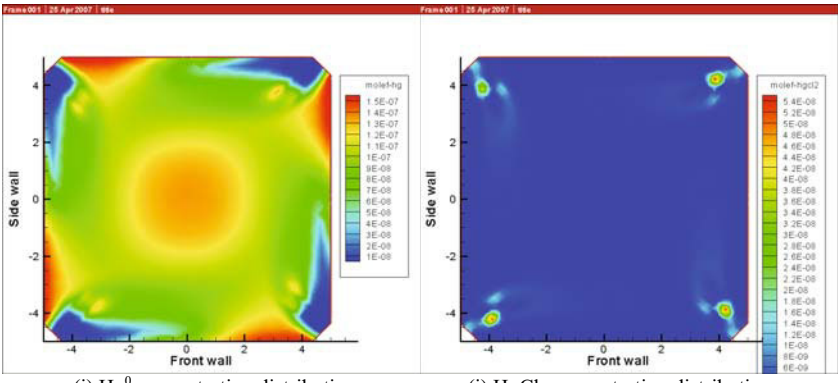

(i) Hg^0 concentration distribution (j) $HgCl_2$ concentration distribution

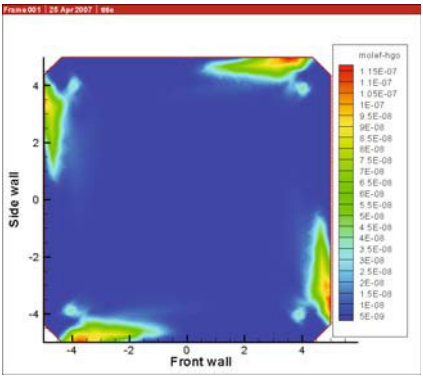

(k) HgO concentration profile

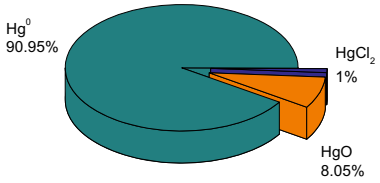

(l) Mercury species distribution at horizontal level of downdraft secondary air

Fig. 4.77 Gas components and mercury species distribution at updraft primary air

concentration of it near the wall is much lower, which is good for protecting Shenhua coal from slagging. Fig. 4.76(e) shows the distribution of the concentration of H_2S. Originally, we considered that S in the coal will all change into SO_2. In the reducing atmosphere, a lot of H_2S generates. The highest concentration is about 50 ppm, which is possibly helpful for desulfurazation technology. Figs. 4.76(f), (g), (h) show the distribution of the concentration of HCl, Cl and Cl_2. We can find that Cl almost exists as a form of HCl. The maximum concentration of HCl is up to 28 – 30 ppm, and HCl is distributed homogeneously in the furnace. A lot of Cl free radical generates in the high temperature of the flame. The maximum concentration of Cl is 1.8 – 2 ppm, while that of Cl_2 is as low as 0.5 ppm and narrowly ranged. The location of Cl_2 is partly homogeneous with Cl and it is much closer to the center of the furnace. Figs. 4.76(i), (j), (k) represent the features of the distribution of Hg, $HgCl_2$ and HgO. In Fig. 4.76(i), Hg^0 is well-distributed in the furnace. There is a large amount of Hg^0 in the center of the furnace and near the wall. Hg^0 is diluted by the incoming secondary air. The amount of $HgCl_2$ is extremely low. The most interesting phenomenon is that the character of its distribution is related to Cl_2 which fits well with the observation by Hou Wenhui, who reported that the three dimensional concentration distribution of mercury within the cylindrical stack was simulated with different concentrations of Cl_2 and HCl by using CHEMKIN3.7 coupled with FLUENT6.2 software[33]. The result showed that even a small amount of Cl_2 was much more effective on oxidation of Hg^0 than HCl. The temperature range for the higher oxidizing rate of the Hg^0 focused on 950 – 1150 K.

HgO is mainly distributed in the axis of the air jet, which is similar to O_2 distribution. Fig. 4.76(l) shows the percentage of each Hg speciation with its integration in the section of secondary air. The percentage of Hg^0 was 95.29%, which took up the most part. The percentage of HgO was 4.18%, and that of $HgCl_2$ was 0.53%, which was quite rare. This was matched with the fact that Hg existed mainly in a form of Hg^0 at high temperature. There was also some Hg^{2+} in the furnace, and HgO was the main form of Hg^{2+}.

Fig. 4.77 shows the distribution of temperature, velocity, components and the concentration of Hg at the updraft primary air section. The distribution is different from that of the downdraft secondary air. Primary air is used for taking the coal to the furnace. The temperature is below 160 centigrade and the velocity is below 30 m/s. It is mainly affected by the updraft and downdraft secondary air, which makes the circle of contact bigger and the temperature average. The distribution of Hg was highly correlated to Cl_2 and O_2. The integral result in Fig. 4.77(l) shows the percentage of Hg^0 decreased, which was 95.29% at the downdraft secondary air section to 90.95%. The percentages of HgO and HgCl both increased and the former achieved 8.05% gradually. The concentration of HgO in updraft primary air was enhanced definitely due to the high concentration of oxygen injection. Similarly, with the Cl released from the coal, the concentration of $HgCl_2$ appeared to be highlighted.

4.5.2.3 Correlation between Hg and Cl Distribution

Fig. 4.78 shows the Hg's form and concentration distribution on the section plane of the furnace. Fig. 4.78(a) is Hg^0 distribution in the furnace, Fig. 4.78(b) is $HgCl_2$ distribution in the furnace, and Fig. 4.78(c) shows the HgO distribution in the furnace. According to Fig. 4.78(a), the highest concentration of Hg^0 appeared at the bottom of the main combustion area, just above the cold ash bucket. That might be attributed to the fact that the heavy metal element Hg had large molecular weight (200 g/mol), and easily sank by gravity. Relatively, the Hg^0 concentration was quite low at the burner area, only because a lot of HgO and $HgCl_2$ was generated in this area. Figs. 4.78(b) and (c) also showed this phenomenon. According to Figs. 4.78(b) and (c), HgCl and HgO were mainly generated at the burner area and the outlet area of the burner chamber. Besides, there was a process happening by which Hg^0 transforms to Hg^{2+} because of the cooling process at the outlet area of the burner chamber.

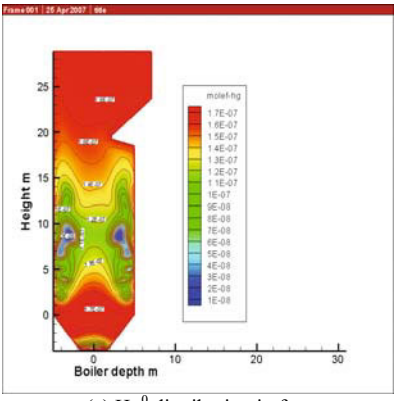

(a) Hg^0 distribution in furnace

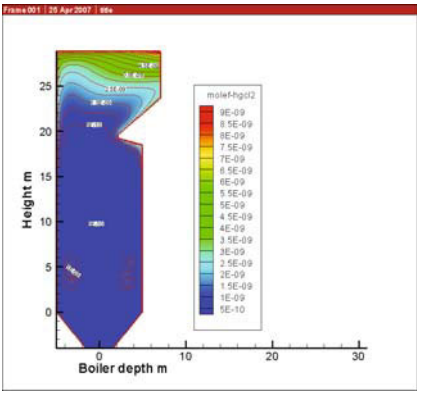

(b) $HgCl_2$ distribution in furnace

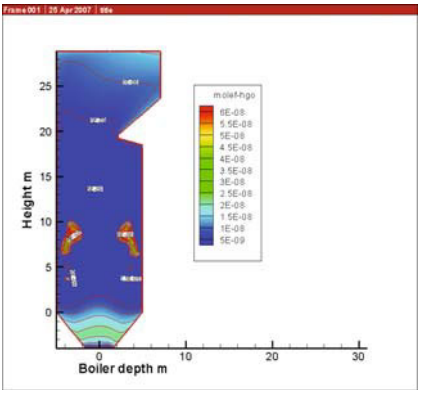

(c) HgO distribution in furnace

Fig. 4.78 Hg species distribution in furnace

Fig. 4.79 is the distribution characteristic of the Cl species in the furnace. Figs. 4.79(a), (b), (c) show the HCl, Cl_2, and Cl concentration distribution respectively. According to the figures, in the high temperature environment of the furnace, the Cl element mainly existed in the form of HCl. We could also see a band of high HCl concentration which was brought about by the pulverized coal in the primary air. Fig. 4.79(b) shows the Cl_2 concentration distribution is surprisingly similar to $HgCl_2$ in Fig. 4.78(b). It might prove that $HgCl_2$'s generation was mainly dependent on the chemical reaction of Hg and Cl_2. At the outlet region of the furnace chamber, along with the decreasing temperature, there was a large amount of Cl_2 generated here. But the absolute amount was still small compared with HCl. We could also find from Fig. 4.79(c) that in the high temperature environment of the main combustion region there was a lot of free radical Cl. But when the height of the furnace chamber was further increased, the temperature decreased gradually, and the Cl free radical disappeared.

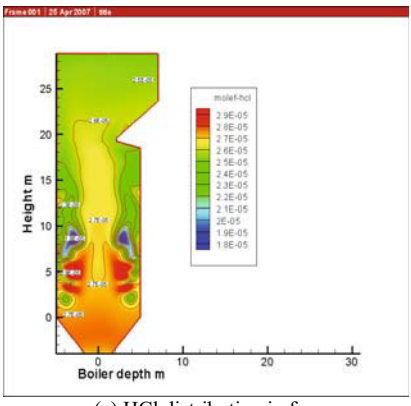

(a) HCl distribution in furnace

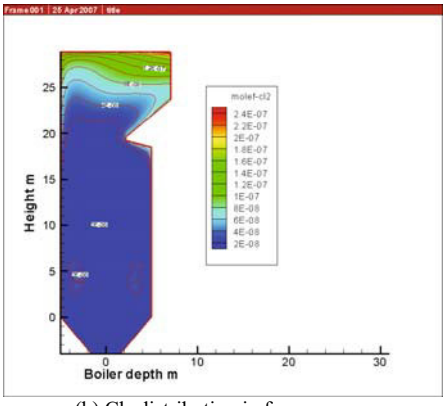

(b) Cl_2 distribution in furnace

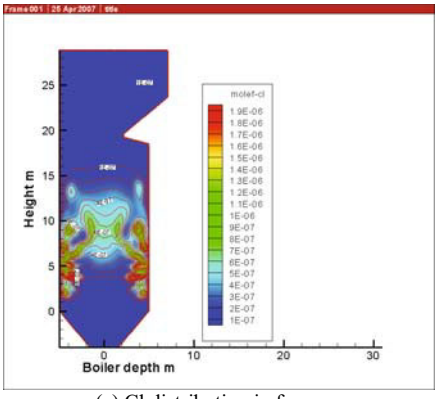

(c) Cl distribution in furnace

Fig. 4.79 Cl species distribution in furnace

Fig. 4.80 shows not only the Hg species distributed along the height of furnace chamber, it also shows the connection between the average temperature, the O_2 concentration and the Hg species distribution along the furnace. The black line is the migration curve of Hg^0. It shows that the Hg in the furnace mainly existed in the form of Hg^0. The figure also shows that, in the region from the low secondary air to the furnace chamber's outlet, the Hg^0 distribution's overall trend decreased in the burner region and then increased after the tertiary air region, then decreased again from the deflection arch to the outlet region of the furnace. The rapid decrease in Hg^0 near the burner area certainly led to the increase in Hg^{2+} concentration, especially the generation of HgO. With the alternate injection of the primary air and secondary air, the oxygen concentration was fluctuating from 0% to 3%. And with the injection of the secondary air, the oxygen was fully supplemented, which induced a small quantity of HgO generation. The highest concentration of HgO was 16.19%. When the flue gas left the burner area, the reactive oxygen component was exhausted gradually, and the HgO generating amount decreased rapidly. Then the HgO concentration remained low in part of the next region after the burner area. When the flue gas went through the outlet region of the furnace, the temperature of the flue decreased rapidly, so that it caused the HgO and $HgCl_2$ to generate again. Apart from this we could also find that because the burner area (the furnace chamber's elevation was 12670–17355 mm) had obviously high-low alternate temperature band areas, with the alternate injection of the primary air whose temperature was lower, the combustion was further intensifying after the injection of the secondary air, and the local temperature was increasing rapidly. The Hg form distribution was largely affected by the frequent variety of the flue gas component, especially the oxygen, of the burner region and the combustion condition.

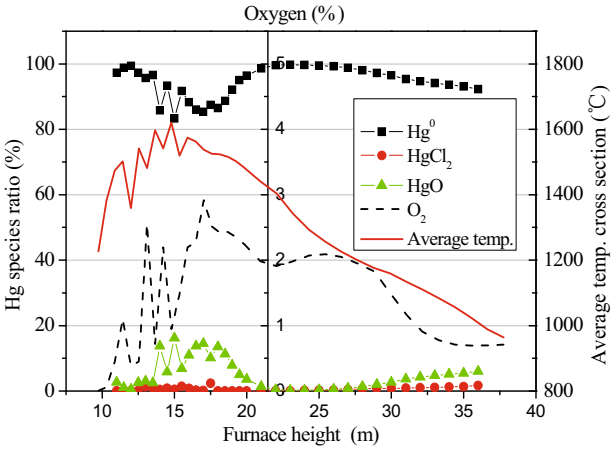

Fig. 4.80 Distribution characteristics of mercury species relative to furnace chamber height

Fig. 4.81 shows the Hg's component as percentage of each burner spout at the burner region. It was found that at different heights of the furnace chamber, the Hg speciation was slightly different. The Hg^0 concentration was relatively lower, and

the generation of Hg^0 greatly changed with the alternate injection of primary air and secondary air. The concentration improved at the primary air surface, and decreased at the secondary air surface. It was only after the injection of the primary air, that the Hg in the pulverized coal released rapidly, and led to the Hg concentration increase. Hg^0 concentration increased to nearly 100% at a height of 23–25 m just above the main burner, and then slightly decreased again.

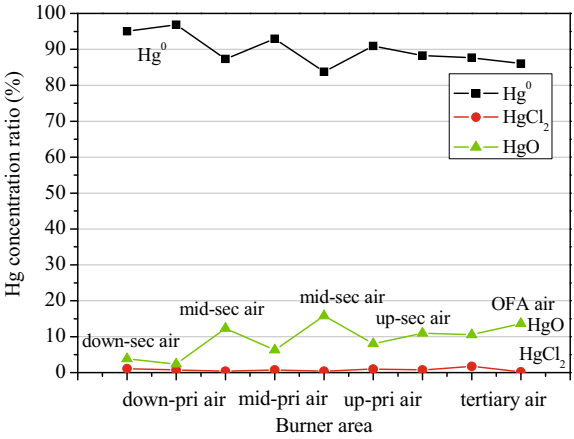

Fig. 4.81 The Hg species distribution at the burner area

The decrease in the Hg^0 in the furnace surely caused an increase in the other two Hg species, i.e. HgO and $HgCl_2$. According to the figure, the HgO concentration changed frequently, and at the Hg^0 decreasing region the HgO concentration universally increased, especially at the burner region. At the height of 15 m, about 16% HgO was generated. At the burner area, the main form was HgO. The generation of HgO greatly changed with the alternate injection of primary air and secondary air. The concentration decreased at the primary air surface, and increased at the secondary air surface. With the injection of secondary air, the rise in O_2 concentration stimulated HgO generation. And above 25 m, HgO concentration slightly rose. So while the furnace chamber temperature further reduced, the HgO concentration tended to increase.

Figs. 4.82 and 4.83 are the distribution ratios of Hg and Cl after integration into the whole three-dimensional furnace chamber. As Fig. 4.82 shows, Hg^0 in the furnace was greatest and was about 94.22% of the total. Then HgO was about 4.96%. $HgCl_2$ was only 0.82% and was the smallest. The Hg^{2+} in major form was HgO. It was different from the flue gas at the end of the flue where the major form was $HgCl_2$. Fig. 4.83 is the distribution ratio of element Cl. As can be seen from the figure, HCl was 99.23%, Cl was 0.64%, and Cl_2 was only 0.13%. Although the concentration of HCl was several orders of magnitude higher than Hg, it was still a trace element compared with O_2. So it was at a disadvantaged position during reaction competition with Hg and the Hg^{2+} in major form was HgO.

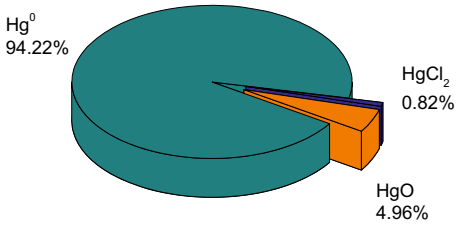

Fig. 4.82 Hg species distribution ratio after integration with the whole three dimensional furnace chamber

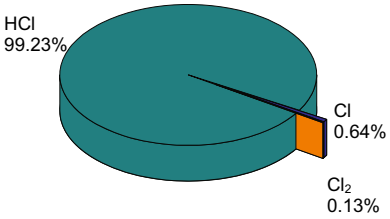

Fig. 4.83 Cl distribution ratio after integration with the whole three dimensional furnace chamber

4.5.2.4 Comparison between One-Dimensional Dynamics Simulation of Rear Heating Surface and Experimental Results

The rear low temperature section must be calculated due to the fact that the accuracy of numerical simulation did not validate test data in the high temperature section, although three-dimensional Hg formation and concentration in the furnace above were precisely simulated. A simple one-dimensional model was employed in numerical calculation of the complicated rear heating surface owing to the difficulty of three-dimensional numerical calculation. According to temperature and velocity parameters, the mean residence time of all temperature sections were calculated. Then component concentrations in the three-dimensional furnace outlet were taken into account by the one-dimensional model.

A one-dimensional dynamics simulation was employed to explore homogeneous mercury speciation along the rear heating surfaces with help of CHEMKIN3.7. While it's well recognized that under actual combustion conditions mercury formation and oxidation would be subject to kinetic control, Hall *et al*. and Widmer *et al*. proposed one-step global reaction mechanisms to model the observed depletion of Hg^0 in the presence of Cl_2 or HCl[11,34,3]. Lia *et al*.[8] studied theoretical chlorine reaction in the publication. But such mechanisms provided little insight into the details of the conversion process, let alone investigated the impact of the other flue gas components. Recently, much progress has been achieved in unraveling the reaction mechanism for homogeneous mercury oxidation through a sequence of elementary reactions. Such investigations had been done by Sliger *et al*. [6,28,34]. Of those efforts, in particular Edward *et al*. [36] provided the most complete mercury

chlorination pathways to date as well as a pathway involving HgO, with model predictions in good accord with experimental data for higher reactor temperatures but drastic under-prediction of mercury chlorination for lower temperatures. Niksa[7] developed and evaluated an elementary reaction mechanism for homogeneous Hg^0 oxidation with an emphasis on major interactions among Cl-species and other pollutants in coal-derived exhausts. Xu *et al*.[37] also developed the kinetic model consisting of 107 reactions and 30 species. This kinetic model included the oxidation and chlorination of key flue-gas components, as well as six mercury reactions involving HgO with new reaction rate constants calculated neither from experimental data nor by estimation, which was commonly used by other investigators before, but directly from transition state theory (TST). Furthermore, approximately 10% of the mercury was observed to be present as HgO at lower temperature as seen by Gullett *et al*.[38]. Senior *et al*. [1] suggested that HgO production might be significant for coals with low chlorine content. Therefore a mechanism for HgO should be involved, especially under conditions of high oxygen concentration and low chlorine concentration at low temperature.

Consequently, based on the achievements and efforts beforehand, the homogeneous mercury speciation in combustion-generated flue gases was modeled by a detailed kinetic model consisting of 94 reactions and 31 species which involved free radicals i.e.O_3, OH, O and other reaction agents. This kinetic model included the oxidation and chlorination of key flue-gas components from the NIST database which were well recognized and verified by the experimental data by Sliger *et al*.[6,28,34].

Furthermore, 14 mercury reactions were proposed, involving Hg chlorination (HgCl, $HgCl_2$) which were built by Widmer and West[3] (Reactions from Nos. 1–8 as tabulated in Table 4.17) and also commonly used by other investigators before. And the important and previously unrecognized pathway of homogeneous the Hg oxidation mechanism concerning Hg reactions involving HgO was developed as well. HgO reactions are listed from Nos. 9–13 in Table 4.17. The detailed kinetics model consists of 31 species, i.e. C, CO, CO_2, Cl, Cl_2, ClO, ClO_2, H, H_2, HCl, H_2O, HO_2, O_3, H_2O_2, HOCl, O, O_2, OH, N_2, Hg, HgCl, $HgCl_2$, HgO, SO_2, NO, H_2S, S, NO_2, NO_3, HNO and HNO_3.

The formulation of the homogeneous mercury reaction mechanism started with the kinetic framework of Widmer *et al*., the key flue-gas components and together with our work with HgO reaction as tabulated in Table 4.17 [3]. The rate coefficients are in the modified Arrhenius form, $k=AT^{\beta}\exp(-E_a/(RT))$. The external factors considered involved a temperature from 400 K to 1800 K and constant pressure of 1.0 atm. And the sub-mechanisms were taken directly from the literature and used without modification. Sub-mechanisms involving other key gas components typically found in flue gas included Cl/H/OH reaction systems developed by Baulch *et al*.[39]. They were adopted here, and other sub-mechanisms include those of Atkinson *et al*.[40] for Cl/HO_2/HOCl systems, Tsang *et al*. for H/HO_2/HNO/OH systems, Boughton *et al*. for HNO_3/H/NO reaction systems and other reaction systems in Table 4.17 in their entirety. In total, 94 elementary reactions and 31 species were involved in this present kinetic model.

Table 4.17 Detailed kinetic parameters of 94 reactions and 31 species

No.	Reactions	A (cm^3/(mol·s))	β	E_a (cal/mol)	Resources
1	Hg+Cl+M=HgCl+M	2.40E8	1.4	−14400	Widmer and West[3]
2	Hg+Cl_2=HgCl+Cl	1.39E14	0.0	34000	Widmer and West[3]
3	HgCl+Cl_2=$HgCl_2$+Cl	1.39E14	0.0	1000	Widmer and West[3]
4	HgCl+Cl+M=$HgCl_2$+M	2.19E18	0.0	3100	Widmer and West[3]
5	Hg+HOCl=HgCl+OH	4.27E13	0.0	19000	Widmer and West[3]
6	Hg+HCl=HgCl+H	4.94E14	0.0	79300	Widmer and West[3]
7	HgCl+HCl=$HgCl_2$+H	4.94E14	0.0	21500	Widmer and West[3]
8	HgCl+HOCl=$HgCl_2$+OH	4.27E13	0.0	1000	Widmer and West[3]
9	Hg+NO_3=HgO+NO_2	2.41E09	0.0	0.0	This work
10	H_2O_2+Hg=HgO+H_2O	5.12E05	0.0	0.0	This work
11	Hg+ O_3=HgO+O_2	1.8E04	0.0	0.0	This work
12	Hg+OH=HgO+H	7.23E10	0.0	0.0	This work
13	O+Hg=HgO	7.23E10	0.0	0.0	This work
14	Hg+Cl=HgCl	8.37E11	0.0	−413	This work
15	Cl+Cl+M=Cl_2+M	2.23E14	0.0	−1800	Baulch *et al.*[39]
16	H+Cl+M=HCl+M	7.19E21	−2.0	0.0	Baulch *et al.*[39]
17	HCl+H=H_2+Cl	1.69E13	0.0	4133	Adusei *et al.* [44]
18	H+Cl_2=HCl+Cl	8.59E13	0.0	1172	Baulch *et al.*[39]
19	O+HCl=OH+Cl	4.26E10	2.87	3517	Mahmud *et al.* [45]
20	OH+HCl=Cl+H_2O	3.27E11	1.65	−223	Ravishankara *et al.* [46]
21	O+Cl_2=ClO+Cl	6.17E12	0.0	3577	Bradley *et al.* [47]
22	O+ClO=Cl+O_2	1.57E13	0.0	−193	Ongstad *et al.* [48]
23	Cl+HO_2=HCl+O_2	1.08E13	0.0	−338	Atkinson *et al.* [49]
24	Cl+HO_2=OH+ClO	2.47E13	0.0	894	Atkinson *et al.* [49]
25	Cl+H_2O_2=HCl+HO_2	12.800	0.0	1947	Atkinson *et al.* [50]
26	ClO+H_2=HOCl+H	6.03E11	0.0	14100	Atkinson *et al.* [50]
27	H+HOCl=HCl+OH	1.69E13	0.0	4133	Adusei *et al.* [51]
28	Cl+HOCl=HCl+ClO	4.17E09	4.07	−337	Wang *et al.* [52]
29	Cl_2+OH=Cl+HOCl	1.02E12	0.0	1810	Boodaghian *et al.* [53]
30	O+HOCl=OH+ClO	6.03E12	0.0	2583	Atkinson *et al.* [40]
31	OH+HOCl=H_2O+ClO	1.81E12	0.0	994	DeMore *et al.* [54]
32	HOCl+M=OH+Cl+M	10.250	−3.0	56720	Atkinson *et al.* [49]
33	Cl+Cl=Cl_2	2.0E15	0.0	0.0	Song *et al.* [55]
34	HCl+O_3=HOCl+O_2	2.83	0.0	0.0	Leu *et al.* [56]
35	H+HO_2=OH+OH	8.22E12	0.75	0.0	Shaw [57]

36	$NO_2+HO_2=HNO_2+O_2$	2.2E-01	0.0	0.0	Glaenzer *et al.* [58]
37	$NO+HO_2=HNO+O_2$	5.84E05	0.0	5600	Howard [59]
38	$NO+HO_2=NO_2+OH$	6.32E11	0.58	1430	Chakraborty *et al.* [60]
39	$NO+HO_2=HNO_3$	3.47E12	0.0	−5720	Howard [59]
40	$H_2O+HO_2=H_2O_2+OH$	2.80E13	0.0	32790	Lloyd [61]
41	$H_2O_2+HO_2=O_2+H_2O+OH$	6.03E10	0.0	0.0	Vardanyan *et al.* [62]
42	$SO_2+HO_2=SO_3+OH$	1.21E07	0.0	0.0	Burrows *et al.* [63]
43	$OH+HO_2=O_2+H_2O$	4.28E13	−0.21	110	Gonzalez *et al.* [64]
44	$HO_2+HO_2=H_2O_2+O_2$	1.87E12	0.0	1540	Baulch *et al.* [39]
45	$CO+HO_2=OH+CO_2$	1.50E14	0.0	23650	Warnatz [65]
46	$HO_2=H+O_2$	1.45E16	−1.18	48490	For [41]
47	$O_3+H_2S=H_2O+SO_2$	1.58E12	0.0	5210	Glavas *et al.* [66]
48	$H_2S=S+H_2$	1.90E14	0.0	65380	Woiki [67]
49	$CO+OH=CO_2+H$	0.151E08	1.300	−758.000	Warnatz [65]
50	$NO_2+NO_3=N_2O_5$	7.98E17	−3.9	0.0	DeMore *et al.* [54]
51	$N+NO_2=O+O+N_2$	1.30E-01	0.0	0.0	Phillips *et al.* [68]
52	$NO_2+SO_2=NO+SO_3$	6.31E12	0.0	27030	Armitage *et al.* [69]
53	$NO_2+H=NO+OH$	2.41E14	0.0	680	DeMore *et al.* [54]
54	$NH+NO=N_2+OH$	3.53E12	−0.5	120	Bozzelli *et al.* [70]
55	$NO+NO=O_2+N_2$	3.10E13	0.0	63190	Yuan *et al.* [71]
56	$NO+N_2O=NO_2+N_2$	1.73E11	2.23	46300	Mebel *et al.*.[72]
57	$H+O_2+M=HO_2+M$	3.61E17	−0.72	0.0	Michael *et al.* [73]
58	$H+H+M=H_2+M$	1.0E18	−1.0	0.0	Cohen *et al.* [74]
59	$H+H+H_2=H_2+H_2$	9.2E16	−0.6	0.0	Baulch *et al.* [39]
60	$H+H+H_2O=H_2+H_2O$	6.0E19	−1.25	0.0	Baulch *et al.* [39]
61	$H+OH+M=H_2O+M$	1.6E22	−2.0	0.0	Baulch *et al.* [39]
62	$H+O+M=OH+M$	6.2E16	−0.6	0.0	Tsang *et al.* [41]
63	$O+O+M=O_2+M$	1.89E13	0.0	−1788	Tsang *et al.* [41]
64	$H_2O_2+M=OH+OH+M$	1.3E17	0.0	45500	Baulch *et al.* [39]
65	$H_2+O_2=2OH$	1.7E13	0.0	48100	Jachimowski *et al.* [75]
66	$OH+H_2=H_2O+H$	1.17E9	1.3	3626	Baulch *et al.* [39]
67	$O+OH=O_2+H$	3.61E14	−0.5	0.0	Miller [76]
68	$O+H_2=OH+H$	5.06E4	2.67	6290	Baulch *et al.* [39]
69	$O+HO_2=O_2+OH$	1.4E13	0.0	1073	Baulch *et al.* [39]
70	$2OH=O+H_2O$	6.0E8	1.3	0.0	Tsang *et al.* [41]
71	$H+HO_2=H_2+O_2$	1.25E13	0.0	0.0	Tsang *et al.* [41]
72	$H_2O_2+H=HO_2+H_2$	1.6E12	0.0	3800	Baulch *et al.* [39]

73	$N+O_2=NO+O$	6.40E09	1.0	6280	Baulch *et al.* [77]
74	$N+OH=NO+H$	3.80E13	0.0	0.0	Baulch *et al.*[78]
75	$N+CO_2=NO+CO$	1.90E11	0.0	3400	Avramenko *et al.* [79]
76	$NO+OH=HNO_2$	5.45E17	0.0	0.0	Pagsberg *et al.* [80]
77	$O+HNO_2=NO_2+OH$	1.21E13	0.0	5962	Tsang *et al.* [41]
78	$NO_2+NH_3=NH_2+HNO_2$	6.70E08	3.41	29810	Mebel *et al.* [72]
79	$H+HNO_2=HNO+OH$	7.57E12	0.86	4968	Hsu [81]
80	$H+HNO_2=NO_2+H_2$	1.37E12	1.55	6617	Hsu [81]
81	$H+HNO_2=NO+H_2O$	3.85E11	1.89	3855	Hsu [81]
82	$O_3+HNO_2=O_2+HNO_3$	3.01E05	0.0	0.0	DeMore *et al.* [54]
83	$HNO_3+O=NO_3+OH$	1.81E07	0.0	0.0	DeMore *et al.* [54]
84	$HNO_3+H=NO_3+H2$	3.4E12	1.53	16332	Boughton *et al.* [81]
85	$HNO_3+H=NO_2+H_2O$	8.39E09	3.29	6280	Boughton *et al.* [81]
86	$HNO_3+NO=NO_2+HNO_2$	4.48E03	0.0	0.0	Svensson *et al.* [82]
87	$HNO_3+OH=NO_3+H_2O$	4.82E10	0.0	0.0	Smith *et al.* [83]
88	$HNO_3+OH=NO_2+H_2O_2$	4.82E08	0.0	0.0	Connell *et al.* [84]
89	$HNO_3=NO_2+OH$	6.90E17	0.0	45900	Chakraborty *et al.* [60]
90	$HNO+O=NO+OH$	2.29E13	0.0	0.0	Inomata *et al.* [85]
91	$HNO+HNO=N_2O+H_2O$	2.55E07	3.98	1192	He *et al.* [86]
92	$HNO+H=NO+H_2$	2.7E13	0.72	654	Soto *et al.* [87]
93	$HNO+NO_2=NO+HNO_2$	6.03E11	0.0	1987	Tsang *et al.* [41]
94	$HNO+OH=NO+H2O$	4.82E+13	0.0	994	Tsang *et al.* [41]

In general, coal-fired gas was released from combustion in the furnace and injected into the rear heating surfaces, which followed a platen superheater, high temperature superheater, high temperature reheater, steering room, updraft economizer, updraft air preheater, downdraft economizer, downdraft air reheater, electrostatic precipitator along the rear flue, as stated in this unit. According to the operating condition, temperature from the furnace outlet to electrostatic precipitator was measured on line and arranged from 1，434 K to 373 K. Here, total residence time was defined as about 5 s as estimated from the platen superheater, so the corresponding residence time of each surface is given in Fig. 4.84.

Table 4.18 included components in a one-dimensional dynamics model derived from the mean value calculated in a three-dimensional furnace outlet surface and the typical species consisting of N_2, O_2, CO_2, H_2O, CO, SO_2, NO, H_2S, HCl, Cl_2, Cl, H_2, H, OH, and three forms of mercury compound (Hg, $HgCl_2$, HgO) were taken into consideration in the model. Key gas and Hg formation distribution in the rear heating surface was calculated by SENKIN module from CHEMKIN3.7. And the calculation results with Hg^0 and mercury oxide forming along the rear surfaces, corresponding to the reduction in the rear temperature, are demonstrated in Figs. 4.85 and 4.86. The Hg^0 remained constant at the beginning, and slightly decreased

with the temperature decrease along the rear heating surface, and Hg^0 dropped dramatically after 3.4 s, especially at the exit of the downdraft economizer. Whereas the mercury oxide such as $HgCl_2$, HgCl and HgO appeared and increased a little with the resident time increase, the amount of $HgCl_2$ appearing was dominant, fitting in well with Hg^{2+} production. Definitely, $HgCl_2$ speeded up greatly after a residence time of 3.4s corresponding to the area between downdraft air preheaters and the electrostatic precipitator (temperature 540 – 383 K).

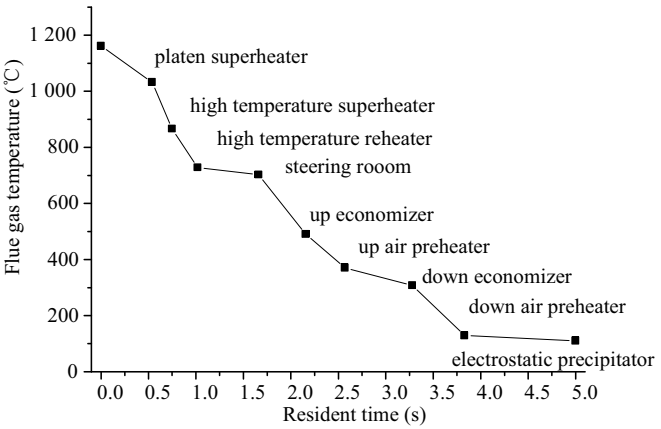

Fig. 4.84 Rear heating surface temperature distribution and its residence time

Table 4.18 Simulation input component parameter (mole fraction)

N_2	O_2	CO_2	H_2O	CO	SO_2	NO	H_2S	HCl
0.74	0.03	0.17	0.06	5.23E-04	3.00E-04	3.00E-04	5.84E-05	2.51E-05
Cl_2	Cl	H_2	H	OH	Hg	$HgCl_2$	HgO	
1.80E-07	1.70E-10	1.52E-04	1.71E-04	1.20E-04	9.54E-10	3.90E-11	7.02E-11	

Note: All parameters derive from integral value calculated in three-dimensional furnace outlet surface

From Fig. 4.86, Hg^0 concentration at the furnace outlet was about 8.52 μg/m^3, and Hg^{2+} content was 1.15 μg/m^3. HgO and $HgCl_2$ were 0.68 and 0.47 μg/m^3 individually. Hg^0 concentration reduced with rear flue temperature decrease. Meanwhile, Hg^{2+} concentration was constantly enhanced due to a great deal of $HgCl_2$ generation instead of HgO. However, the rear temperature hardly had an effect on HgO production, so HgO concentration continuously remained constant with the resident time going up. That was because the low temperature helped $HgCl_2$ production with the existence of Cl_2. Sometimes Cl_2 was actively superior to oxygen, and HgO was oxidized to $HgCl_2$ possibly. Furthermore, intermediate production HgCl slightly increased with an Hg^0 concentration decrease and Hg^{2+} concentration enhancement by comparison between Figs. 4.85 and 4.86.

Hg^{2+} content rose to 4.3 μg/m^3 in flue gas at the outlet of the electrostatic precipitator. Fig. 4.87 illustrated that the temperature decrease induced Cl_2 generation

employing the occurrence of an oxidizing reaction with Hg^0. Cl component concentration varied with residence time as shown in Fig. 4.87. Free radical Cl had a peak value of 0.4 ppm at the beginning of the reaction, whereas it was fast reduced. Cl_2 gradually generated 1 s of residence time later, the highest concentration 0.1 ppm appeared by undergoing stable steps of 1–1.7 s and 2.5–5 s. Consequently, $HgCl_2$ generated was due to the existence of Cl_2. The influence of HCl concentration on Hg oxidization was very little (Fig. 4.88), although its concentration had a high value of 25 ppm. HCl concentration had a fluctuation trend at an earlier stage. Moreover, there was little obvious concentration variety at 2–5 s reaction stage. Definitely, Cl_2 was the key active component participating in Hg oxidizing reaction in the rear flue instead of other chlorine compounds, as the model indicated, which was in good accordance with the literature[7]. Nevertheless, the oxidation was governed primarily by HCl concentration, quench rate and background gas composition[6]. The mercury oxidation mechanism bears further investigation.

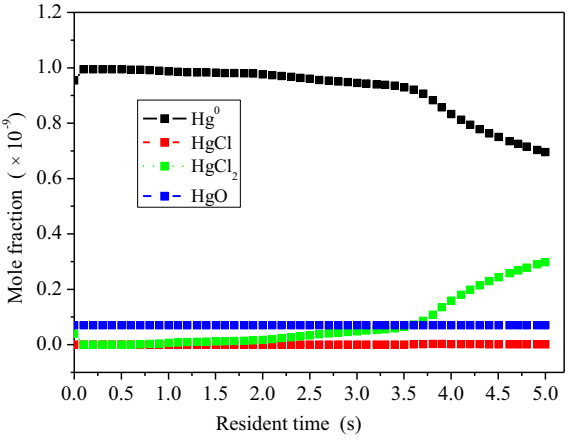

Fig. 4.85 Hg transformation in rear flue

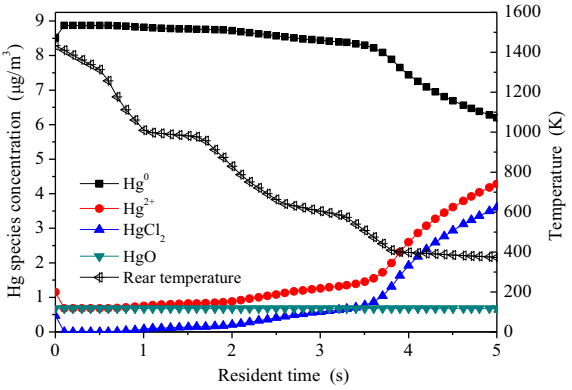

Fig. 4.86 Hg distribution proportion in rear flue

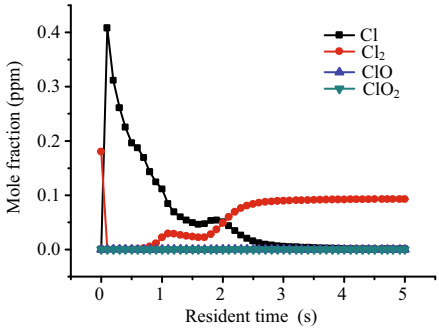

Fig. 4.87 Cl component transformation

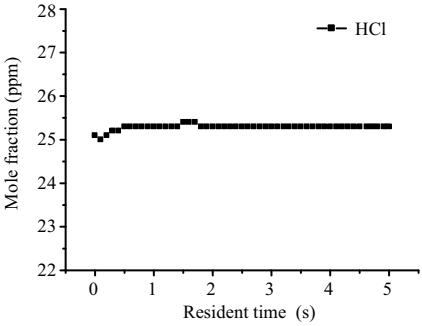

Fig. 4.88 HCl concentration transformation

The comparative result between the field test results on the 410 tons/h station boiler and the calculation results were identified here. The field test data came from CEM in-situ measurement on line at the outlet of the electrostatic precipitator (ESP). The results data derived from the gaseous Hg^0 and gaseous Hg^{2+} content were 51.63% and 48.37% by field test, respectively, while those of content of gaseous Hg^0 and gaseous Hg^{2+} were denoted as 59.18% and 40.82% by simulation calculation. Usually, the field testing of mercury could not be precisely enough conducted owing to mercury being absorbed by flying ash, low residue, heating surfaces and mercury oxidation or catalyzed by mineral substances in fly ash during the practical boiler operation.

Although a small deviation occurred between them, the simulation data was satisfactory, fitting well with CEM in-situ measurement data of mercury species concentrations. Therefore, this kind of CFD model was validated to do the modeling of mercury distribution during the combustion process, and even the 1-D dynamic model for the rear flue worked as well. But of course, it needs to be investigated further.

4.6 Summary

In this chapter, the mercury speciation transformation during coal combustion was discussed completely using different research methods.

In the research of mercury emissions from coal of different combustion types, the behavior of mercury emissions was checked by heating coal in a fixed quartz tube furnace, a pulverized coal boiler and circulating fluidized-bed bench tests, respectively. From the experimental results of coal burning in a fixed bed and a state of suspension, the ratios of $Hg_{(g)}$ and Hg^p were found to be similar. The ratio of $Hg_{(g)}$, Hg^p in the flue gas from the three different combustion methods indicated that $Hg_{(g)}$ was the main speciation emission when coal was fired. Given the conditions of the three different combustion methods, the speciation distributions of Hg^{2+} and Hg^0 were similar. Coal burning in a fixed bed increased the Hg^0 concentration, which

may be attributed to the shorter gas cooling process and the shorter reaction time in the experiment. The concentration of $Hg_{(g)}$, when using the fluidized-bed combustion method, was slightly lower than that when using the suspension combustion method. This may be attributed to the high proportion of burning stone coal, the addition of limestone in some conditions, and the high concentration of fly ash. These factors enhanced the mercury adsorption by particles, thus reducing the concentration of $Hg_{(g)}$.

Based on the previous studies and the experiments, the apparent reaction kinetic model for the combination of mercury and HCl was established. The model was used to predict the degree of transformation from Hg^0 to Hg^{2+} in a coal-fired flue gas. The model mainly considered the reaction between mercury and HCl which could be applied to predict the impact of HCl concentration, residence time, reaction temperature, Hg/Cl, etc., on the oxidation of Hg^0 to Hg^{2+}.

With increasing HCl concentration during the same residence time, the Hg^0 concentration reduced. It was because increasing HCl was equivalent to increasing Cl as the mercury oxidant. In addition, with a low HCl concentration, the impact on mercury transformation from increased HCl concentration was relatively significant. The reaction temperature increased while the Hg^0 concentration dropped, indicating that a higher temperature in a certain temperature range promoted the oxidation of Hg^0. At lower HCl concentration, when the residence time was shorter, the transformation of mercury speciation was less affected by temperature; when the residence time was longer, the impact became more significant. When all other conditions were unchanged, the increase in gas residence time decreased the amount of Hg^0. It meant that a longer retention period increased the oxidation of Hg^0, and that mercury oxidation in flue gas usually was far from a theoretically balanced state because the residence time was usually less than reaction time in theory. With the increasing concentration of Hg^0 inlet mercury in the same residence time, the concentration of Hg^0 gradually increased, thus leading to a reduced transformation rate. Cl/Hg increased while the concentration of Hg^0 dropped. It meant that higher Cl/Hg increased the oxidation rate of Hg^0 under certain conditions. Cl/Hg could be considered as a parameter in the discussion of regulating mercury oxidation in coal-fired flue gas.

Based on the chemical thermodynamic equilibrium calculation result, mercury speciation was dominating as Hg^0 in high temperature combustion conditions. The thermodynamic equilibrium calculations suggested that mercury oxidation was the most sensitive to inlet O_2, HCl, SO_2, and insensitive to NO. But by comparison, HCl displayed a stronger oxidation ability than O_2 and SO_2. With the concentration of O_2, HCl, SO_2 improvement, Hg^0 began to be oxidized at higher temperature and also kept a similar tendency. If HCl gas is typically included in flue gas, mercury oxidation could be achieved at higher temperature. As the flue gas cools along the tail surface area, mercury oxidation would happen, altering from Hg^0 into mercuric chloride, transferring from mercuric chloride into mercuric sulfate sometimes. In particular, mercury was a mixture of mercuric sulfate, gaseous mercuric chloride and gaseous mercury oxide in the flue gas entering the desulfurization tower according to estimations from the model. In general, mercuric chloride and mercury

oxide are water-soluble oxidized species, and are more readily removed from flue gases in scrubber systems. And mercuric sulfate consists of small particle-bounded species, which would be absorbed and deposited by serous fluid in the desulfurization tower. Therefore, mercury oxide would be preferred in the stack gases and eliminated easily.

Modelling and numerical simulation of combustion and mercury species formation, distribution and transformation process in a 410 tons/h coal-fired boiler was conducted based on the platform supplied by FLUENT6.2 software, integrated with a sub-model with mercury reaction kinetics. The simulation results were calculated continuously according to various retention times of the rear flue, which were obtained from the 1-D dynamic model. The simulation data fits well with CEM in-situ measurement data of mercury species concentrations at a real 250 M. The kind of CFD model was validated to do the mercury modeling distribution during the combustion process, and even the 1-D dynamic model for the rear flue worked as well. The 1-D dynamic model was utilized to do calculation with the platform of CHEMKIN4.7.

In regard to the 3-D simulation during the combustion process, the mechanism of mercury species formation, reaction, oxidation, transformation was employed to study, complicated phenomena of physical or chemical reaction were revealed in the furnace, esp. mercury species at higher temperatures, divalent mercury oxide (HgO) exists as well except for Hg^0, which differed with the previous literature, which helps to limit mercury emission in an appreciate way efficiently and economically. In some cases, activated carbon was injected into the furnace to absorb the mercury possibly.

In view of the simulation data agreeing well with measurement in-situ data, the simulation work seems to be accurate and reliable both with the 3-D model in the furnace and the 1-D dynamic model. In terms of the CFD simulation result, mercury exists predominantly in gaseous Hg^0 in the furnace, a little amount of HgO and $HgCl_2$ coexist. Stemming from three-dimensional integration, Hg^0 is 94.22% of the total amount, HgO, $HgCl_2$ are 4.96%, 0.82%, respectively.

It is inferred that HgO formation has a close correlation with O_2, $HgCl_2$ formation has a comparatively strong correlation with Cl_2. which originates from HCl existing as a dominant Cl element, over 99%. This is attributed to the fact that Cl_2 has an extremely active impact on mercury oxidation instead of Cl.

With the temperature down along the back-end surface, Hg^0 was oxdized into $HgCl_2$, especially in a temperature range from 373–540 K, $HgCl_2$ formed swiftly, and the 10% ratio at the outlet of the furnace was increased to 40.8% rapidly. Therefore, this kind of CFD model was validated to do the modeling of mercury distribution during the combustion process, and even a 1-D dynamic model for the rear flue worked as well.

References

[1] Senior C.L., *et al*. Gas-phase transformations of mercury in coal-fired power plants. *Fuel Processing Technology*, 68(3): 197-213, 2000.

[2] Carpi A. Mercury from combustion sources: A review of the chemical species emitted and their transport in the atmosphere. *Water, Air and Soil Pollution*, 98: 241-254, 1997.

[3] Widmer N.C., West J. Thermochemical Study of Mercury Oxidation in Utility Boiler Fuel Gases. 93rd Annual Meeting, Air&Waste Management Association, Salt Lake City, Utah, 2000.

[4] Lee T.G. Hg Reactions in the presence of chlorine species: homogeneous gas phase and heterogeneous gas-solid phase. *Journal of the Air & Waste Management Association*, 52: 1316-1323, 2002.

[5] Dunham G.E., DeWall R.A., Senior C.L. Fixed-bed studies of the interactions between mercury and coal combustion fly ash. *Fuel Processing Technology*, 82(2-3): 197-213, 2003.

[6] Sliger R.N., Kramlicha J.C., Marinov N.M. Towards the development of a chemical kinetic model for the homogeneous oxidation of mercury by chlorine species. *Fuel Processing Technology*, (65-66): 423-438, 2000.

[7] Niksa S. Kinetic modeling of homogeneous mercury oxidation: the importance of NO and H_2O in predicting oxidation in coal-derived system. *Environmental Science & Technology*, 35: 3701-3706, 2001.

[8] Liu J., Wand M.H., Zheng C.G., *et al.* Reaction mechanism of mercury and gases during coal combustion. *Journal of Engineering Thermophysics*, 24(1): 161-164, 2003.

[9] Mamani-Paco R.M., Helble J.J. Bench-Scale Examination of Mercury Oxidation under Non-Isothermal Conditions. 93rd Annual Meeting & Exhibition, Air & Waste Management Association, Salt Lake City, Utah, June 18-22, 2000.

[10] Dajnak D., Lockwood F.C. Modelling of toxic heavy metal mercury partitioning from pulverized fuel combustion. *IFRF Combustion Journal*, Article Number 200103, 2001.

[11] Hall B., Schager P., Lindqvist O. Chemical reactions of mercury in combustion flue gases. *Water, Air & Soil Pollution*, 56: 3-14, 1991.

[12] Matsumura Y. Adsorption of mercury vapor on the surface of activated carbons modified by oxidation or iodization. *Atmospheric Environment*, 8: 1321-1327, 1974.

[13] Senior C.L., Morency J.R. Prediction of Mercury Speciation in Coal-Fired Power Plant Flue Gas: A Fundamental Study. Managing Hazardous Air Pollutants, Fourth International Conference, Washington, DC, November 12-14, 1997.

[14] Schager P. The Behavior of Mercury in Flue Gases. Department of Inorganic Chemistry, University of Goteburg, Goteburg, Sweden, 1990.

[15] Liu Y.H. The Migration of Trace Elements in Coal Combustion Process Changes in Behavior. Huazhong University of Science and Technology, 2002.

[16] Ren J.L. Experimental and Theoretical Study on Mercury Transformation and Sorbents Adsorption in Simulated Combustion Flue Gases. College of Mechanical and Energy Engineering, Zhejiang University, Hangzhou, 71-73. 2003.

[17] U.S. Environmental Protection Agency. U.S. EPA Clean Air Mercury Rule. Washington, DC, 2005. Available at http://www.epa.gov.
[18] He S., *et al*. Mercury oxidation over a vanadian-based selective catalytic reduction catalyst. *Energy & Fuels*, 23: 253-259, 2009.
[19] Zhou J.S., *et al*. Investigation on mercury emission during coal combustion process. *Combustion Science and Technology*, 8(2): 103-108, 2002.
[20] Wu X.J. Research on Mercury Control with Semi-Dry Adsorption During Coal Combustion. College of Mechanial and Energy Engineering, Zhejiang University, Hangzhou, 4-5, 2004.
[21] Hall B., *et al*. Mercury chemistry in simulated flue gases related to waste incineration conditions. *Environmental Science and Technology*, 24(1): 108-111, 1990.
[22] Frandsen F., *et al*. Trace element partitioning during coal gasification. *Fuel*, 20(3): 115-138, 1996.
[23] Bob H. Chemical reactions of mercury in combustion flue gases. *Water, Air and Soil Pollution*, 56(4): 3-14, 1991.
[24] Qiao Y., *et al*. The oxidation kinetics of mercury in Hg/O/H/Cl systems. *Proceedings of the CSEE*, 22(12): 138-141, 2002.
[25] Wang Q.H., *et al*. Investigation on mercury emission during coal combustion process. *Thermal Power Engineering*, 17(6): 547-550, 2002.
[26] Hall B., *et al*. The gas phase oxidation of elemental mercury by ozone. *Water, Air and Soil Pollution*, (80): 301-315, 1995.
[27] Musmarra A.L.D., *et al*. Adsorption of mercuric chloride vapors from incinerator flue gases on calcium hydroxide particle. *Combustion Science Technology*, 93(4): 277-289, 1993.
[28] Sliger R.N., *et al*. Kinetic Investigation of the High-Temperature Oxidation of Mercury by Chlorine Species. Fall Meeting, Western State Section/The Combustion Institute, Seattle, 1998.
[29] Fransden F., *et al*. Rasmussen. Progress Energy Combustion Science, 1994.
[30] Zhao Y., *et al*. Research reviews of mercury control technology in the coal-fired power plants. *Electric Power Technology and Environmental Protection*, 26(2): 31-33, 2001.
[31] Jones C. Consensus on air toxics eludes industry to date. *Power*, 138: 51-59, 1994.
[32] Chow W., Miller M.J., Torrens I.M. Pathways of trace elements in power plants: interim research results and implications. *Fuel Processing Technology*, 39: 5-20, 1994.
[33] Hou W.H., *et al*. Numerical simulation of homogeneous mercury oxidation by chemical kinetic coupled with computation fluid dynamics. *Proceedings of the CSEE*, 30(5): 23-27, 2010.
[34] Sliger R.N., Kramlicha J.C., Marinov N.M. Towards the development of a chemical kinetic model for the homogeneous oxidation of mercury by chlorine species. *Fuel Processing Technology*, (65-66): 423-438, 2000.
[35] Roesler J.F., *et al*. Kinetic interactions of CO, NO_x, and HCl emissions in post combustion gases. *Combustion and Flame, February*, 100(3): 495-504, 1995.
[36] Edwards J.R., *et al*. A study of gas-phase mercury speciation using detailed chemical kinetics. *Air & Waste Management Association*, 51: 869-877, 2001.
[37] Xu M.H., *et al*. Modeling of homogeneous mercury speciation using detailed chemical kinetics. *Combustion and Flame*, 132: 208-218, 2003.

[38] Gullett B.K. Sorbent Injection for Dioxin/Furan Prevention and Mercury Control. Multipollutant Sorbent Reactivity Workshop, Research Triangle Park, NC, July 1994.
[39] Baulch D.L.C., *et al*. Evaluated kinetic data for combustion modelling. *Journal of Physical and Chemical Reference Data*, 21: 411-429, 1992.
[40] Atkinson R.B., *et al*. Evaluated kinetic, photochemical and heterogeneous data for atmospheric chemistry: supplement V, IUPAC subcommittee on gas kinetic data evaluation for atmospheric chemistry. *Journal of Physical and Chemical Reference Data*, 26: 521-1011, 1997.
[41] Tsang W.H., *et al*. Chemical kinetic data base for combustion chemistry. Part I. Methane and related compounds. *Journal of Physical and Chemical Reference Data*, 15, 1986.
[42] Tsang W.H., *et al*. Chemical kinetic data base for propellant combustion. I. Reactions involving NO, NO_2, HNO, HNO_2, HCN and N_2O. *Journal of Physical and Chemical Reference Data*, 20: 609-663, 1991.
[43] Sommar J.H., *et al*. On the gas phase reactions between volatile biogenic mercury species and the nitrate radical. *Journal of Atmospheric Chemistry*, 27: 233-247, 1997.
[44] Adusei G.Y.F., *et al*. A high-temperature photochemistry study of the H + HCl → H_2 + Cl reaction from 298 to 1192 K. *Journal of Physical Chemistry*, 97, 1993.
[45] Mahmud K.K., *et al*. A high-temperature photochemical kinetics study of the O + HCl reaction from 350 to 1480 K. *Journal of Physical Chemistry*, 94: 2994-2998, 1990.
[46] Ravishankara A.R.W., *et al*. Kinetic study of the reaction of OH with HCl from 240-1055 K. *International Journal of Chemical Kinetics*, 17, 1985.
[47] Bradley J.N.W., *et al*. Electron spin resonance study of the reaction of O(3P) atoms with chlorine and nitrosyl chloride. *Journal of the Chemical Society, Faraday Transactions*, 1:69, 1973.
[48] Ongstad A.P.B., *et al*. Studies of reactions of importance in the stratosphere. VI. Temperature dependence of the reactions O + NO_2 → NO + O_2 and O + ClO → Cl + O_2. *Journal of Physical Chemistry*, 85, 1986.
[49] Atkinson R.B., *et al*. Summary of Evaluated Kinetic and Photochemical Data for Atmospheric Chemistry. 1-56, 2001.
[50] Atkinson R.B., *et al*. Evaluated kinetic and photochemical data for atmospheric chemistry: Volume III-gas phase reactions of inorganic halogens. *Atmospheric Chemistry and Physics*, 7: 981-1191, 2007.
[51] Adusei G.Y.F., *et al*. A high-temperature photochemistry study of the H + HCl → H_2 + Cl reaction from 298 to 1192 K. *Journal of Physical Chemistry*, 97: 1409-1412, 1993.
[52] Wang L.L., *et al*. Theoretical Study and Rate Constant Calculation of the Cl + HOCl and H + HOCl Reactions. *Journal of Physical Chemistry A*, 107: 4921-4928, 2003.
[53] Boodaghians R.B.H., *et al*. Kinetics of the reactions of the hydroxyl radical with molecular chlorine and bromine. *Journal of the Chemical Society, Faraday Transactions*, 2: 83, 1987.
[54] DeMore W.B.S., *et al*. Chemical kinetics and photochemical data for use in stratospheric modeling. Evaluation number 12. *JPL Publication*, 97(4): 1-266, 1997.

[55] Song T.T.S., *et al*. Recombination reactions of atomic chlorine in compressed gases. 2. Geminate and nongeminate recombinations and photolysis quantum yields with argon pressure up to 180 bar. *Journal of Physical Chemistry*, 100: 13554-13560, 1996.

[56] Leu M.T., *et al*. Rate constants for reactions between atmospheric reservoir species. 1. HCl. *Journal of Physical Chemistry*, 93: 5778-5784, 1989.

[57] Shaw R. Estimation of rate constants as a function of temperature for the reactions W + XYZ = WX + YZ, where W, X, Y, and Z are H or O atoms. *International Journal of Chemical Kinetics*, 9, 1977.

[58] Glaenzer K.T., *et al*. HO_2 formation in shock heated HNO_3-NO_2 mixtures. *Berichte der Bunsengesellschaft für physikalische Chemie*, 79, 1975.

[59] Howard C.J. Temperature dependence of the reaction $HO_2 + NO \rightarrow OH + NO_2$. *Journal of Chemical Physics*, 91, 1979.

[60] Chakraborty D.P., *et al*. Theoretical study of the $OH + NO_2$ reaction: formation of nitric acid and the hydroperoxyl radical. *Journal of Chemical Physics*, 231: 39-49, 1998.

[61] Lloyd A.C. Evaluated and estimated kinetic data for phase reactions of the hydroperoxyl radical. *International Journal of Chemical Kinetics*, 6: 169-228, 1974.

[62] Vardanyan I.A.S., *et al*. Kinetics and mechanism of formaldehyde oxidation-II. *Combustion and Flame*, 22: 153-159, 1974.

[63] Burrows J.P.C., *et al*. Atmospheric reactions of the HO_2 radical studied by laser magnetic resonance spectroscopy. *Proceedings of the Royal Society of London A*, 368: 463-481, 1980.

[64] Gonzalez C.T., *et al*. Kinetics of the reaction between OH and HO_2 on the triplet potential energy surface. *Journal of Physical Chemistry*, 96: 1767-1774, 1992.

[65] Warnatz J. Rate coefficients in the C/H/O system. *Combustion Chemistry*, 1984.

[66] Glavas S.T., *et al*. Reaction between ozone and hydrogen sulfide. *Journal of Physical Chemistry*, 79, 1975.

[67] Woiki D.R., *et al*. Kinetics of the high-temperature H_2S decomposition. *Journal of Physical Chemistry*, 98: 12958-12963, 1994.

[68] Phillips L.F.S., *et al*. Mass-spectrometric studies of atomic reactions. V. The reaction of nitrogen atoms with NO_2. *Journal of Chemical Physics*, 42: 3171-3174, 1995.

[69] Armitage J.W.C., *et al*. Studies of the reaction between nitrogen dioxide and sulfur dioxide. *Combustion and Flame*, 16, 1971.

[70] Bozzelli J.W.C., *et al*. Analysis of the reactions $H + N_2O$ and NH + NO: pathways and rate constants over a wide range of temperature and pressure. *Symposium (International) on Combustion*, 25: 965-974, 1994.

[71] Yuan E.L.S., *et al*. Kinetics of the decomposition of nitric oxide in the range 700-1800 °C. *Journal of Physical Chemistry*, 63: 952-956, 1959.

[72] Mebel A.M.L., *et al*. Reactions of NO_x with nitrogen hydrides. *International Reviews in Physical Chemistry*, 16: 249-266, 1997.

[73] Michael J.V.S., *et al*. Rate constants for $H + O_2 + M \rightarrow HO_2 + M$ in seven bath gases. *Journal of Physical Chemistry A*, 106: 5297-5313, 2002.

[74] Cohen N.W., *et al*. Chemical kinetic data sheets for high-temperature chemical reactions. *Journal of Physical Chemistry Reference Data*, 12, 1983.

[75] Jachimowski C.J.H., *et al*. Shock-tube study of the initiation process in the hydrogen-oxygen reaction. *Combustion and Flame*, 17, 1971.
[76] Miller J.A. Nonstatistical effects and detailed balance in quasiclassical trajectory calculations of the thermal rate coefficient for O + OH → O_2 + H. *Journal of Chemical Physics*, 84, 1986.
[77] Baulch D.L.C., *et al*. An assessment of rate data for high-temperature systems. *Symp. Int. Combust. Proc.*, 14: 107-118, 1973.
[78] Baulch D.L.C., *et al*. Evaluated kinetic data for combusion modelling. Supplement I. *Journal of Physical Chemistry Reference Data*, 23: 847-1033, 1994.
[79] Avramenko L.I., *et al*. Reactions of nitrogen atoms communication 6. Rate constant and mechanism of the elementary reaction of nitrogen atoms with carbon dioxide. *Bulletin of the Academy of Sciences of the USSR, Division of Chemical Science (Engl. Transl.)*, 501-503, 1967.
[80] Pagsberg P.B., *et al*. Kinetics of the gas phase reaction OH + NO(+M) → HONO(+M) and the determination of the UV absorption cross sections of HONO. *Chemical Physics Letters*, 272: 383-390, 1997.
[81] Boughton J.W.K., *et al*. Theoretical study of the reaction of hydrogen with nitric acid: ab initio MO and TST/RRKM calculations. *Journal of Chemical Physics*, 214: 219-227, 1997.
[82] Svensson R.L., *et al*. A kinetic study of the decomposition of HNO_3 and its reaction with NO. *International Journal of Chemical Kinetics*, 20, 1988.
[83] Smith I.W.M.Z., *et al*. Rate measurements of OH by resonance absorption. IV. Reactions of OH with NH_3 and HNO_3. Proc. Symp. Chem. Kinet. Data Upper Lower Atmos, 1974, 1975.
[84] Connell P.S.H., *et al*. Kinetics study of the reaction HO + HNO_3. *International Journal of Chemical Kinetics*, 17, 1985.
[85] Inomata S.W., *et al*. Rate constants for the reactions of NH_2 and HNO with atomic oxygen at temperatures between 242 and 473 K. *Journal of Physical Chemistry A*, 103: 5023-5031, 1999.
[86] He Y.L., *et al*. Effects of nitric oxide on the thermal decomposition of methyl nitrite: overall kinetics and rate constants for the HNO + HNO and HNO + 2NO reactions. *International Journal of Chemical Kinetics*, 24: 743-760, 1992.
[87] Soto M.R.P., *et al*. Ab initio variational transition-state-theory reaction-rate calculations for the gas-phase reaction H + HNO → H_2 + NO. *Journal of Chemical Physics*, 97: 287-7296, 1992.

5

Mercury Control and Mercury Stability in Byproducts

5.1 Introduction

As stated previously, coal burning is one of the major sources of mercury pollution in China. Here, Hg^0 and Hg^{2+} are main mercury speciation in flue gas from coal-fired power plants. Generally, water-soluble Hg^{2+} is relatively easy to remove by water scrubber. However, Hg^0 is very difficult to control[1,2]. Currently, more studies have focused on using activated carbon or other sorbents to remove $Hg_{(g)}$ from coal-fired flue gas.

Powdered carbon has been used for removing mercury from flue gas from incinerator plants[3]. According to previous studies, powdered carbon can adsorb $Hg_{(g)}$ with high efficiency[4,5,6,7]. Activated carbon, which is usually modified by adding iodine, chlorine, sulfur compounds, etc., can enhance the adsorption of Hg^0. However, modified activated carbon can increase production costs. Many factors, including the characteristic of activated carbon, the running condition of adsorption, etc., influence the adsorption efficiency of mercury; thus, the adsorption mechanism of mercury using activated carbon remains unclear[8,9].

Mercury removal using activated carbon can be conducted in two ways: through the injection of powdered activated carbon (PAC) before a particle removal device[5], and through the utilization of the adsorption bed of granular activated carbon (GAC)[10]. Other types of sorbents, which mainly include fly ash, calcium-based sorbents, precious metals, etc., are not very efficient in mercury adsorption[11,12,13].

Zhejiang University and several other domestic universities and research institutions have been engaged in various projects on coal-fired mercury control technology for over 20 years, and the researchers have achieved some results during these years. This section introduces the findings of Zhejiang University on the adsorbent control of mercury emissions in flue gas, including the adsorption performance of different mercury sorbents, the development of new adsorbents, the mechanism of activated carbon adsorption of mercury in flue gas, and the stability of mercury in the adsorption product.

5.2 Experimental Research System for the Absorption of $Hg_{(g)}$

5.2.1 Introduction of the Mercury Adsorption Experiments

A fixed bed was used in the test system for the mercury adsorption mechanism. The study focused on the influences of simulated flue gas composition, adsorption temperature, different mercury inlet concentrations, etc., on mercury adsorption by activated carbon. The diagram of the experimental mechanism is shown in Fig. 5.1.

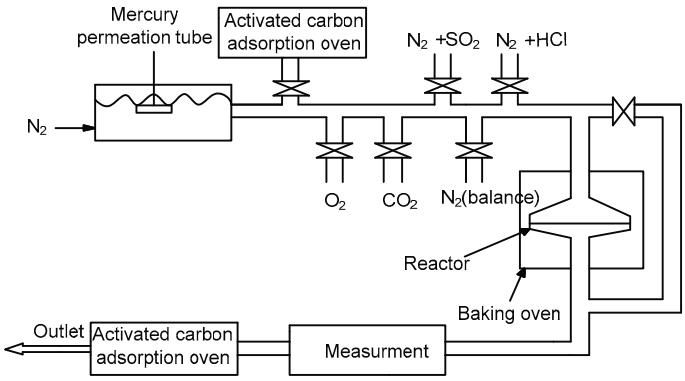

Fig. 5.1 Diagram of the experimental mechanism

The simulated flue gas consisted of $Hg_{(g)}$ from a penetration tube and stand gases of O_2, CO_2, N_2, SO_2, HCl, etc. The concentrations of each basic component in the simulated flue gas are shown in Table 5.1. The mixture of O_2, CO_2, and N_2 was labelled as "BL."

Table 5.1 Concentrations of several basic components in simulated flue gas

Component	O_2	CO_2	SO_2 (ppm)	HCl (ppm)	Hg^0 (μg/m^3)	N_2
Concentration	6%	12%	0	0	5–55	Balance
			400	25		
			800	50		
			1600	75		

The sample analysis during the experimental process was conducted according to the OH method. Under the same conditions, the stabilization and reliability of the test system for the mercury adsorption mechanism in simulated flue gas was conducted. The results of the four contrastive experiments are shown in Table 5.2. As can be seen, the error fell within the permitted range, and the test system was stable and reliable.

Table 5.2 Reliability of the adsorption mechanism test system

Contrastive experiment	Inlet of Hg concentration ($\mu g/m^3$)	Outlet of Hg concentration ($\mu g/m^{3)}$	Percent (%)
No. 1	17.75	15.75	88.76
No. 2	17.75	20.84	117.42
No. 3	17.75	17.48	98.47
No. 4	17.75	19.42	109.40

5.2.2 Adsorption Efficiency and Adsorption Capacity

Adsorption efficiency and adsorption capacity were both used to represent the adsorption ability of mercury by the sorbent. The breakthrough curve shows the change in mercury concentration at the exit of the fixed bed over time. The ordinate ($C/C_0\times100\%$) of the breakthrough curve is the ratio of mercury concentration (C) at the exit of the fixed bed to the initial mercury concentration (C_0) at the entrance of the fixed bed. The breakthrough curve represents the mercury concentration changes within the adsorptive layer, and its shape relies on the type of sorbent and the characteristics of simulated flue gas. The break is defined as the appearance of mercury at the exit of the fixed bed during the adsorption process. Break time is the accumulated total time between the start of adsorption and the break appearance. Adsorption efficiency can be defined as $(1-C/C_0)\times100\%$, which is the percentage of mercury removal from simulated flue gases by sorbent.

The adsorption capacity of a unit sorbent at some time t (μg Hg/g) is the ratio of the amount of mercury adsorbed to unit mass of the sorbent during the start of the adsorption up to the moment of t, as shown in the following expression:

$$q = [\int_0^t (1 - C / C_0)\mathrm{d}t] \cdot C_0 / m$$

In the next subsection, we will firstly introduce the different types of adsorbents and modified adsorption properties. Subsection 5.4 presents the mercury adsorption mechanism of activated carbon, and after that subsection 5.5 discusses the stability of the mercury in the sorbent.

5.3 Experimental Research on Mercury Absorption of Different Sorbents

The mercury adsorption performances of different types of adsorbents are the basis of studies on sorbent injection mercury control. Corresponding modifications were

needful to obtain an economic and efficient adsorbent for mercury control in the coal-fired flue gas.

Through experiments on sorbents and chemically modified sorbents, those with good Hg^0 adsorption abilities were identified. These include activated carbon (AC), AC-MnO_2, ZS-MnO_2, PT-MnO_2, FS-MnO_2, AC-$FeCl_3$, ZS-$FeCl_3$, and activated carbon treated by sulphurization at different temperatures (AC-S).

5.3.1 Hg^0 Adsorption Ability of Normal Sorbents

The Hg^0 adsorption ability of fly ash, calcium-based sorbents (hydrated lime, lime, MFC), zeolite, bentonite, vermiculite, bimomass semicoke, activated carbon, etc. were studied on the bench-scale test of the mercury controlling mechanism in simulated flue gas (BL).

5.3.1.1 Hg^0 Adsorption Ability of Fly Ash

Fly ash can remove some mercury from coal-fired flue gas through adsorption. Carbon-in-ash is one of the factors influencing Hg^0 adsorption by fly ash. Experiments were conducted under the same conditions (Hg^0 concentration: 19.4 μg/m^3; simulated gas: BL; temperature: 125 °C; flow: 1 L/min; fly ash: 70 mg). The adsorption kinetic curves of Hg^0 by 3 kinds of fly ash (FA, LFA1 and LFA2) with different carbon content are shown in Fig. 5.2.

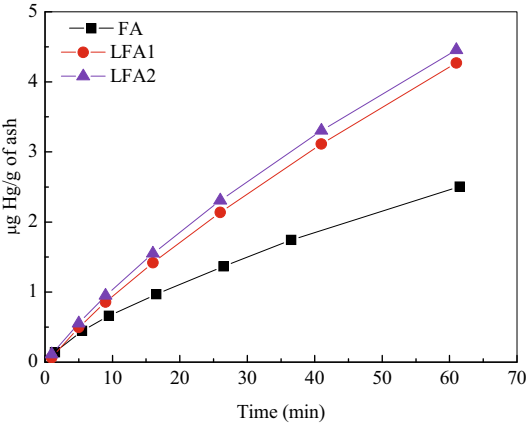

Fig. 5.2 Hg^0 adsorption by three kinds of fly ash

According to a previous research, the mercury adsorption ability of fly ash is related to its carbon residue content; however, carbon content alone cannot determine the mercury adsorption ability of fly ash[14]. As shown in Fig. 5.2, the Hg^0

adsorption quantities of LFA1 with 17.51% carbon and LFA2 with 39.87% carbon were similar, and these values were larger than that of FA with 6.13% carbon. The adsorption ability of fly ash was not proportional to its carbon content. Other elements in fly ash and the composition of flue gas might have great effects on mercury adsorption by fly ash.

5.3.1.2 Hg^0 Adsorption Ability of Calcium-Based Sorbent

Three different sorbents, namely hydrated lime ($Ca(OH)_2$ of 97.6%), lime (CaO of 87.6%) and MFC (mixture of fly ash and lime), were chosen in the study of the Hg^0 adsorption ability of calcium-based sorbents.

● *Hg^0 adsorption ability of hydrated lime*

Adsorption experiments were conducted on two kinds of simulated flue gas: 1) BL and 2) BL added with 800 ppm SO_2. Other conditions were the same (Hg^0 concentration: 19.9 μg/m^3; temperature: 125 °C; flow: 1 L/min). The adsorption kinetic and adsorption efficiency curves of Hg^0 by hydrated lime on the two kinds of simulated flue gas are shown in Fig. 5.3. The existence of SO_2 was favorable for hydrated lime adsorbing Hg^0 because SO_2 reacted with the hydrated lime, promoting the adsorption of Hg^0. Reaction equations are as follows:

$$Ca(OH)_2 + SO_2 + O_2 \rightarrow CaSO_4 + H_2O + O\,, \tag{5-1}$$

$$2Hg^0 + O \rightarrow Hg_2O\,, \tag{5-2}$$

$$Ca(OH)_2 + SO_2 + O_2 + 2Hg^0 \rightarrow CaSO_4 + H_2O + Hg_2O\,, \tag{5-3}$$

$$Ca(OH)_2 + SO_2 \rightarrow CaSO_3 + H_2O\,. \tag{5-4}$$

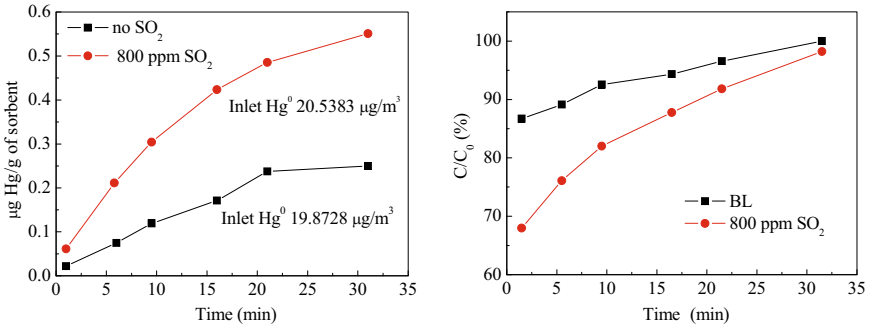

Fig. 5.3 Hg^0 adsorption by hydrated lime on two kinds of simulated flue gas

● *Hg^0 adsorption ability of lime*

Adsorption experiments were conducted on two kinds of simulated flue gas: 1) BL and 2) BL added with 800 ppm SO_2. Other conditions were the same (Hg^0 concentration: 18.4 μg/m^3; temperature: 125 °C; flow: 1 L/min). The adsorption kinetic and

adsorption efficiency curves of Hg^0 by lime on the two kinds of simulated flue gas are shown in Fig. 5.4. The existence of SO_2 was favorable for lime adsorbing Hg^0.

Based on experiments of Hg^0 adsorption by hydrated lime and lime, chemical adsorption was found to be the key in the process of Hg^0 adsorption by calcium-based sorbents. SO_2, improved Hg^0 adsorption by calcium-based sorbents through the chemical adsorption mechanism.

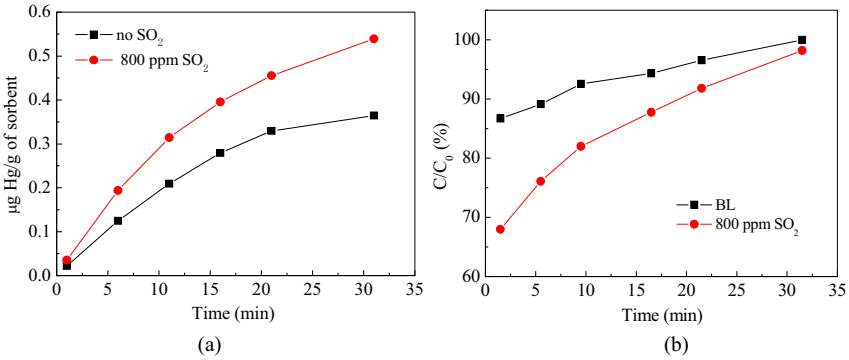

Fig. 5.4 Hg^0 adsorption by lime on two kinds of simulated flue gas

● *Hg^0 adsorption ability of MFC*

MFC is a mixture of fly ash LFA1 and lime with a mass ratio of 3:1. Adsorption experiments were conducted on two kinds of simulated flue gas: 1) BL and 2) BL added with 800 ppm SO_2. Other conditions were the same (Hg^0 concentration: 21.5 μg/m^3; temperature: 125 °C; flow: 1 L/min). The adsorption kinetic and adsorption efficiency curves of Hg^0 by lime on the two kinds of simulated flue gas are shown in Fig. 5.5. The existence of SO_2 was favorable for MFC adsorbing Hg^0.

The three kinds of calcium-based sorbents, namely hydrated lime, lime and MFC, had higher adsorption capacities and absorption efficiencies in flue gas with SO_2. Calcium-based sorbents are widely used as flue gas desulfurizers, indicating a certain ability for Hg^0 removal. A combined removal technology of SO_2 and Hg^0 through injection of calcium-based sorbents can be considered.

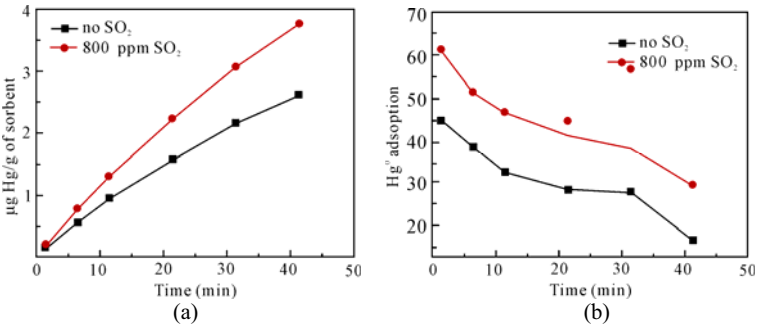

Fig. 5.5 Hg^0 adsorption by MFC on two kinds of simulated flue gas

5.3.1.3 Hg^0 Adsorption Ability of Zeolite

Hg^0 adsorption experiments by different zeolites were conducted under the same conditions (Hg^0 concentration: 19.5 μg/m^3; temperature: 125 °C; simulated flue gas: BL; flow: 1 L/min; amount of sorbent: 100 mg). The respective adsorption kinetic curves of Hg^0 by zeolite (FS), hydrogen-zeolite (H-FS), sodium-zeolite (N-FS), and ammonium-zeolite (A-FS) are shown in Fig. 5.6. The sodium-zeolite had the maximum Hg^0 adsorption quantity.

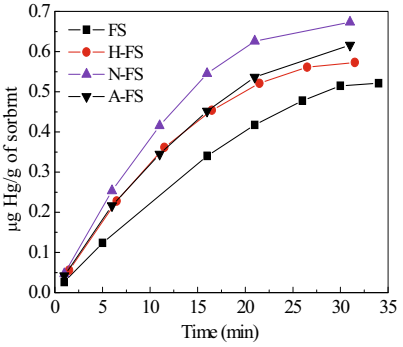

Fig. 5.6 Hg^0 adsorption by different zeolites

5.3.1.4 Hg^0 Adsorption Ability of Bentonite

Hg^0 adsorption experiments by bentonite and cetyltrimethylammonium bromide (CTMAB)-modified bentonites were conducted under the same conditions (Hg^0 concentration: 18.4 μg/m^3, temperature: 125 °C, simulated flue gas: BL, flow: 1 L/min, amount of sorbent: 100 mg). The adsorption kinetic curves of Hg^0 by bentonite (PT), 1% CTMAB-modified bentonite (PT1), 3% CTMAB-modified bentonite (PT2), and 6% CTMAB-modified bentonite (PT3) are shown in Fig. 5.7. PT3 had the maximum adsorption quantity of Hg^0, which had the biggest interlamellar spacing of 2.78 nm through 6% CTMAB-modified bentonites.

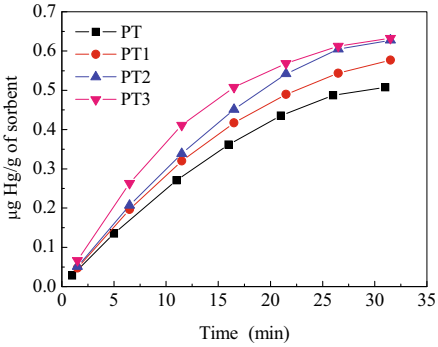

Fig. 5.7 Hg^0 adsorption by different bentonites

5.3.1.5 Hg^0 Adsorption Ability of Vermiculite

As with the others, Hg^0 adsorption experiments by vermiculite and CTMAB-modified vermiculite were conducted under the same conditions (Hg^0 concentration: 18.3 μg/m^3; temperature: 125 °C; simulated flue gas: BL; flow: 1 L/min; amount of sorbent: 100 mg). The adsorption kinetic curves of Hg^0 by vermiculite (ZS), 1% CTMAB-modified vermiculite (ZS1), 3% CTMAB-modified vermiculite (ZS2), and 6% CTMAB-modified vermiculite (ZS3) are shown in Fig. 5.8. Of these, ZS3 had the maximum adsorption quantity of Hg^0, which had the biggest interlamellar spacing of 3.47 nm through 6% CTMAB-modified bentonites.

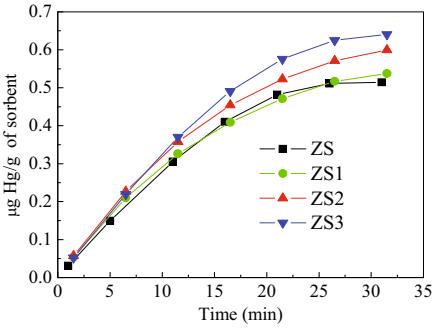

Fig. 5.8 Hg^0 adsorption by different vermiculites

5.3.1.6 Hg^0 Adsorption Ability of Biomass Semicoke

Hg^0 adsorption experiments by biomass semicoke from straw were conducted under the same conditions (Hg^0 concentration: 18.1 μg/m^3; temperature: 125 °C; simulated flue gas: BL; flow: 1 L/min; amount of sorbent: 1.045 g). The adsorption kinetic curves of Hg^0 by semicoke are shown in Fig. 5.9. Biomass semicoke had a low adsorption quantity of Hg^0 because of its poor surface characteristic, only 8.13 m^2/g specific surface area, 0.011 cm^3/g micropore volume adn 3.32 nm average pore size.

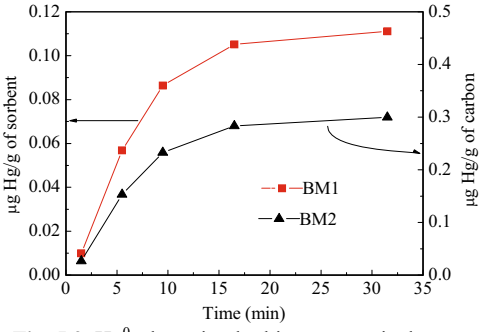

Fig. 5.9 Hg^0 adsorption by biomass semicoke

5.3.1.7 Hg^0 Adsorption Ability of Activated Carbon

Two different groups of C/Hg (mass ratio of active carbon to mercury) were determinated from the same entrance concentration of Hg^0 by changing the quality of AC. The adsorption experiment was conducted in BL gas, with a temperature of 125 °C. Other experimental conditions are shown in Table 5.3.

Table 5.3 Experimental conditions of different C/Hg ratio

Sorbent	Quality (mg)	Hg^0 (μg/m^3)	Gas flow (L/min)	Adsorb time (min)	C/Hg
AC1	10.3	19.3	1	65	8210:1
AC2	44.7	19.3	1	135	17156:1

The adsorption kinetic curves of Hg^0 obtained through AC under different C/Hg ratios are shown in Fig. 5.10. The adsorption efficiency of Hg^0 by AC under high C/Hg was higher than that under a low ratio. However, the adsorption quantity of unit AC decreased under high C/Hg and reduced the utilization efficiency of AC. In the course of practical engineering application, a mere increase in C/Hg was sometimes insufficient to ensure good results.

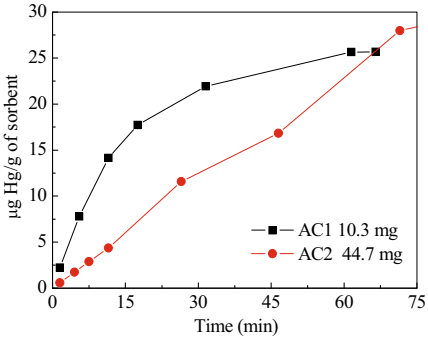

Fig. 5.10 Hg^0 adsorption by AC at different C/Hg ratios

5.3.2 *Mercury Adsorption Ability of Modified Sorbents*

Experimental research on mercury adsorption with modified sorbents was conducted in order to screen out those with high efficiency and low cost. Several sorbents, including coal-fired fly ash, zeolite, vermiculite and bentonite, were modified according to the following modified methods:

1) Dipping treatment of Na_2S;
2) Dipping treatment of $KMnO_4$;
3) Dipping treatment of active MnO_2;
4) Dipping treatment of $Mn(NO_3)_2$;

5) Dipping treatment of $FeCl_3$;
6) Sulphurization with different temperature.

The mercury adsorption abilities of modified fly ash, modified zeolite, modified bentonite, and modified vermiculite are discussed below.

5.3.2.1 Hg^0 Adsorption Ability of Modified Fly Ash

In order to improve Hg^0 adsorption ability, various methods were used to modify fly ash. The experiments showed that the Hg^0 adsorption ability of modified fly ash remained at the same level as that of regular fly ash. The main reason for this was that the carbon-in-ash was lower; hence, modification did not change the physical surface structure of fly ash.

5.3.2.2 Hg^0 Adsorption Ability of Modified Zeolite

After modification, there was some improvement in the Hg^0 adsorption ability of zeolite. The zeolite treated by dipping into active MnO_2 had the best Hg^0 adsorption ability (as shown in Fig. 5.11) among all modified zeolites. The time for 100% mercury breakthrough increased significantly, extending the effective absorption time and improving the Hg^0 adsorption ability of zeolite.

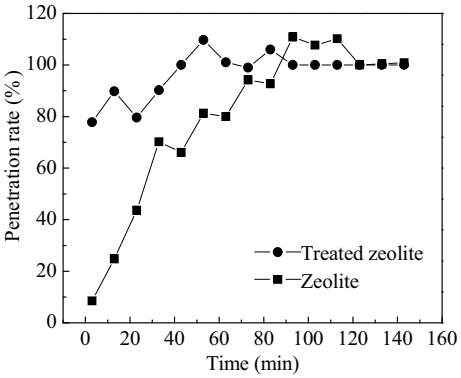

Fig. 5.11 Hg^0 adsorption ability of zeolite treated by dipping of active MnO_2

The zeolite treated by dipping into active MnO_2 had a strong Hg^0 adsorption ability, which can be attributed to several factors including: (1) Mn had multivalence as a cation; (2) valence transformation of Mn ions was easier, hence the number of valence Mn ions was reduced more easily than that by mercury; (3) the adsorption product had a catalytic action, which accelerated Hg^0 adsorption of modified zeolite; and (4) active MnO_2 was widely distributed on the surface of zeolite, which enhanced the contact probability of Hg^0 and Mn.

5.3.2.3 Hg^0 Adsorption Ability of Modified Bentonite

After modification, the Hg^0 adsorption ability of bentonite improved greatly. The Hg^0 adsorption ability of bentonites treated by dipping into active MnO_2 and $FeCl_3$ were much improved compared to other modified zeolites (Fig. 5.12 and Fig. 5.13).

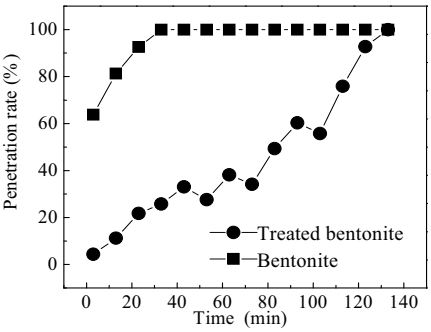

Fig. 5.12 Hg^0 adsorption ability of bentonite treated by dipping into active MnO_2

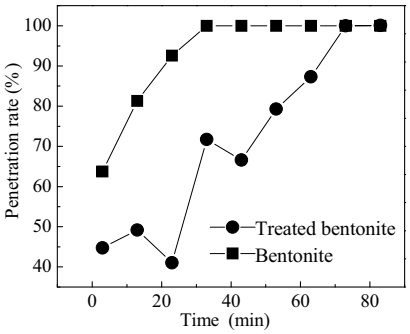

Fig. 5.13 Hg^0 adsorption ability of bentonite treated by dipping into $FeCl_3$

5.3.2.4 Hg^0 Adsorption Ability of Modified Vermiculite

There was a great improvement in the Hg^0 adsorption ability of vermiculite after modification. The Hg^0 adsorption ability of vermiculites treated by dipping into active MnO_2 and $FeCl_3$ were also much improved compared to other modified zeolites (Fig. 5.14 and Fig. 5.15).

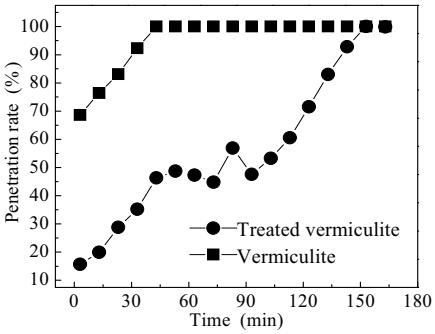

Fig. 5.14 Hg^0 adsorption ability of vermiculite treated by dipping of active MnO_2

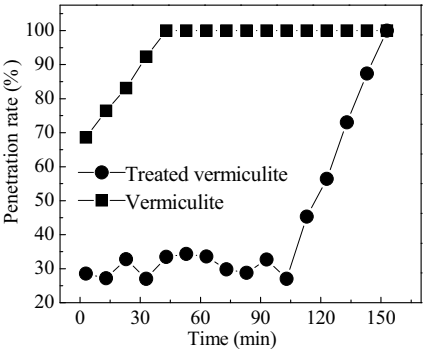

Fig. 5.15 Hg^0 adsorption ability of vermiculite treated by dipping of $FeCl_3$

5.3.2.5 Evaluation of the Mercury Adsorption Ability of Modified Sorbents

Adsorption efficiency, cost and operation complexity of the modified method were the three important factors considered in the project application of adsorption technology. The effective adsorption times of modified sorbents with good Hg^0 adsorption abilities were all acquired at reasonable cost. These modified sorbents included the following: activated carbon treated by dipping into active MnO_2 (AC-MnO_2), vermiculite treated by dipping into active MnO_2 (ZS-MnO_2), bentonite treated by dipping into active MnO_2 (PT-MnO_2), zeolite treated by dipping into active MnO_2 (FS-MnO_2), activated carbon treated by dipping into ferric trichloride (AC-$FeCl_3$), and vermiculite treated by dipping into ferric trichloride (ZS-$FeCl_3$).

A comparison of the preparation process of three modification methods showed that the simplest modification method was the dipping treatment of $FeCl_3$, which merely required the addition of a certain amount of $FeCl_3$ into HCl and mixing. The dipping treatment of active MnO_2 was prepared by mixing $Mn(NO_3)_2$, $KMnO_4$, and HNO_3 in a fixed way for a combined reaction. The process of sulphurization was the

most complicated among the three methods. It required that sorbent and powdered sulfur be mixed first in a porcelain boat and then penetrated for two hours at a certain temperature in a protective gas flow of N_2. Finally, the mixture must be cooled from the penetrative temperature to the environmental temperature in a protective gas flow of N_2.

5.4 Research on Hg Chemical Absorption on the Surface of Actived Carbon

The adsorption process of mercury in the coal-fired flue gas is complicated. Adsorption of Hg^0 by AC is determined by several factors, including the surface characteristic of AC, temperature, and composition of the flue gas. A number of studies have been conducted to understand the mercury adsorbing mechanism of AC. However, most of these studies considered a complex external environment, which made it difficult to expound on the basic mercury adsorption mechanism of activated carbon.

Physical adsorption mainly uses a large specific surface area of activated carbon, whereas chemical adsorption uses chemical groups on the surface of activated carbon. There is a fundamental difference in the adsorption mechanisms between physical and chemical adsorptions. In this section, we firstly introduced mercury adsorption using different activated carbons in the N_2 atmosphere. It aimed to distinguish fundamentally the surface physical and chemical properties of activated carbon through the different kinds of surface modifications and clean methods. Secondly, we showed the influence of simulated coal-fired flue gas composition on mercury adsorption ability of activated carbon. Thirdly, the roles of the physical and chemical adsorptions in the process of mercury adsorption by activated carbon through studying the surface chemical components and physical structure of activated carbon are discussed.

5.4.1 Cleaning System of the Surface Functional Group on the Surface of Activated Carbon

The properties of the surface functional group (SFG) with oxygen of activated carbon are related to the contact temperature of oxygen and carbon[1,15-21]. An experimental system was used to remove the SFGs on the surface of AC by decomposing SFGs with protective inert gas at a temperature of 1200 °C, cleaning the surface of the activated carbon, and ensuring that no chemical elements except carbon exist on the surface. The process could eliminate the effect of surface chemical factors on the process of mercury adsorption by activated carbon.

5.4.1.1 Physical Characteristics of Activated Carbon After High Temperature Removal

Table 5.4 shows the changes in the physical structure characteristics of ACs treated by decomposing SFGs with protective inert gas at temperatures of 1200 °C. The surface physical characteristics of ACs were determined by Autosorb/1/C, a type of automated chemisorption/physisorption analyzer for surface area and pore size measurements.

The specific surface area, total pore volume, and micropore volume of treated ACs decreased. The decrease in the specific surface area of AC was about 20% except for C-AC, which was about 10%. Based on changes in the characteristics of total pore and micropore volumes, the influence of the decomposing process on micropore volume was less than that on other pore volumes.

The fractal dimension also indicated that the surface roughness of treated AC increased but the overall physical structure characteristics of treated AC did not change a lot.

Table 5.4 Changes in the physical structure characteristics of ACs treated by decomposing SFGs

ACs	Treated by decomposing SFGs	Specific surface area (m^2/g)	Total pore volume (cm^3/g)	Micropore volume (<20Å) (cm^3/g)	Average pore size (Å)	Fractal dimension (D)
A-AC	YES	1515	0.94	0.72	24.7	2.62
	NO	1218	0.71	0.58	23.6	2.70
B-AC	YES	1561	1.46	0.74	37.4	2.53
	NO	1220	1.03	0.58	33.8	2.60
C-AC	YES	1091	0.59	0.51	21.7	2.86
	NO	1004	0.52	0.47	22.0	2.86
D-AC	YES	1070	0.81	0.48	30.4	2.76
	NO	799	0.68	0.38	33.9	2.79

5.4.1.2 Chemical Characteristics of Activated Carbon After High Temperature Removal

The surface chemical compositions of ACs were analyzed using a JEOL JEM/2010 electron microscope with the INCA energy dispersive X-ray microanalysis.

Fig. 5.16 shows the Transmission Electron Microscopy (TEM) micrographs and energy dispersive X-ray microanalysis of element compositions at locations 1 (0.2 μm observation) and 2 (0.5 μm observation) on the surface of A-AC. The atoms and weight distribution proportion of elements at locations 1 and 2 on the surface of A-AC are shown in Tables 5.5 and 5.6, respectively. Among the elements found on the surface of A-AC, Cu was composed of a device for supporting the sample during the analyzing.

Table 5.5 Atoms and weight distribution proportion of elements at location 1 on the surface of A-AC

Detected elements	Weight (%)	Atom (%)
C	93.07	96.97
O	2.69	2.10
S	0.23	0.09
Cl	0.30	0.11
Cu	3.71	0.73

Table 5.6 Atoms and weight distribution proportion of elements at location 2 on the surface of A-AC

Detected elements	Weight (%)	Atom (%)
C	92.58	96.57
O	2.85	2.23
F	0.45	0.29
S	0.28	0.11
Cl	0.22	0.08
Cu	3.63	0.72

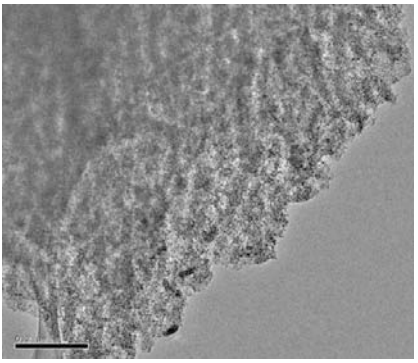

Location 1 (A)

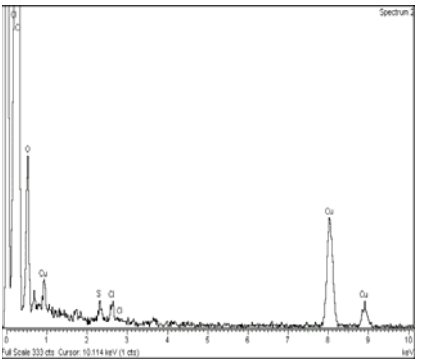

Location 1 (B)

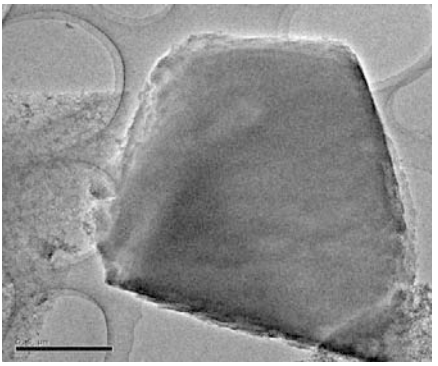

Location 2 (A)

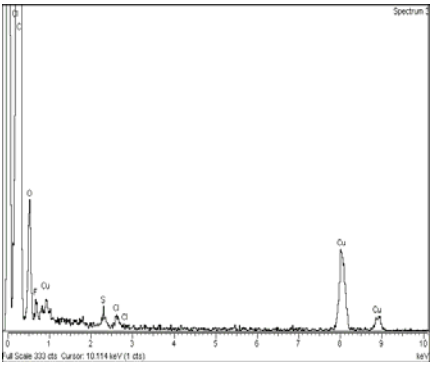

Location 2 (B)

Fig. 5.16 TEM micrographs and energy dispersive X-ray microanalysis of element compositions on the surface of A-AC

The results of the analysis indicated that many other elements exited on the surface of AC, including O F, S, Cl, and Cu. These elements might exist on the surface of AC as groups or other forms during the activation process, with O being the most dominant element.

Fig. 5.17 shows surface chemical characteristics at locations 3 (0.2 μm observation) and 4 (0.05 μm observation) on the surface of A-AC treated by high temperature removal. Almost all elements, except C, were desorbed by decomposing SFGs for 10 h with protective inert gas at 1200 °C temperatures. The surface of the treated A-AC became very clean. However, there were still extremely low traces of O and Si elements at location 3, which may be due to incomplete desorption at some complex surface structures.

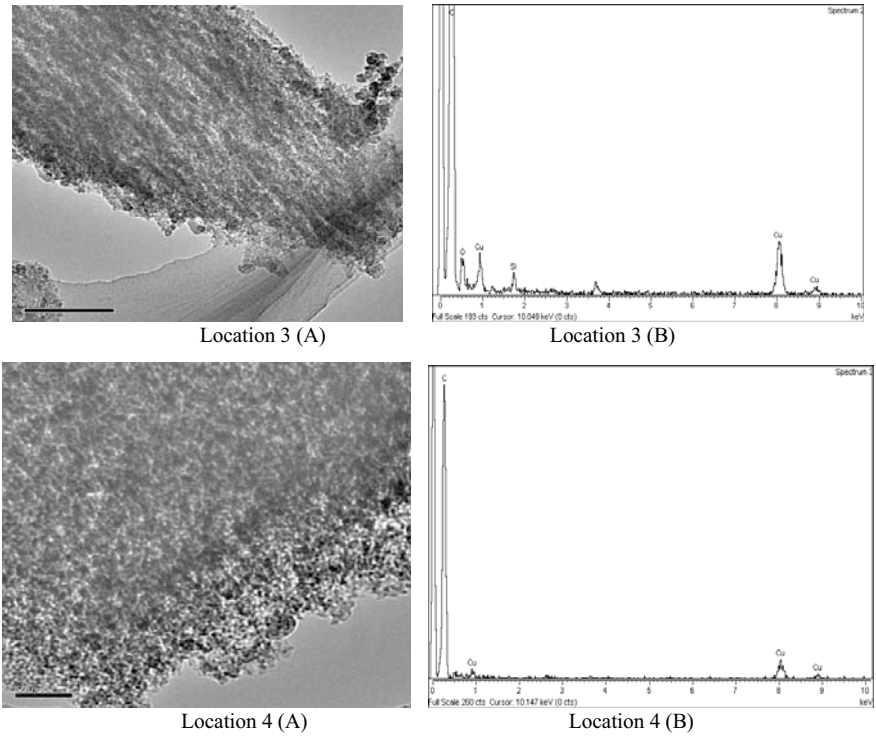

Fig. 5.17 TEM micrographs and energy dispersive X-ray microanalysis of element compositions on the surface of treated A-AC

5.4.2 Type of AC Sorbents

Four kinds of AC samples were used in the adsorption experiments, namely, AC(XK), AC(YK), AC(MJ), and AC(MZ). All ACs were dried at a temperature of 100 °C for 2 h. Table 5.7 provides information on ACs, including their raw material,

production technique, form and supplier.

The three ACs, namely, AC(XK), AC(YK) and AC(MJ), were prepared by steam activation from apricot shells, coconut shells and coal, respectively. These activations were carried out at temperatures within 800–1100 °C with the presence of steam, and ACs prepared using this method only had hydrogen and oxygen elements on their surfaces. On the other hand, AC(MZ) was generated from wood by chemical activation using $ZnCl_2$ at a temperature of 600 °C. As a result, some Cl and Zn elements remained on the surface of AC(MZ). All ACs were in powder form except for AC(MJ), which was in granular form.

Table 5.7 Detailed information on ACs used in the experiments

Sorbent	Raw material	Production technique	Form
AC(XK)	Apricot shell	Steam activation	Powder
AC(YK)	Coconut shell	Steam activation	Powder
AC(MJ)	Coal	Steam activation	Granule
AC(MZ)	Wood	Chemical activation	Powder

The surface physical characteristics of ACs were determined by Autosorb/1/C. The surface chemical compositions of ACs were analyzed using a JEOL JEM/2010 electron microscope with INCA energy dispersive X-ray microanalysis. The surface physical characteristics of AC(XK), AC(YK), AC(MJ), and AC(MZ) are shown in Table 5.8. A continuous emission monitor (CEM) of DM/6A/MS/1A for mercury speciation was used in the experiments.

Table 5.8 Surface physical characteristics of ACs

Sorbent	Specific surface area (m^2/g)	Pore volume (cm^3/g)	Micropore volume (<20Å) (cm^3/g)	Particle size (mm)	Porosity (%)
AC(XK)	1070	0.81	0.48	0.08	57
AC(YK)	846	0.48	0.38	0.08	43
AC(MJ)	791	0.41	0.37	1.5	34
AC(MZ)	1450	0.94	0.72	0.09	67
AC(MZ-T)	1218	0.71	0.58	0.09	62

Prior to the adsorption of Hg^0, AC was placed on a fixed bed reactor, and sample gas was adjusted to the desired flux in the bypass. All the experimental projects are shown in Table 5.9. Every kind of powder AC sorbent was controlled at about 0.05 g (the height of the adsorption column was about 2 mm) except for AC(MJ), which was about 0.10 g (the height of the adsorption column was about 2.5 mm). Adsorption temperatures were all maintained at 130 °C. Initial Hg^0 concentrations ranged from 13.7 to 19.4 $\mu g/(N \cdot m^3)$. For each project, the total flux was controlled at 1 or 1.3 L/min using a mass flowmeter.

Table 5.9 Experimental project of Hg^0 onto activated carbon in N_2

No.	Sorbent	Amount of sorbent (g)	Adsorption temperature (°C)	Initial Hg^0 concentration (μg/(N·m^3))	Flux (L/min)
1	AC(XK)	0.0501	130	18.8	1.3
2	AC(XK)	0.0503	130	18.8	1.3
3	AC(YK)	0.0505	130	19.4	1
4	AC(YK)	0.0516	130	14.2	1.3
5	AC(MJ)	0.1002	130	16.9	1.3
6	AC(MZ)	0.0514	130	16.4	1
7	AC(MZ)	0.0508	130	14.2	1.3
8	AC(MZ-T)[a]	0.0500	130	16.9	1.3
9	AC(MZ-T)[a]	0.0507	130	13.7	1.3

[a]: AC(MZ) has been treated by high temperature treating system

5.4.3 Hg^0 Adsorption by Four Commercial ACs in the N_2 Environment

In order to estimate the influence of the surface characteristics of AC, Hg^0 adsorption studies on AC(XK), AC(YK), AC(MJ), and AC(MZ) were conducted on a fixed bed reactor in the N_2 environment. The results indicated that the adsorption process was only influenced by the surface characteristics of AC. The results also reflected the impact of the surface characteristics of AC on Hg^0 adsorption.

Fig. 5.18 shows the Hg^0 adsorption by AC(XK) in N_2 environment. At the beginning of the experiment, the initial Hg^0 concentration was 18.8 μg/(N·m^3). The outlet Hg^0 concentration fell about 5 min after the start of the experiment when the gas flow was switched from the bypass to the fixed bed reactor. This was due to the presence of air in the tube between the end of the fixed bed reactor and the entrance of the CEM. About 1 min later, the outlet Hg^0 concentration in the tail-end gas rose back to the initial concentration. This indicated that all the Hg^0 penetrated through the fixed adsorption bed of AC(XK) in the N_2 environment. The results of the two repeated experiments were almost the same (Fig. 5.18). Consequently, it can be concluded that AC(XK) did not adsorb any Hg^0 when the Hg^0-N_2 gas flowed through the fixed bed. The experiments of Hg^0 adsorption by AC(YK) were conducted with different initial Hg^0 concentrations (19.4 and 14.2 μg/(N·m^3)). Moreover, AC(YK) had no capability to adsorb Hg^0 in the N_2 environment (Fig. 5.19), either.

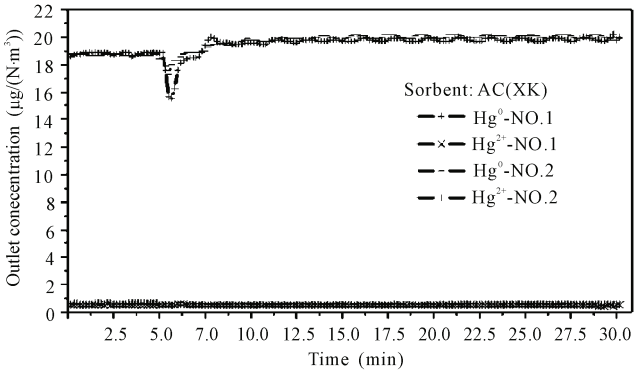

Fig. 5.18 AC(XK) Hg^0 adsorption in the N_2 environment

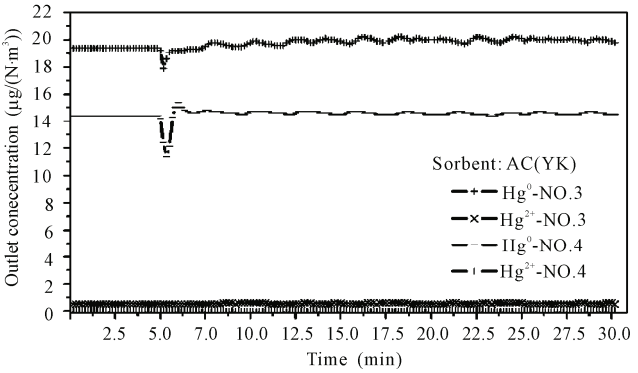

Fig. 5.19 AC(YK) Hg^0 adsorption in the N_2 environment

The granular AC(MJ) was prepared from coal. In the adsorption experiment, the gas flow was switched from the bypass to the fixed bed reactor 30 min after the start of the experiment (Fig. 5.20). After the switch of the gas flow, the curves of outlet Hg^0 concentrations in Fig. 5.20 started to fluctuate. The fluctuation resulted from the influence of the pressure drop in the gas flow on CEM when it went through the granular fixed bed. However, the fluctuation did not change the trend of the curve. The centerline of the fluctuant outlet concentration curve of Hg^0 was at the same level as the initial one. Thus, AC(MJ) did not adsorb Hg^0 in the N_2 environment.

The Hg^0 adsorption results of AC(MZ) in the N_2 environment are described in Fig. 5.21. The adsorption curves of AC(MZ) were completely different from those of AC(XK), AC(YK), and AC(MJ) under nearly the same conditions. Both of the outlet Hg^0 concentration adsorption lines of AC(MZ) decreased steeply to almost zero when the Hg^0-laden gas flow was switched to a fixed bed reactor. Moreover, AC(MZ) exhibited good capability to adsorb Hg^0 in the N_2 environment, because it adsorbed almost all of the Hg^0 after the switch.

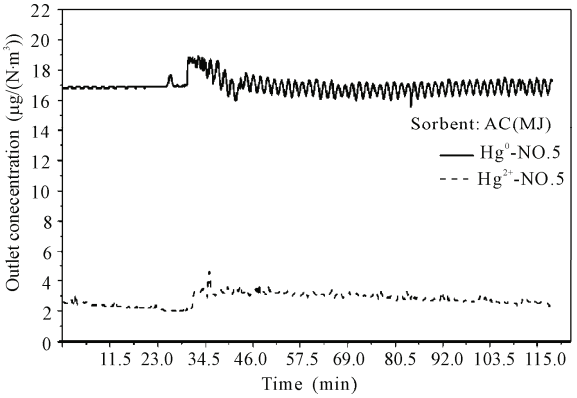

Fig. 5.20 AC(MJ) Hg^0 adsorption in the N_2 environment

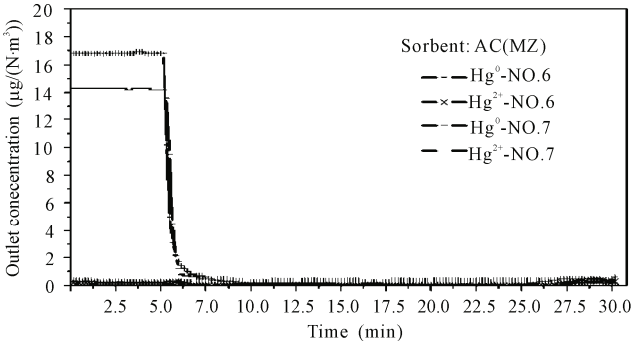

Fig. 5.21 AC(MZ) Hg^0 adsorption in N_2 environment

There were also significant differences in the adsorption of Hg^0 between AC(XK)\AC(YK)\AC(MJ) and AC(MZ). The reason for the different adsorption phenomena had no connection with the form of AC (Figs. 5.18 to 5.21). Further analyses were conducted using Autosorb/1/C in order to explore the influences of surface physical characteristics on AC adsorbing Hg^0.

The surface physical characteristics of AC(XK), AC(YK), AC(MJ), and AC(MZ) were basically similar, except for quantity (Table 5.8). For example, the pore volume of AC(YK) was 0.48 cm^3/g, whereas that of AC(MZ) was 0.94 cm^3/g. However, the difference in quantity was unlikely to induce such significant differences in the adsorption of Hg^0 between AC(XK)\AC(YK)\AC(MJ) and AC(MZ).

The three samples (AC(XK)/AC(YK)/AC(MJ)) were derived from different raw materials, namely apricot shell (XK), coconut shell (YK) and coal (MJ), and were all activated by steam. Steam activation is a common activation technique for AC production and is effective in creating more surface area physically by opening up more micropores. The surfaces of AC(XK), AC(YK), and AC(MJ) had no spe-

cific active element apart from possible hydrogen and oxygen elements, according to the steam activation method. However, it was obvious that the oxygen functional groups did not work in the process of Hg^0 adsorption by ACs in the N_2 environment in this study. Hence, steam activation was not a good choice for preparing ACs to capture Hg^0.

In contrast to the steam activation methods of AC(XK)/AC(YK)/AC(MJ), AC(MZ) was prepared through a chemical method using $ZnCl_2$. Then, some $ZnCl_2$ was left in the AC(MZ). Previous studies have shown that the Cl element can facilitate the adsorption of AC to Hg^0. Table 5.10 shows the results of the analysis of the surface chemical element of AC(MZ) and treated-AC(MZ). The percentage of Cl was 0.31% (weight) or 0.11% (atom), whereas the percentage of S was 0.24% (weight) or 0.09% (atom) on AC(MZ). The proportions of Cl and S were lower than those of other elements in AC(MZ), but the amounts of Cl and S were greater than those of Hg^0 in the N_2 environment. For the purpose of proving the importance of the chemical elements (e.g., Cl and S) in the Hg^0 adsorption by AC, a high temperature treatment system was utilized to remove SFGs from the surface of AC(MZ). The treated AC(MZ) was labeled as AC(MZ-T). Furthermore, there was nothing on the surface of AC(MZ-T) except for C.

Table 5.10 Percentage of elements in AC(MZ) and AC(MZ-T)

ACs	Element	Peak value	Weight (%)	Atom (%)
AC(MZ)	C	33474	96.66	97.68
	O	1179	2.79	2.12
	S	195	0.24	0.09
	Cl	248	0.31	0.11
AC(MZ-T)	C	1759	100	100

Fig. 5.22 shows the Hg^0 adsorption curves of AC(MZ-T) in the N_2 environment. When the gas flow was switched to adsorption, there were noticeable decreases for both the outlet Hg^0 concentrations with initial Hg^0 concentrations of 16.9 and 13.7 $\mu g/(N{\cdot}m^3)$, respectively. The decreases were around 30% of the initial Hg^0 concentrations. The adsorption curves quickly rose back to the initial Hg^0 concentrations at about 5 min (Fig. 5.22). Thus, AC(MZ-T) only had limited adsorption capability of Hg^0 in the N_2 environment, which could be the result of incomplete surface cleaning (Fig. 5.22). In other words, if it did not have the chemical element on its surface, the Hg^0 adsorption capability of AC(MZ) in the N_2 environment would have been similar to those of AC(XK), AC(YK), and AC(MJ).

The results of determining by Autosorb/1/C indicated that the surface physical structure of AC(MZ-T) was almost the same as that of AC(MZ). Compared with AC(MZ), there was a decrease of approximately 20% in the specific surface area and pore volume of AC(MZ-T) (Table 5.8). However, the 20% loss in porosity resulting from high temperature treatment did not cause the observed elimination of the Hg^0 adsorption capacity of the treated sample.

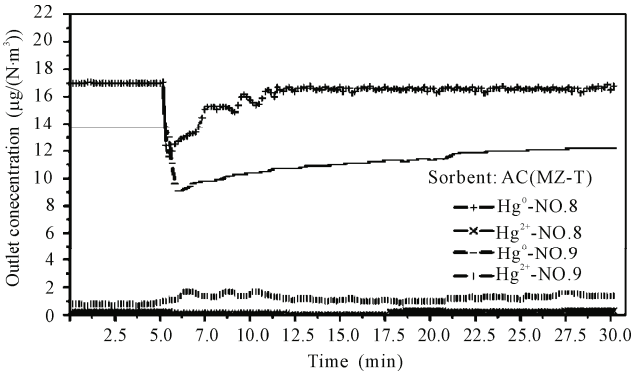

Fig. 5.22 AC(MZ-T) Hg^0 adsorption in the N_2 environment

According to the experimental results of the Hg^0 adsorptions in the N_2 environment of four kinds of commercial ACs, as well as the discussion on the influence of surface physical characteristics and surface chemical characteristics on the adsorption, it can be concluded that the Hg^0 adsorption by AC was a chemical adsorption process in the N_2 environment. The Hg^0 was possibly oxidized to $HgCl_2$ or HgS by Cl or S during the adsorption process of AC(MZ).

Understanding the adsorption mechanism of Hg^0 by AC is valuable for improving Hg^0 adsorption capability of the sorbent, which is necessary for increasing mercury emission control efficiency in AC injection technology. In this paper, the key focus was to understand the mechanism. Accordingly, the adsorption experiment was carried out primarily in order to study the influence of physical and chemical adsorptions in the process of AC adsorbing Hg^0 in the N_2 environment. The experimental results showed that AC(XK), AC(YK) and AC(MJ), which were all prepared by steam activation with relatively clean surfaces, had no adsorption capability of Hg^0 in the N_2 environment. However, the AC(MZ) that was prepared using a chemical activation method with $ZnCl_2$ showed high Hg^0 adsorption capability in the same experimental condition. Using the high temperature treatment system, AC(MZ) was modified to remove SFGs and was renamed AC(MZ-T). The AC(MZ-T) showed no Hg^0 adsorption capability in the N_2 environment.

Based on the adsorption experimental results of AC(XK), AC(YK), AC(MJ), AC(MZ) and AC(MZ-T), as well as the surface analysis of its physical and chemical characteristics, the Hg^0 adsorption by AC was a chemical adsorption process in the N_2 environment. Hg^0 was likely to be oxidized and retained by the oxidative elements produced on the AC surface through chemical activation. Without the oxidative elements capable of oxidizing Hg^0, AC was unable to adsorb Hg^0 in the N_2 environment through physical adsorption.

5.4.4 Hg^0 Adsorption by ACs in Simulated Flue Gas Environment

The Hg^0 adsorption by AC is a chemical process in the N_2 environment. This chemical force may be attributed to elements on the surface of AC as well as to the adsorption environment. During the process of adsorbing Hg^0 from coal-fired flue gas, AC confronted many kinds of flue gas components, such as SO_2, NO_2, O_2, H_2O, HCl and so on, except for mercury.

Here, Hg^0 adsorption by AC(YK), AC(XK), and AC(MZ-T) in the simulated flue gas was conducted, following the work conditions shown in Table 5.11. The experiment was divided into three stages: first, the stabilization of the Hg^0 source in the balance of N_2 gas through bypass; second, the adsorption of Hg^0 in the N_2 atmosphere by ACs; and third, the adsorption of Hg^0 in the simulated flue gas atmosphere by ACs.

Table 5.11 Work conditions of Hg^0 adsorption using ACs in the simulated flue gas

Work condition	AC	Flow (L/min)	Hg^0 ($\mu g/(N \cdot m^3)$)	Sorbent (g)	Thickness of fixed bed (mm)	Temperature (°C)
No.1	YK-AC	1	19.4	0.0505	About 2	130
No.2	XK-AC	1.3	14.1	0.0505	About 2	130
No.3	MZ(sm)-AC	1.3	13.7	0.0507	About 2	130

When the absorption atmosphere was switched from N_2 to simulated flue gas, AC(YK), AC(XK), and AC(MZ-T) showed good Hg^0 adsorption capacities and had an initial Hg^0 adsorption efficiency of 80% (Fig. 5.23). This result showed that simulated flue gas composition promoted Hg^0 chemical adsorption by ACs. How was the chemical adsorption formed? Was Hg^0 first oxidized into Hg^{2+} in the simulated flue gas and then adsorbed by ACs? Was Hg^0 chemically adsorbed directly by ACs? This section focuses on the influence of flue gas composition, Hg^0, and activated carbon surface on Hg^0 adsorption by ACs in a simulated flue gas environment.

5.4.4.1 Influence of Simulated Flue Gas Components on Hg^0 Speciation

The influence of the simulated flue gas component on Hg^0 speciation was studied at the temperature of a flue tail. In this experiment, the mercury speciation was monitored in real-time when simulated flue gas components were changed step by step. The simulated flue gas components were changed in four phases described below.

In the first phase, the amount of carried Hg^0 gas was 300 ml/min, the balance gas of N_2 was 966 ml/min, and total flow of simulated flue gas was 1266 ml/min. As a result, the concentration of Hg^0 was 14.1 $\mu g/(N \cdot m^3)$ and that of Hg^{2+} was 0.7 $\mu g/(N \cdot m^3)$. In the second phase, simulated flue gas components were added (except for H_2O): $O_2/CO_2/SO_2/ NO_2/NO/HCl$. In the third phase, H_2O was added based on

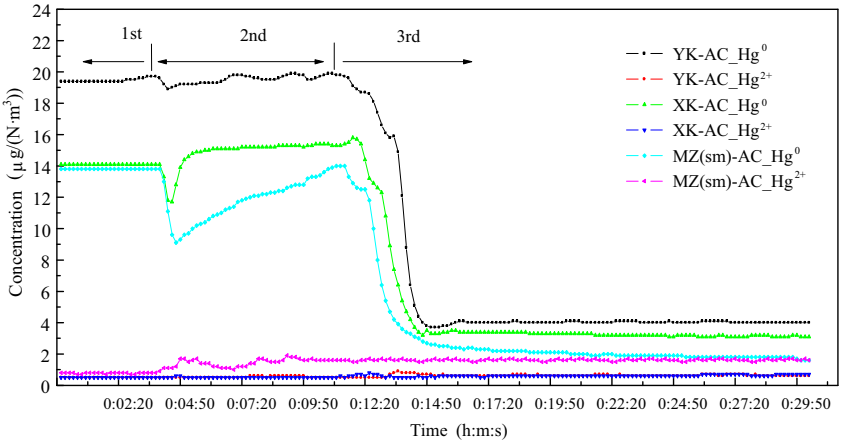

Fig. 5.23 Hg^0 adsorption by ACs in simulated flue gas environment

the second phase. In the fourth phase, the simulated flue gas components were turned off one by one as follows: H_2O/HCl, NO, NO_2, SO_2, O_2, and CO_2.

In the process of changing the gas components, the total simulated flue gas flow was maintained at 1266 ml/min. The influence of the simulated flue gas components on mercury speciation is shown in Fig. 5.24. The horizontal axis showed the experiment time in h:m:s. There were four ordinate axes, namely, A, B, C, and D. The A axis showed the mercury concentration in simulated flue gas in μg/(N·m^3); the B axis showed the O_2 and CO_2 concentrations in simulated flue gas as a percentage; the C axis showed the NO and NO_2 concentration in simulated flue gas in ppm; and the D axis showed the SO_2 concentration in simulated flue gas in ppm. The water and HCl concentrations were adjusted to 10% and 50 ppm, respectively, based on standard gas.

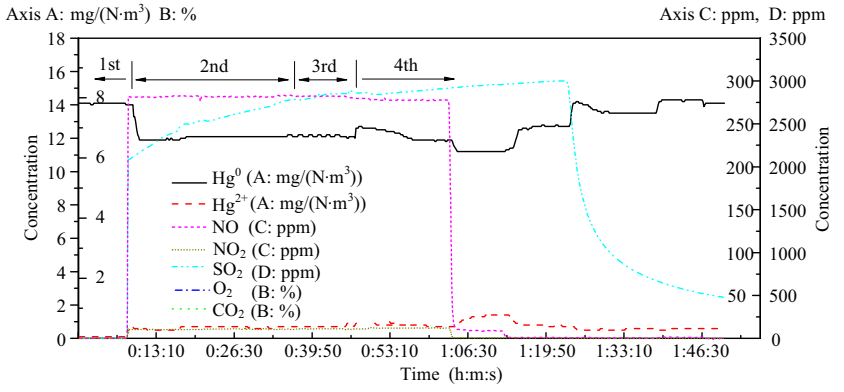

Fig. 5.24 Influence of simulating flue gas components on mercury speciation

Approximately 14% of Hg^0 was oxidized to Hg^{2+} with the action of the simulated flue gas components (Fig. 5.24). However, AC had a good adsorption capability for Hg^0 (the initial adsorption efficiency was about 80%, as shown in

Fig. 5.23). In contrast to the above-mentioned experiments, the method for Hg^0 adsorption by AC in simulated flue gas should cause Hg^0 to be first oxidized into Hg^{2+} by simulated flue gas components and then be adsorbed by AC.

5.4.4.2 Hg^0 Adsorption by AC(XK) that Previously Adsorbed Simulated Flue Gas Components

During the experiment, the adsorption temperature was controlled at 130 °C, the amount of AC(XK) was 0.0506 g, and the total flow of simulated flue gas was maintained at 1.3 L/min, including the 6.9% O_2, 282 ppm NO, 8.7% CO_2, 1,786 ppm SO_2, 23.4 ppm NO_2 components.

As shown in Fig. 5.25, AC(XK) was the first simulated flue gas component to be adsorbed within about 1 h and was then switched to adsorbed Hg^0 in an N_2 atmosphere. As a result, AC(XK) obtained the capability to adsorb Hg^0 in an N_2 atmosphere, similar to AC(YK), AC(XK), and AC(MZ-T) (Fig. 5.23). This experiment showed that the promotion of simulated flue gas components on Hg^0 adsorption by XK-AC materialized on the surface of AC.

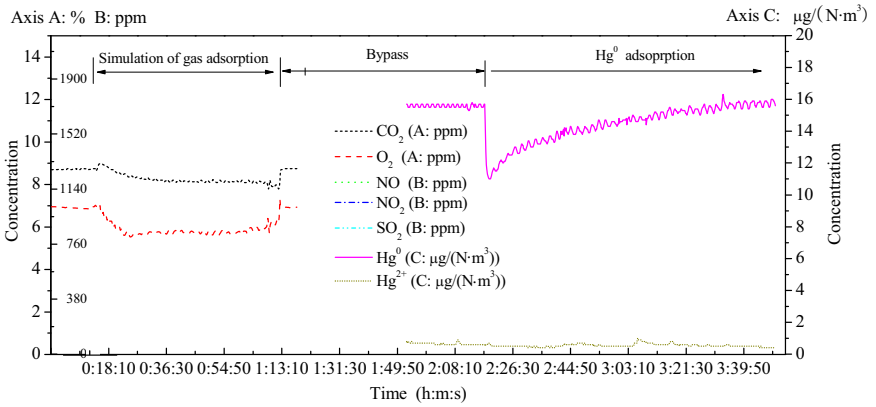

Fig. 5.25 Hg^0 absorption of AC(XK) after the simulation of flue gas in the N_2 environment

5.4.4.3 Influence of Simulated Flue Gas Components on Hg^0 Adsorption by XK-AC

During the experiment, the adsorption temperature was controlled at 130 °C, the amount of AC(XK) was 0.0505 g, and the total flow of simulated flue gas was maintained at 1.3 L/min. The main concentrations of simulated flue gas components at the outlet of the adsorption bed are shown in Fig. 5.26. The horizontal axis showed experimental time in h:m:s. There were three ordinate axes, namely, A, B, and C. Of these A showed O_2 and CO_2 concentrations in simulated flue gas as a percentage; B showed the NO and NO_2 concentrations in simulated flue gas in ppm;

and C showed the SO_2 concentration in simulated flue gas in ppm. The HCl concentration was adjusted to 50 ppm based on standard gas. The experiment results on the influence of simulated flue gas components on Hg^0 adsorption by AC(XK) are shown in Fig. 5.27.

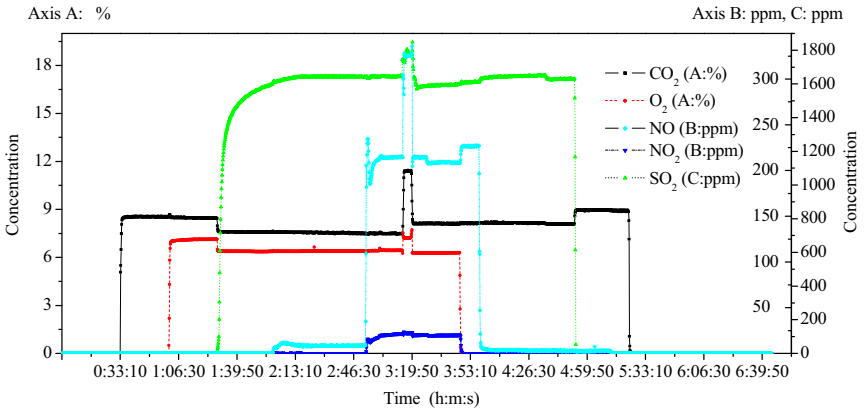

Fig. 5.26 Main concentrations of simulated flue gas components at the outlet of the adsorption bed

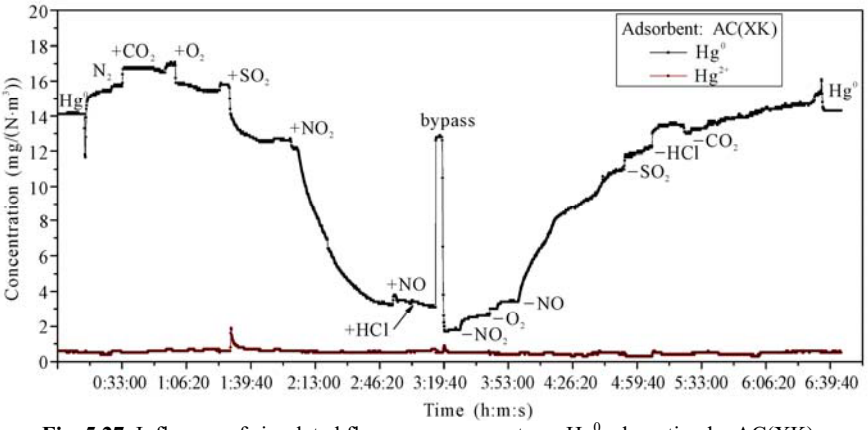

Fig. 5.27 Influence of simulated flue gas components on Hg^0 adsorption by AC(XK)

The experiment on the influence of simulated flue gas components on Hg^0 adsorption by AC(XK) was divided into two parts. First, simulated flue gas components were added one by one (from CO_2 to HCl), and second, simulated flue gas components were subtracted one by one (from NO_2 to CO_2).

As shown in Fig. 5.27, CO_2 and O_2 did not affect Hg^0 adsorption by AC(XK) when they were added. When SO_2 was added, the concentrations of CO_2 and O_2 decreased slightly. Here, SO_2 may have promoted adsorption of O_2 and CO_2 on AC. With the combined action of O_2, CO_2 and SO_2, Hg^0 adsorption by AC(XK) was promoted, Meanwhile, Hg^{2+} exhibited a small peak, which indicated that Hg^{2+} was formed during the process of Hg^0 adsorption by AC(XK).

When NO_2 was added to the simulated flue gas, Hg^0 adsorption by AC(XK) increased substantially. On the other hand, the concentration of NO increased more than that of NO_2 (Fig. 5.27). Based on the concentration changes of Hg^0, NO_2 and NO, Hg^0 was oxidized by NO_2 with the catalysis of surface carbon, which can be expressed as the following reaction: $Hg+NO_2 \rightarrow HgO+NO$. When NO and HCl were added, respectively, both did not affect Hg^0 adsorption by AC(XK) in this experiment.

As confirmed in subsection 5.4.4.1, the impact of simulated flue gas components on the changing speciation of Hg^0 was limited. When simulated flue gas was switched to bypass in the middle of experiment, the concentration of Hg^0 reverted to the initial concentration of the Hg^0 source (Fig. 5.27). This is similar to the conclusions obtained in subsection 5.4.4.1.

When the simulate flue gas switched back through the adsorption bed, Hg^0 was again immediately adsorbed by AC(XK) in the simulated flue gas. When the simulated flue gas components were added one by one, NO_2 was one of the best components in terms of the promotion of Hg^0 adsorption by AC(XK).

In addition, NO_2 was first subtracted from the simulated flue gas components. The subtraction of NO_2 from simulated flue gas did not have a great influence on Hg^0 adsorption by AC(XK). This result can be attributed to the fact that the subtraction of NO_2 did not obviously change the concentration of NO_2 and merely induced a slight decrease in NO concentration (Fig. 5.26). Moreover, NO_2 was easily produced through the reaction between the O_2 and NO.

In the next stage, O_2 was removed from the simulated flue gas, which resulted in a significant increase in NO concentration and a rapid decrease in NO_2 concentration. As a result, the outlet Hg^0 concentration of the adsorption bed increased. As NO was consumed, the Hg^0 adsorption capability of AC(XK) was further reduced. Among the other simulated flue gas components, HCl also had a greater influence on Hg^0 adsorption by AC(XK), as shown in Fig. 5.27.

Prior to the individual removal of simulated flue gas components, AC(XK) had already adsorbed the Hg^0 from simulated flue gas for nearly 3 h. This reaction changed the composition on the surface of AC(XK) (see the discussion in subsection 5.4.4.2), which induced differences in the Hg^0 adsorption dynamic curves between the process of adding simulated flue gas components and that of subtracting simulated flue gas components. However, both Hg^0 adsorption dynamic curves were generally symmetrical, indicating chemical adsorption. Moreover, Hg^0 adsorption by AC, which was produced using the physical method in simulated flue gas, was a complicated chemical adsorption process relying on the both acidic simulated flue gas components and surface carbon. In this experiment, NO_2 played a major role in Hg^0 chemical adsorption by AC.

5.4.5 Saturated Hg^0 Adsorption Experiments by ACs in Simulated Flue Gas

Based on the obtained results, the adsorption process of Hg^0 by AC was found to be the chemical adsorption in N_2 gas or in simulated coal-fired flue gas. The Hg^0 gas was probably oxidized to Hg^{2+} and adsorbed by AC. Thus, when the adsorption capacity of AC for Hg^0 was close to the maximum, Hg^{2+} could be detected at the outlet of the adsorption bed. To further confirm the above-mentioned conclusions and discover the mercury adsorption mechanism of AC, saturated Hg^0 adsorption experiments using ACs were conducted in simulated flue gas.

5.4.5.1 Saturated Hg^0 Adsorption Experiments by AC(MZ) in Simulated Flue Gas

The adsorption experiments were conducted by the bench-scale experiment system with a fixed adsorption bed in the simulated flue gas (Fig. 5.1). The AC sorbent was controlled to about 0.05 g (the height of the adsorption column was about 2 mm). The heating temperature of the gas channel and the operating temperature of the fixed adsorption bed were all kept constant at (130±1) °C. The Hg^0 adsorption experiment by AC was divided into four steps, which were conducted continuously. The time consumed for the experiment was about 60 h, as shown in Fig. 5.28.

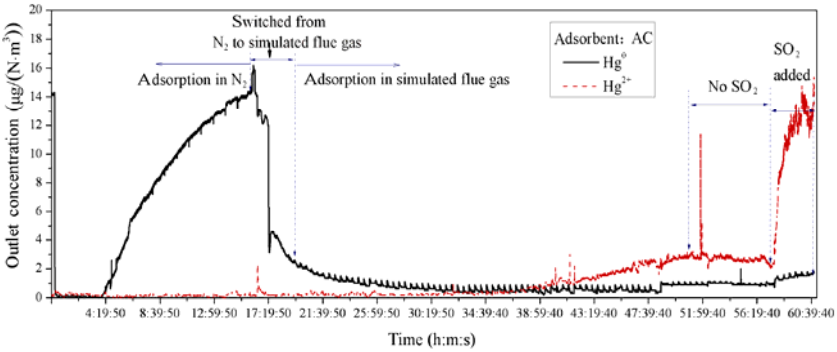

Fig. 5.28 Hg^0 adsorption by AC in N_2 and in simulated flue gas

Step 1 consumed 16 min in total. Here, AC was first placed in the fixed bed reactor, and the concentration of Hg^0 was controlled at 14.2 μg/(N·m^3) with a total flow of 1.3 L/min in the bypass. Through this step, a consistent and stable initial condition was established.

In Step 2, the adsorption Hg^0 by AC was first conducted in N_2 gas. This step was performed to investigate the adsorption between the surfaces of AC and Hg^0. This step was maintained for about 16 h and 33 min.

When Step 2 was finished, the simulated flue gas components were introduced into the gas flow one by one. Meanwhile, the total flow was kept constant by adjusting the N_2 balance gas. The effect of different flue gas components on Hg^0 adsorption was evaluated in this step.

Once all the gas components were added, the adsorption of Hg^0 by AC in the complete simulated flue gas started. The adsorption time in the Step 4 was quite long at approximately 41 h and 22 min. The effect of flue gas components on Hg^0 adsorption and the mechanism of Hg^0 adsorption by AC were studied.

Fig. 5.28 shows the outlet Hg concentration on the fixed adsorption bed. Initially, the rate of Hg^0 adsorption by AC was very high. As the experiment proceeded, Hg^0 was detected 4 h later, and its concentration reached 14.2 μg/(N·m^3) at the 16th hour; Hg^{2+} never emerged during the entire process. The above-mentioned Hg^0 adsorption phenomenon seemed to indicate that the Hg^0 adsorption by AC in N_2 may be a physical adsorption. When the Hg^0 adsorption by AC was a physical adsorption, the saturated adsorption of the AC was reached at the 16th hour (Fig. 5.28). Then, more Hg^0 would no longer be adsorbed by AC because all the pores in the surface of AC were filled by Hg^0 when the AC had reached the saturated adsorption. However, the following adsorption in the simulated coal-fired flue gas provided interesting and important results.

When the gas flow into the reactor was switched from N_2 to simulated gas components one by one, the concentration of Hg^0 dropped (Fig. 5.28) (Step 3). The influence of different gas components on Hg^0 adsorption was observed during switching from N_2 gas to the simulated flue gas from 15:59:50 to 19:29:50 (Fig. 5.29). Excluding CO_2, almost all other gas components, especially NO, enhanced Hg^0 adsorption by AC.

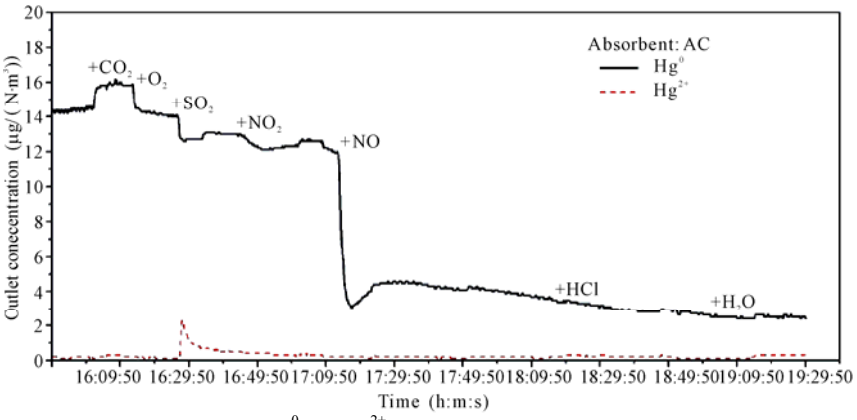

Fig. 5.29 Concentrations of Hg^0 and Hg^{2+} during switching from N_2 gas to simulated flue gas

Competitive adsorption also existed between CO_2 and Hg^0 on AC. Accordingly, Hg^0 concentration increased because surface conditions of AC favored CO_2 adsorption when CO_2 was added at 15:59:50.

There was also a peak of Hg^{2+} when SO_2 was added to the simulated flue gas at 16:26:50 (Fig. 5.29). The chemical oxidation of Hg^0 to Hg^{2+} can be expressed in the following equation:

$$Hg^0{}_{(g)} + SO_{2\,(g)} + O_{2\,(g)} \rightarrow HgSO_{4\,(s,\,g)}\,, \tag{5-5}$$

However, this peak disappeared very quickly. The Hg^{2+} produced by oxidization was adsorbed by AC, especially when NO_2 and NO were added in the simulated flue gas. The oxidization of Hg^0 to Hg^{2+} by NO and NO_2 may have occurred through reactions Eqs. (5-6) to (5-8), which are respectively given by:

$$NO_{(g)} + O_{2\,(g)} \rightarrow NO_{2\,(g)} + O, \tag{5-6}$$

$$Hg_{(g)} + O \rightarrow HgO_{(s,\,g)}\,, \tag{5-7}$$

$$Hg_{(g)} + NO_{2\,(g)} \rightarrow HgO_{(s,\,g)} + NO_{(g).} \tag{5-8}$$

During the adsorption of Hg^0 by AC in the simulated flue gas (Step 4), the concentration of Hg^0 continued to decrease, and there was no rebound of Hg^0 concentration during the remainder of the adsorption experiment. However, the outlet concentration of Hg^{2+} slowly increased. Finally, the outlet concentration of Hg^{2+} reached the same level as the initial concentration of Hg^0. The conversion of Hg^0 to Hg^{2+} occurred during adsorption in the presence of the simulated coal-fired flue gas.

There was a relatively stable curve of Hg^{2+} when the SO_2 flow into the simulated flue gas was stopped between 48:37:20 and 57:39:20; when SO_2 was added again at 57:39:20, the concentration curve of Hg^{2+} increased rapidly (Fig. 5.28). There was a competitive adsorption between SO_2 and Hg^{2+} on AC; thus, SO_2 hampered the adsorption of Hg^{2+} by AC. The Hg^{2+} concentration measured in the outlet of the bench system was even higher than the inlet concentration (14.2 $\mu g/(N{\cdot}m^3)$) at some periods. This result can be attributed to Hg^{2+}, which was already adsorbed on the surface of AC and desorbed at a temperature of 130 °C.

Here, Hg^0 was measured at the outlet of the fixed bed when AC reached saturation in terms of Hg^0 adsorption in the presence of N_2 (Fig. 5.28). However, Hg^{2+} was found at the outlet of the fixed bed when AC reached saturation in the presence of the simulated flue gas.

Such observations suggested the conversion of Hg^0 to Hg^{2+} occurred during adsorption in the presence of the simulated coal-fired flue gas. Furthermore, the conversion rate of Hg^0 to Hg^{2+} was quite high and reached nearly 100%, based on the results of Hg^0 saturation adsorption by AC in the simulated flue gas.

The results of Hg^0 adsorption by AC in N_2 gas showed that AC was not capable of inducing high Hg^0 conversion. When only flue gas was present without AC, only part of the Hg^0 was converted to Hg^{2+}. The obtained results suggested the occurrence of oxidation with the help of both AC and flue gas during Hg^0 adsorption in the presence of flue gas.

Huggins[22] found that mercury can be captured by bonding to I, Cl, S, or O anionic species on the surfaces of AC and other sorbents (e.g., coal char sorbents, zeolite-based sorbents, coal fly-ash sorbents, and so on), but only as ionic Hg^{2+}.

None of the observations made by the reported XAFS spectroscopy study are consistent with the capture of mercury in the elemental state, i.e., physisorption. Physisorption seemed to be very unlikely in the adsorption Hg^0 by AC in simulated flue gas.

Based on previous experience with saturated adsorption, the adsorption of Hg^0 by AC in N_2 may be physical adsorption. However, further research suggests that the adsorption of Hg^0 by AC in N_2 gas may also occur through a chemical adsorption process. The AC used in the current study was produced by a chemical activation method using $ZnCl_2$, which may reside on the surface of AC. The Cl element has been suggested to be strongly supportive for AC adsorption of Hg^0 in previous studies.

For the purpose of proving the key chemical element (e.g., Cl) in the Hg^0 adsorption by AC, a high temperature desorption system was utilized to remove the element on the surface of AC. After heat treatment at a temperature of 1200 °C, AC had almost the same physical characteristics, but the chemical elements were all removed by decomposition.

The Hg^0 adsorption curves of the treated AC in N_2 gas are shown in Fig. 5.30. When the gas flow was switched to the adsorption bed at 5 min, the decrease in Hg^0 concentrations was about 30% of the initial Hg^0 concentration. The adsorption curve rose quickly, reaching the initial level of Hg^0 concentration about 5 min later. This finding was completely different from the adsorption phenomena in N_2 (Fig. 5.28).

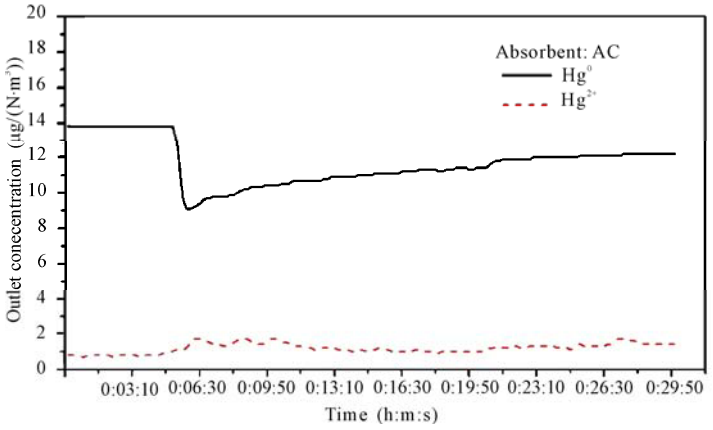

Fig. 5.30 The Hg^0 adsorption curves of treated AC in the N_2 gas

The treated AC only had limited adsorption capacity for Hg^0 in N_2 gas (Fig. 5.30). After losing the supply of surface chemical elements (e.g., Cl, among others), AC was unable to develop the capability to adsorb Hg^0 in N_2 gas. The Hg^0 adsorption capacities of ACs produced by the physical activation method were also compared. The three ACs produced by the physical activation method showed almost no capacity for Hg^0 adsorption in N_2 gas. However, those ACs had high Hg^0 adsorption capacities in simulated flue gas.

5.4.5.2 Saturated Hg^0 Adsorption Experiment by AC(MJ) in Simulated Flue Gas

In this part of the experiment, AC(MJ) was a granular AC prepared from coal using the steam activation method. During the experiment, the concentration of Hg^0 was controlled at 16.9 μg/(N·m^3) with a total flow of 1.3 L/min. The AC(MJ) sorbent was controlled at about 0.1 g. The heating temperature of the gas channel and the operating temperature of the fixed adsorption bed were all kept at (130±1) °C. The Hg^0 adsorption experiment by AC(MJ) was divided into four steps, which were conducted continuously. The time consumed for the experiment was about 25 h. The experimental result is shown in Fig. 5.31.

With similar Hg^0 adsorption results as those of other powder ACs produced using steam activation, granular AC(MJ) did not have a capability for Hg^0 adsorption in an N_2 atmosphere (Fig. 5.31). AC(MJ) started to adsorb Hg^0 when simulated flue gas components, such as NO_2, NO and so on, were added one by one. As the adsorption continued, Hg^{2+} began to appear increasingly at the outlet of the adsorption bed. Finally, the concentration of Hg^{2+} was almost the same as the initial concentration of Hg^0. Finally, Hg^0 adsorption by AC(MJ) reached true saturation.

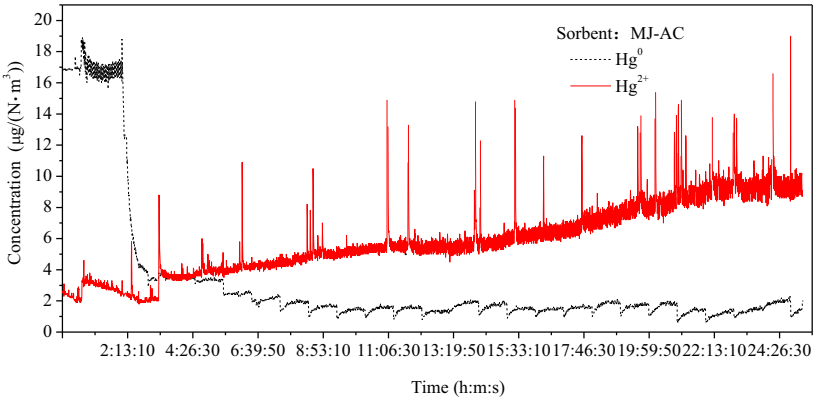

Fig. 5.31 Saturated Hg^0 adsorption experiment by AC(MJ) in simulated flue gas

5.4.6 Brief Summary

The bench-scale experimental study of adsorption of Hg^0 by AC in N_2 and in the simulated flue gas produced some important results that can help in further understanding the Hg adsorption mechanism by AC. The obtained results suggested that the adsorption of Hg^0 by AC proceeded through a chemical adsorption process either in N_2 gas or in simulated flue gas. In addition, Hg^0 was possibly oxidized to $HgCl_2$ by the Cl element remaining on the carbon surface, and then adsorbed by AC in N_2 gas. This finding indicated that chemical modification enhanced the Hg adsorption capability of AC in certain flue gas environments.

The Cl element was consumed as adsorption proceeded; thus, AC lost the capability to adsorb Hg^0 through chemical oxidization. Breakthrough occurred as Hg^0 was measured at the outlet of the reactor; however, the adsorption of Hg^0 by AC did not reach its full capacity.

When the gas flow was switched from N_2 to the simulated flue gas compounds, AC again started to adsorb Hg^0. However, with the help of carbon on the AC surface, the oxidation factor of Hg^0 was not promoted by the Cl element on AC, but by the components of simulated flue gas, such as NO, NO_2, HCl, and so on. When the adsorption capacity of AC for Hg^0 reached its full capacity, Hg^0 oxidation proceeded continuously, and the breakthrough occurred when Hg^{2+} was detected at the reactor outlet.

5.5 Mercury Stability in Pollution Control Production

The existing flue gas pollution control systems of SCR+ESP+WFGD and the injection of AC upstream by a particle control device were both potential and effective mercury emission control technologies for coal-fired power plants. However, the mercury stability in control products is very important to avoid possible mercury reemission. Thus, the mercury stabilization in both FGD gypsum and simulated mercury adsorption production of AC were studied in this research.

5.5.1 Mercury Stability in Desulfurization Gypsum

5.5.1.1 Mercury Speciation Analysis of Desulfurization Gypsum

Mercury stability was found to be intimately connected with mercury speciation in desulfurization gypsum. In order to further understand the mercury speciation in desulfurization gypsum, a chemical thermodynamic equilibrium model from Factsage software was used. This model was based on the principle of minimum Gibbs free energy, and was used to solve the possible direction of the chemical reaction and speciation of mercury in desulfurization gypsum.

First, the model hypothesized that $Hg_{(g)}$ and gypsum slurry was uniformly mixed, and the entire system was in equilibrium. In the calculation model, gypsum slurry components (CaO, SiO_2, Al_2O_3, Fe_2O_3, MgO, SO_3, and H_2O) and three kinds of $Hg_{(g)}$ (i.e., Hg^0, $HgCl_2$, HgO) were considered. According to the calculation results of the chemical thermodynamics model, the concentrations of Hg^0, $HgCl_2$, and HgO were set at 56%, 34% and 10%, respectively. The concentration of O_2 was 7%, CO_2 was 13%, N_2 was 79%, SO_2 was 1200 ppm, and HCl was 60 ppm.

The calculation results of mercury speciation in a desulfurizing tower based on a chemical thermodynamics model are shown in Fig. 5.32. In a desulfurizing tower

temperature range of 50 – 60 °C, the mercury speciation had $HgCl_{2(g)}$, $HgO_{(s)}$, $Hg_{(g)}$, $HgO_{(g)}$ and $HgS_{(g)}$, which were mainly gaseous $HgCl_2$ and solid HgO.

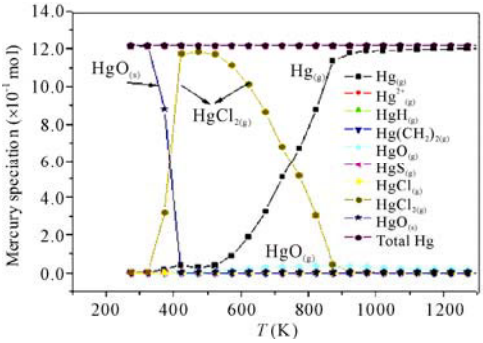

Fig. 5.32 The calculation results of mercury speciation in desulfurizing tower

The experimental study of the second emission and mercury stability on desulfurization gypsum as influenced by temperature, humidity, time and so on, is important for preventing environmental pollution and promoting the effective use of gypsum.

5.5.1.2 Mercury Stability on Desulfurization Gypsum in Natural Storage

The stability of mercury on gypsum at an environmental temperature was studied. Fig. 5.33 shows the result of mercury that escaped from gypsum at different temperatures in natural storage. The mercury-escaped ratio of gypsum was relative to time of storage at environmental temperature. In the natural environment, more mercury generally escapes within a longer period of time. Compared with mercury stability in gypsum at an environmental temperature of 50 °C (Fig. 5.33), the mercury release curve at an environmental temperature was gentler than that at 50 °C, which meant that the amount of mercury that escaped at low temperature was relatively small.

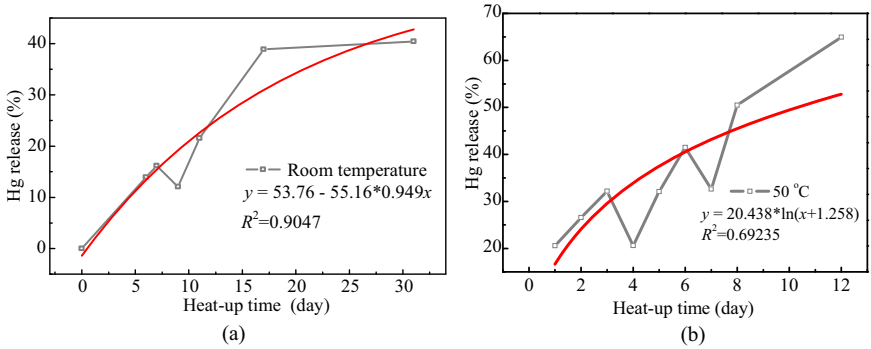

Fig. 5.33 Mercury escaped from gypsum at different temperatures in natural storage

5.5.1.3 Mercury Stability in Desulfurization Gypsum Used in an Environment at High Temperature

A wide heating temperature range was chosen to study the mercury stability in desulfurization gypsum used in an environment at high temperature. Four mercury release curves at 100, 200, 300, and 400 °C are shown in Fig. 5.34. The trend of the four curves was the same. However, different temperatures had enormous implications on mercury stability in desulfurization gypsum. 40% mercury in gypsum was stable at 100 °C for 16 days, 35% – 40% mercury in gypsum was stable at 200 °C for 20 days, 25% mercury in gypsum was stable at 300 °C for 12 days, and 10% mercury in gypsum was stable at 400 °C for 12 days.

The key factor that affected mercury stability in gypsum was the initial period of heating time (Fig. 5.34). The factor that affected the influence of mercury in plaster was the most stable initial period of heating time. The mercury release phenomenon was the same at varying high temperatures. The mercury escaped very quickly during the initial period. The mercury release ratio was much bigger at higher temperatures. After the initial period when mercury rapidly escaped, the mercury release ratio dropped due to the stronger adhesion between the remaining mercury and gypsum.

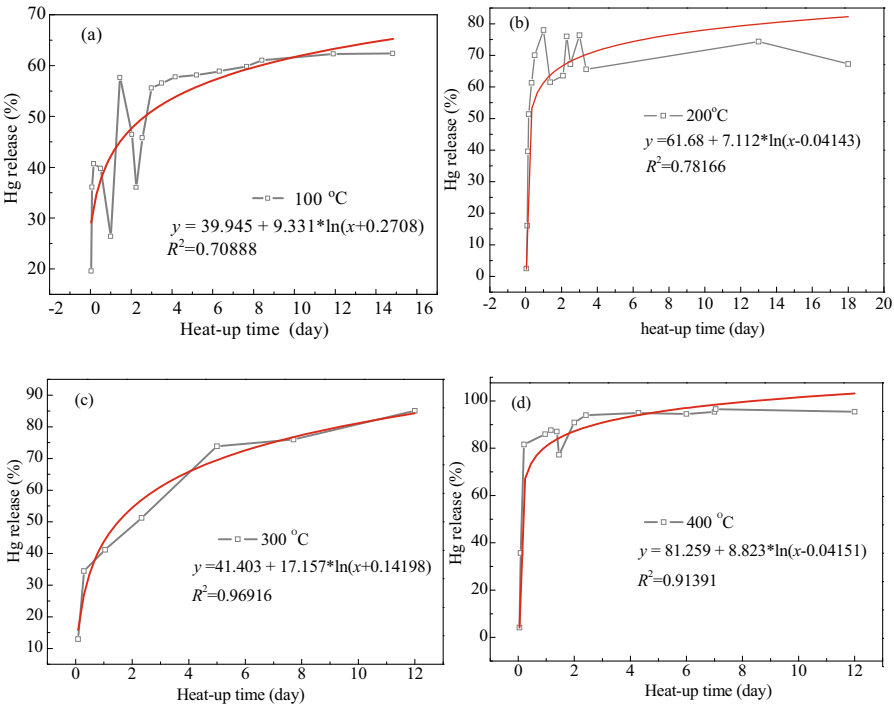

Fig. 5.34 Mercury release at 100, 200, 300 and 400 °C

5.5.2 Mercury Stability in Actived Carbon Surface

The injection of AC upstream by either an ESP or an FF is a retrofit control technology that can be potentially applied to all coal-fired power plants, since it can control almost all kinds of mercury. The stability of mercury captured on the AC is very important to avoid possible mercury reemission.

Coal combustion byproducts (e.g., fly ash, bottom ash and slag, fluidized combustion bed materials, and FGD residues) are either disposed of or utilized. These byproducts are often used as cement replacement in concrete/grout, structural fill, stability components for waste and soil, road base, mineral filler, concrete block, blasting grit, wallboard, etc. Currently, the amount of mercury leached from coal combustion byproducts is extremely low and does not appear to present a serious hazard to humans. However, only limited information has been reported on the stability of mercury captured in sorbents. This section aims to investigate the released properties of mercury captured in AC under conditions of disposal and reuse using leaching and thermal desorption techniques.

The stability of mercury in AC with respect to its potential disposal and reuse conditions was studied using two techniques: leaching and thermal desorption. Leaching was carried out using a leaching protocol called the toxicity characteristic leaching procedure (TCLP) and a column test with five different leaching solutions. TCLP is an accelerated experimental method designed to simulate conditions in an anaerobic landfill; therefore, it is supposed to represent the worst-case leaching conditions in a landfill where organic wastes are co-disposed.

The TCLP is a batch test and involves leaching a mass of waste material with an acetic acid solution, using a 20:1 liquid-to-solid (L/S) mass ratio, and rotating the mixture for (18±2) h at 30 rpm. TCLP pollutant concentrations are also used to determine whether hazardous waste complies with land disposal restrictions and whether waste may be disposed of in an unlined landfill that contains co-disposed organic wastes.

Mercury released from AC was studied at air temperatures of 60 and 90 °C. An aqueous thermostat was used to maintain the desired temperature. The results of thermal desorption experiments can verify whether fly ash containing AC, which has adsorbed mercury on its surface, is suitable for disposition in some thermal conditions.

5.5.2.1 Mercury Stability in Three Activated Carbon Sorbents with TCLP

Three types of AC were used in the experiments. The first was the commercially available untreated AC prepared from wood by the zinc chloride method [AC(MZ)] and supplied by Shanghai Activated Carbon Co., Ltd. The other two were modified from as-received AC through impregnation with MnO_2 solution [AC(MnO_2-MZ)] and $FeCl_3$ solution [AC($FeCl_3$-MZ)], respectively. The treated ACs had stronger oxidability than untreated AC.

The TCLP test was carried out on untreated AC, MnO_2-impregnated AC, and $FeCl_3$-impregnated AC. The textural characteristics of AC are provided in Table 5.12. Leaching results are summarized in Table 5.13. The calculated maximum mercury indicated the maximum concentration that was reached if all of the mercury had dissolved during leaching; it also represented the worst-case scenario. Only MnO_2-impregnated AC was detected in the leachate at 0.31 μg/L for adsorbed original Hg^0 and 0.41 μg/L for adsorbed original Hg^{2+}. The content of mercury in the leachate was much lower than the 0.025 mg/L TCLP limit. The mercury appeared to be very stable in the three ACs with respect to leaching.

Table 5.12 Textural characteristics of activated carbon

Activated carbon	Specific surface area (m^2/g)	Bulk specific weight (g/cm^3)	Pore volume (cm^3/g)	Micropore volume (<20 Å) (cm^3/g)	Particle size (mm)	Porosity (%)
AC(MZ)	1850	0.35	1.05	0.35	0.09	67
AC(MnO_2-MZ)	865	0.41	0.29	0.10	0.09	45
AC($FeCl_3$-MZ)	1470	0.38	0.92	0.31	0.09	58

Table 5.13 TCLP leaching results

Type of sample	Type of mercury[a]	Bulk (μg/g)	Calc. Max. (μg/L)	Leaching result (μg/L)
AC(MZ)	Hg^0	0.63	31.4	BDL[b]
	Hg^{2+}	0.22	10.9	BDL
AC(MnO_2-MZ)	Hg^0	0.51	25.6	0.31
	Hg^{2+}	0.21	10.5	0.41
AC($FeCl_3$-MZ)	Hg^0	0.57	28.7	BDL
	Hg^{2+}	0.18	8.8	BDL

[a] The original type of mercury in simulated flue gas; [b] Below detection limit (Hg < 0.01 μg/L)

5.5.2.2 Mercury Stability in Activated Carbon Sorbents with Column Tests

Various laboratory leaching methods have been developed, including batch tests, column tests, serial and sequential leaching tests, etc. Five different kinds of leaching liquids were used in the column tests to simulate various disposal solution environments. These kinds of liquids included deionized water, 1% sulfuric acid solution (1% H_2SO_4), 1% ferric trichloride solution (1% $FeCl_3$), 1% sodium carbonate solution (1% Na_2CO_3), and 1% sodium hydroxide solution (1% NaOH). The flow of the leaching liquid was controlled at about 5 ml/h, after which the leachate was collected every day for analysis.

The Hg content of each AC, which was used in the stability test, was adjusted to about (52±1) μg/g through the Hg adsorption experiment system. Figs. 5.35 to 5.37

show the leaching results of AC(MZ), AC(MnO_2-MZ), and AC($FeCl_3$-MZ) using five different leaching liquids continuously for 14 days and with the standard TCLP. The average Hg concentration in 1% NaOH leachate (pH>14) was about 0.89 μg/L, which was close to the average Hg concentration of about 0.78 μg/L in 1% H_2SO_4 leachate (pH<1) (Fig. 5.35). However, this value was much higher than the average Hg concentrations in H_2O, 1% $FeCl_3$, and 1% Na_2CO_3 leachates (3<pH<10), which mostly ranged from 0.22 to 0.28 μg/L. It seemed that Hg was easily released from the surface of the AC(MZ) in a strong alkaline or acid solution. Compared with the Hg concentration of the TCLP leachate, which was about 0.73 μg/L, the Hg concentrations in all the leachates were still lower than the safe limit defined by the Universal Treatment Standard, which limits content of mercury in the TCLP leachate to 25 μg /L. Based on these experiments, Hg was found to be stable on the surface of the AC(MZ) in the solution.

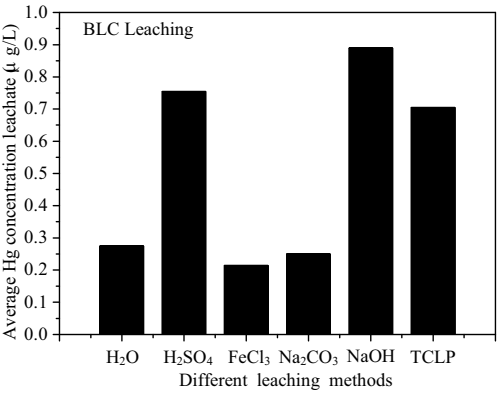

Fig. 5.35 The leaching results of AC(MZ)

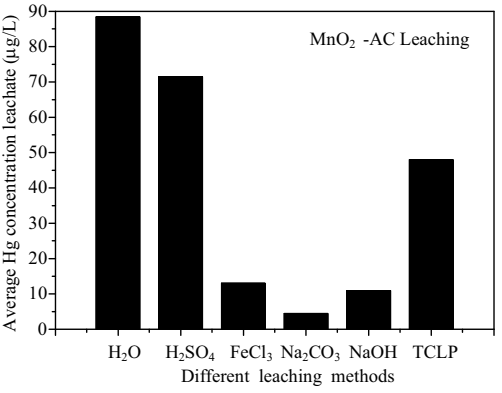

Fig. 5.36 The leaching results of AC(MnO_2-MZ)

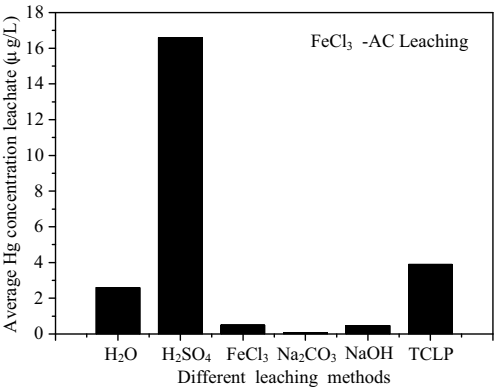

Fig. 5.37 The leaching results of AC($FeCl_3$-MZ)

The leaching results of AC(MnO_2-MZ) are shown in Fig. 5.36. Evidently, the average Hg concentrations in the leachates of H_2O, 1% H_2SO_4, and TCLP were over the safe limit of 25 μg/L. In addition, although the Hg concentrations in the leachates of 1% $FeCl_3$, 1% Na_2CO_3, and 1% NaOH were much lower than those in the leachates of H_2O, 1% H_2SO_4 and TCLP, respectively, those values were still much larger than the results shown in Fig. 5.35. According to these results, it seemed that the Hg adsorbed on the surface of AC(MnO_2-MZ) was not firm. The average Hg concentration in each leachate for AC($FeCl_3$-MZ) was low except in the 1% H_2SO_4 leachate (Fig. 5.37). However, all the leaching results of AC($FeCl_3$-MZ) were still less than the safe limit. Considering both Fig. 5.36 and Fig. 5.37, the Hg adsorbed by the oxidation treatment of ACs, especially by AC(MnO_2-MZ), was not stable in the acid solution environment. The concentrations of Hg were relatively lower in the alkaline solution environment for both. Further research may be done to clarify these facts.

All the conditions in the Hg adsorption experiments and the original Hg-laden were the same for the three kinds of ACs. However, it was very clear that the amounts of Hg that leached out from the AC(MnO_2-MZ) were greater than those from the other two kinds of ACs (Fig. 5.38). There was very little amount of Hg that leached out from the AC(MZ) relative to the AC(MnO_2-MZ) and the AC($FeCl_3$-MZ). The oxidation treatment induced the differences in the stability of mercury on ACs. In other words, the influences of the oxidized or acidic flue gas components, such as O_2, NO_2, NO, SO_2 and HCl, can be omitted as compared with that of the oxidation treatment on the stability of mercury on AC. It can be assumed that the oxidation treatment changed the physical and chemical characteristics of mercury on the surface of the ACs, or the adsorption affinity between the mercury and the surface of ACs. These changes induced the instability of mercury in AC in the solution environment.

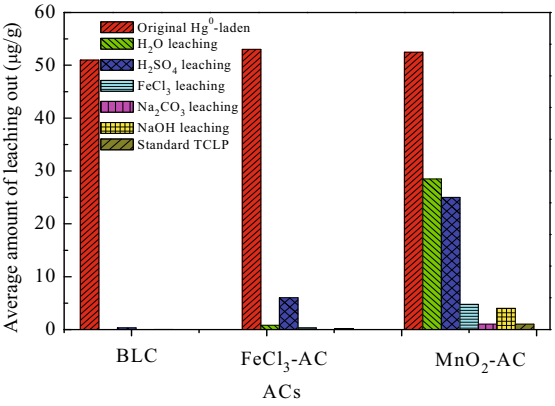

Fig. 5.38 The results of Hg stability on the three Acs

Many forms of mercury that existed on the surface of AC(MnO_2-MZ), such as $Hg(NO_3)_2$, $Hg_2(NO_3)_2$, and some Hg^0, were attributed to the influence of MnO_4, Mn^{4+}, NO_3^-, or others. Furthermore, both forms of mercury were easily soluble in water and in an acid solution. For AC($FeCl_3$-MZ), the amount of Hg that leached out was between that from AC(MZ) and AC(MnO_2-MZ); Fe^{3+} was estimated as the only probable one out of all the possible oxidizing mediums, and Cl^- was the primary anion on the surface of AC($FeCl_3$-MZ). Therefore, the oxidizability of AC($FeCl_3$-MZ) may be weak in contrast with that of AC(MnO_2-MZ). Consequently, both $HgCl_2$ and Hg_2Cl_2 were the most possible existing forms of Hg on the surface of AC($FeCl_3$-MZ). Moreover, Hg_2Cl_2 could be the main existing matter for the number of Cl^-existing on the surface of AC($FeCl_3$-MZ). Consequently, although both AC(MnO_2-MZ) and AC($FeCl_3$-MZ) have high mercury sorption capacities as an effect of the oxidation treatment, mercury is much more stable in AC($FeCl_3$-MZ) than in AC(MnO_2-MZ) in a solution environment because Hg_2Cl_2 is slightly soluble. Hence, it is very important to first consider the stability of mercury on the surface of sorbents after adsorption in certain conditions if using an oxidation treatment to enhance the mercury sorption capacity of sorbents, including AC.

5.5.2.3 Mercury Stability in Activated Carbon Sorbents in Thermal Desorption

For the coal-fired mercury emission control technology of AC injection, the thermal desorption characteristics of mercury on the AC are very important in avoiding re-emission and ensuring safe disposal of combustible byproducts. The experiment was carried out in air with the aid of an aqueous thermostat to maintain the desired temperature. The experiments were conducted to investigate the influence of heating time on mercury released from AC at 60 and 90 °C. The quantity of Hg^0 adsorbed originally in AC was 0.41 μg/g, and the amount of Hg^{2+} adsorbed origi-

nally was 0.44 μg/g.

The influence of heating time on mercury release is shown in Fig. 5.39. The Hg released (%) represented the percentage of mercury released from the original Hg-laden AC. There was much more mercury released from the AC at longer heating times for both kinds of mercury. The higher the temperature, the more the mercury released. Mercury was not stable at longer heating times and at higher temperatures. Consequently, it is disadvantageous to place mercury-contaminated AC under the sun for long periods of time, most especially in the summer.

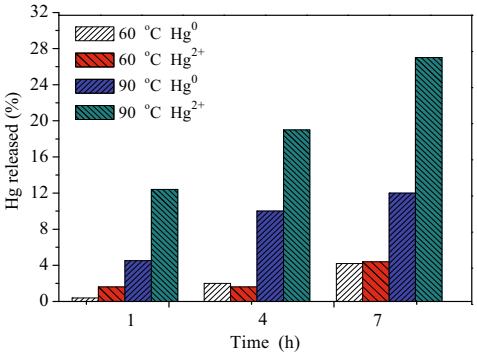

Fig. 5.39 Mercury released as a function of heating time at 60 and 90 °C

It is interesting to note that the Hg^{2+} originally adsorbed was released more easily from AC than the Hg^0 originally adsorbed under the same conditions. However, the action of Hg sorption, especially of Hg^0, is very complicated. Previous research shows that some original Hg^0 reacts with the surface functional group on the AC surface, which results in the formation of Hg–anion (e.g., Hg–O, Hg–S, Hg–Cl, etc.) chemical bonds. Some original Hg^0 was oxidized first in the flue gas and then condensed heterogeneously on the sorbent. In other words, there were almost no differences between original Hg^{2+} and original Hg^0 for AC after adsorption. However, the strength of the bond of the original Hg^0 on AC may be stronger than that of original Hg^{2+} under the same thermal conditions (Fig. 5.39). Further work is in progress to elucidate the differences between original Hg^0 and original Hg^{2+} in terms of bond strength on AC.

At the same heating time of 0.5 h, the stabilities of Hg^0 and Hg^{2+} on AC(MZ) were compared over a broad temperature range (from 150 to 900 °C). The quantity of the original Hg^0 adsorbed on AC(MZ) is 0.41 μg/g, and the quantity of the original Hg^{2+} adsorbed is 0.44 μg/g. The result is shown in Fig. 5.40. As the temperature increased from 150 to 900 °C, more and more mercury (Hg^0 and Hg^{2+}) was released from AC(MZ). Thus, there was a rapid increase in mercury release between the temperatures of 250 and 500 °C. Furthermore, almost all mercury had already escaped before the temperature reached 500 °C. However, after 500 °C, the increase in mercury release changed slowly and even stopped completely after 700 °C. The experiment indicates that AC burns in air at ca. 350 – 400 °C. The burning completely destroyed the texture of AC (MZ), which then induced mercury to lose

to lose its bond on an object; most of the mercury then escaped. Therefore, it was not suitable to use AC(MZ) with mercury as a material at high temperatures in oxygen-rich environments. The two curves intercrossed at ca. 470 °C (Fig. 5.40). Before this point, the curve of Hg^{2+} was always above Hg^0, indicating that more Hg^{2+} was released than Hg^0 under the same conditions and Hg^0 is more stable than Hg^{2+} on AC(MZ).

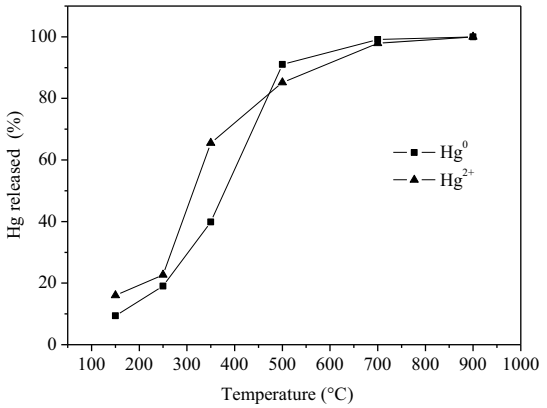

Fig. 5.40 Mercury released as a function of high temperature

5.5.2.4 Mercury Stability in Actual Fly Ash and AC in a Natural Storage Environment

A simulated experiment of mercury stability in sorbent in a natural storage environment was conducted to study the mercury released from actual fly ash and AC(MZ). Mercury stability in fly ash in natural environments was a short-term experiment focused on the relation between the mercury release and natural temperature. The results are shown in Fig. 5.41. The experiment on mercury stability in AC(MZ) in a room environment, was conducted over a period of more than one year. There was exposure to direct sunlight and the temperature ranged from 6 to 25 °C. The results are shown in Fig. 5.42.

Based on the above, the Hg release was quite low in actual fly ash and AC, with a release ratio lower than 1.5%. In addition, Hg was stable in both fly ash and AC, which would not significantly affect the environment.

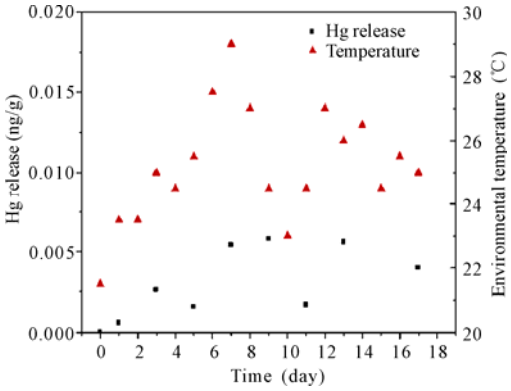

Fig. 5.41 Hg release from fly ash in a natural storage environment

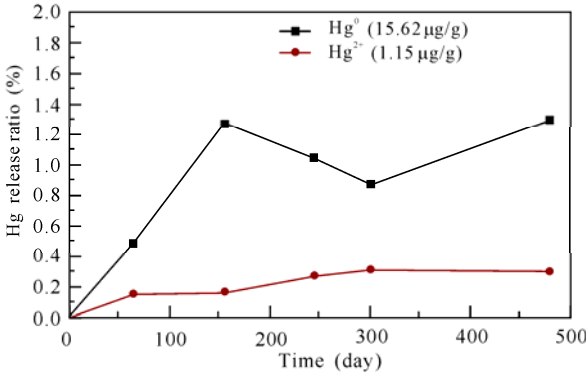

Fig. 5.42 Hg release from AC in a natural storage environment

5.6 Summary

Mercury emissions from coal-fired flue gas comprise one of the major sources of mercury pollution; thus, controlling these emissions is very important. Sorbent injection technology is currently a relatively mature and comprehensive gas mercury removal technology, with fairly extensive adaptability. The removal of mercury can be a cost-effective approach with the use of existing pollution control devices. However, the resulting impact of mercury on the control products should be highlighted. Two kinds of flue gas mercury control methods were featured in this study. The findings of researchers from Zhejiang University about the opening of new adsorbents, the mercury adsorption mechanism of activated carbon, as well as the formation of possible mercury stability using the two methods were also introduced.

Based on the results, ZS-MnO_2, PT-MnO_2, FS-MnO_2, and ZS-$FeCl_3$ were found to be applicable for use in the future because of their better adsorption efficiencies, lower costs and easier modified operation.

The adsorption of Hg^0 by AC proceeded through the chemical adsorption process either in N_2 gas or in simulated flue gas. In addition, Hg^0 was oxidized to $HgCl_2$ by the Cl element that remained on a carbon surface and adsorbed by AC in N_2 gas. Thus, chemical modification enhanced the Hg adsorption of AC in certain flue gas environments. The Cl element was consumed as adsorption proceeded, AC then lost the ability to adsorb Hg^0 through chemical oxidization, and a breakthrough occurred as Hg^0 was measured at the outlet of the reactor. However, the adsorption of Hg^0 by AC did not reach its full capacity. When the gas flow was switched from N_2 to the simulated gas compounds one by one, the AC resumed its absorption of Hg^0. The oxidation factor of Hg^0 was not the Cl element in AC, but the components in the simulated flue gas, such as NO, NO_2, HCl, etc., with the help of carbon on the AC surface. When the adsorption capacity of AC for Hg^0 reached its full capacity, Hg^0 oxidation continued, and the breakthrough occurred when Hg^{2+} was detected at the reactor outlet.

Mercury appeared to be stable in untreated AC according to leaching tests. Thus, when using oxidation treatment to enhance the mercury sorption capacity of sorbents, it is very important to consider first the stability of mercury on the surface of sorbents. As the temperature increases, more mercury is released from the control products of AC and gypsum. Furthermore, it is not a good idea to place mercury-contaminated AC and gypsum under direct sunlight for long periods of time and in high-temperature environments. Finally, Hg was found to be stable on actual fly ash and AC in a natural storage environment.

References

[1] Donnet J.B. Carbon, 6: 161, 1968.
[2] Huggins, F.E., Huffman, G.P., Dunham, G.E., Senior, C.L. XAFS examination of mercury sorption on three activated carbons. *Energy & Fuels*, 13: 114-121, 1999.
[3] Liberti L., Notarnicola M., Amicarelli V., Campanoro V., Roethel F., Swanson L. *Waste Management Research*, 16: 183-189, 1998.
[4] Karatzaa D., Lancia A., Musmarra D., Zucchini C. Study of mercury absorption and desorption on sulfur impregnated carbon. *Experimental Thermal and Fluid Science*, 21: 150-155, 2000.
[5] Matsumura Y. Atmos. *Environment*, 8: 1321-1327, 1974.
[6] Liu W., Vidic R.D. Optimization of sulfur impregnation protocol for fixed bed application of activated carbon-based sorbents for gas-phase mercury removal. *Environmental Science Technology*, 32: 531-538, 1998.
[7] U.S. Environmental Protection Agency. Mercury Study Report to Congress, Volume I: Executive Summary. Office of Air Quality Planning and Standards and Office of Research and Development, EPA-452rR-97-003, December 1997.
[8] Brown T.D., Smith D.N., Hargis R.A., O'Dowd W.J. Mercury measurement and

its control: what we know, have learned, and need to further investigate. *Journal of Air & Waste Management Association*, 6: 1, 1999.

[9] Miller S.J., Dunham G.E., Olson E.S., Brown T.D. Flue gas effects on a carbon-based mercury sorbent. *Flue Processing Technology*, 65-66: 343-363, 2000.

[10] Teller A.J., Quimby J.M. 84th Annual Meeting and Exhibition, AWMA, Vancouver, BC, 91-35.5, 1991.

[11] Roberts D.L., Stewart R.M. Novel Process for Removal and Recovery of Vapor Phase Mercury. Presented at First Joint Power&Flue Systems Contractors conference, Pittsburgh, PA, July 1996.

[12] Yan T.Y. A novel process for Hg removal from gases. *Industrial & Engineering Chemistry Research*, 33: 3010, 1994.

[13] Ghorishi B., Jozewicz W., Gullet B.K., Sedman C.B. Mercury Control: Overview of Bench-Scale Research at EPA/APPCD. Presented at the First Joint Power & Flue Systems Contractors Conference, Pittsburgh, PA, July 1996.

[14] Schager P., Hall B., Linquist O. Retention of Gaseous Mercury on Flyashes. Second International Conference on Mercury as a Global Pollutant. Monterey, CA, June 1992.

[15] Tessmer C.H., Vidic R.D., Uranowski L.J. Impact of oxygen-containing surface functional groups on activated carbon adsorption of phenols. *Environmental Science& Technology*, 31(7), 1997.

[16] Boehm H.P., Voll M. *Carbon*, 8: 227, 1970.

[17] Papirer E., Li S., Donnet J.B. *Carbon*, 25(2): 243, 1987.

[18] Boehm H.P., Diehl E., Heck W., Sappok R. *Angewandte Chemie International Edition in English*, 3(10): 669, 1964.

[19] Garten V.A., Weiss D.E. *Carbon*, 22(1): 19, 1984.

[20] Leon C.A., Solar J.M., Calemma V., Radovic L.R. *Carbon*, 30(5): 797, 1992.

[21] Puri B.R. In Chemistry and Physics of Carbon. New York, 1970.

[22] Huggins F.E., Yap N., Huffman G.P., Senior C.L. XAFS characterization of mercury captured from combustion gases on sorbents at low temperatures. *Fuel Processing Technology*, 82: 167-196, 2003.

Index